A MECHANISTIC STUDY IN METHANOL: CLEAVAGE OF RNA MODELS AND HIGHLY STABLE PHOSPHODIESTERS WITH DINUCLEAR Zn(II)-COMPLEXES

by

STEPHANIE ANDREA MELNYCHUK

A thesis submitted to the Department of Chemistry

in conformity with the requirements for

the degree of Master of Science.

Queen's University

Kingston, Ontario, Canada

August, 2008

Abstract

Phosphoryl transfer reactions are vital to life. In response to the slow intrinsic rates of phosphoryl transfer, Nature has evolved a series of enzymes designed to accelerate these reactions and allow them to occur at biologically relevant rates. These metallo-enzymes are largely characterized by bi- or tri-nuclear active sites with effective dielectric constants that more closely resemble those of organic solvents than water. This project was designed to better understand the mechanisms by which metalloenzymes cleave phosphodiesters with poor leaving groups.

The stability of the phosphodiester is central to the storage of genetic information in DNA and RNA. The cleavage of a series of more reactive RNA models, 2-hydroxylpropyl aryl phosphates **1**a-g, catalyzed by a dinuclear $Zn(II)_2$ complex of **53** in methanol was explored. A solution of **53**:$Zn(II)_2$:($^-OCH_3$) was observed to accelerate the decomposition of **1**a-g with rates that were 10^{11}-10^{12}-fold greater than the methoxide-promoted reaction at ^s_spH 9.47, approaching rate accelerations achieved by natural enzymes.

The remarkable activity of **53**:$Zn(II)_2$:($^-OCH_3$) and **36**:$Zn(II)_2$:($^-OCH_3$) towards the cleavage of **1**a-g probed the study of the decomposition of diribonucleotides (3'→5)UpU and (3'→5')ApC in methanol. The **53**:$Zn(II)_2$:($^-OCH_3$)- and **36**:$Zn(II)_2$:($^-OCH_3$)-catalyzed decomposition of UpU achieved k_2 values of 1.21 ± 0.17 and (7.04 ± 0.99) x 10^{-2} $M^{-1}s^{-1}$. The reactivity of ApC in the presence of these systems was unimpressive, however Zn(II) ions in ethanol resulted in the isomerization of

(3'→5')ApC to (2'→5')ApC providing support for the existence of a pentacoordinate phosphorane intermediate.

The pentacoordinate phosphorane was further explored through the reaction of **36**:$Zn(II)_2$:($^-OCH_3$) with the cyclic phosphate **58** and 2-hydroxylpropyl methyl phosphate (**59**). In the presence of **36**:$Zn(II)_2$:($^-OCH_3$) the rate of isomerization of **59/59a** (k_{obs} = (4.7 ± 0.5) x 10^{-3} s^{-1}) exceeded that of expulsion of the methoxy group (k_{obs} = 1.62 x 10^{-3} s^{-1}), thus confirming the existence of a pentacoordinate phosphorane intermediate (**60**) and providing support for a two-step phosphodiester cleavage reaction.

The catalytic efficiency of **36**:$Zn(II)_2$:($^-OCH_3$) towards the cleavage of stable phosphodiesters probed its application towards the decomposition of dimethyl phosphate (**2**) in methanol-d4. The exchange of OCH_3 for OCD_3 occurred with k_{cat}^{max} = (2.27 ± 0.03) x 10^{-6} s^{-1}.

Acknowledgements

With the submission of this manuscript I am hanging up my lab coat and goggles and trading them for robes and legal briefs. Although my future may be steering me away from the world of Chemistry, I will look back on my time as a graduate student with great fondness towards the experience, the people, and the pursuit and pleasure of finding things out.

Foremost I would like to thank Dr. R. Stan Brown whom I have come to bestow many titles upon. Dr. Brown has been a professor, a supervisor, and most importantly a mentor. He has offered support, encouragement, knowledge and experience for which I am extremely grateful. I would like to thank him for an unexpected, but much appreciated, invitation to join his group of friends and researchers.

One of the group members that I would consider a friend in addition to a supervisor and lab guru is Dr. Alexei Neverov. Alex has provided me with the answers to my many stupid questions and has beared many of the frustrations associated with this project and experiments failed. Simply thanking Alex in text seems feeble and will undoubtedly be done instead over vodka and dill pickles.

Undoubtedly, Mark will be "no fun" and leave the celebration early. I thank Mark for grounding me throughout the completion of my Master's, providing me with encouragement, feed-back, friendship, and an ear to talk off and off. I would also like to acknowledge group members Chris, Tony, Dave, Zhong-Lin, Chaomin, Tam, Benoit, and Pasha who have assisted with the completion of my degree and have been friends and guides throughout the process.

Outside of the doors of Chernoff Hall are a handful of people who have encouraged and supported this journey of mine. My mother, father, sister, aunt Yvonne, and bff Mike have been monumental in my achieving my goals. Thank you, thank you, thank you, thank you, and thank you. And thank you Sean for your love and support during the writing and defending of my thesis. You helped me keep perspective and encouraged my best efforts always. I love you all.

Statement of Originality

To the best of the author's knowledge, the original work presented in this thesis includes the following:

1. Kinetic studies and mechanistic analysis of the transesterification of a series of RNA models, 2-hydroxylpropyl aryl phosphates (**1**a-g), as a function of [**53**:$(Zn(II)_2$:$(^{-}OCH_3)]_{free}$ in methanol.

2. Kinetic studies and mechanistic analysis of the transesterification and isomerization of dinucleotides, uridyl(3'→5')uridine monophosphate (UpU) and adenyly(3'→5')cytidine (ApC), as a function of [**36**:$(Zn(II)_2$:$(^{-}OCH_3)]_{free}$ and [**53**:$(Zn(II)_2$:$(^{-}OCH_3)]_{free}$ in methanol and as a function of [Zn(II):(^{-}OEt)] in ethanol.

3. Kinetic studies and mechanistic analysis of the transesterification and isomerization of an RNA model, 2-hydroxylpropyl methyl phosphate (**59**), catalyzed by [**36**:$(Zn(II)_2$:$(^{-}OCH_3)_{total}$ in methanol and methanol-d4.

4. Kinetic studies and mechanistic analysis of the transesterification of a highly stable DNA model, dimethyl phosphate (**2**) catalyzed by [**36**:$(Zn(II)_2$:$(^{-}OCH_3)]_{total}$ in methanol.

Table of Contents

List of Figures

List of Tables

List of Schemes

List of Abbreviations

[9]aneN_3	1,4,7-triaazacyclononane
[12]aneN_3	1,5,9-triaazacyclododecane
([12]aneN_3)$_2$	1,3-bis[N_1,N_1'-(1,5,9-triazacyclododecyl)]propane
[12]aneN_4	1,4,7,10-tetraazacyclododecane
[30]aneN_6O_4	1,4,7,16,19,22-hexaza-10,13,25,28-tetraoxacyclotriacontane
A	adenine
2'-AMP	adenine 2'-monophosphate
3'-AMP	adenine 3'-monophosphate
2':3'-cAMP	adenine cyclic (2':3')-monophosphate
AP	alkaline phosphatase
ApA	adenyl(3'→5')adenine
ApC	adenyl(3'→5')cytidine
(2'→5')ApC	adenyl(2'→5')cytidine
ApU	adenyl(3'→5')uridine
Bpy	2,2'-bipyridine
BNP	bis *p*-nitrophenyl phosphate
BPAN	2,7-bis[(2-pyridylethyl)aminomethyl]-1,8-naphthyridine
C	cytosine
CAPS	*N*-cyclohexyl-3-aminopropanesulfonic acid

DAG	diacylglycerol
ddH_2O	doubly deionized water
DFT	density functional theory
DMP	dimethyl phosphate
DMSO	dimethylsulfoxide
DNA	deoxyribonucleic acid
E. coli	*Escherichia coli*
ESI	electrospray ionization
EtO^-	ethoxide
EtOH	ethanol
G	guanine
GpG	guanyl(3'→5')guanine
HEPES	4-(2-hydroxyethyl)-1-piperazineethanesulfonic acid
HMP	2-hydroxylpropyl methyl phosphate
HPLC	high-pressure liquid chromatography
HPNPP	2-hydroxylpropyl *p*-nitrophenyl phosphate
MPMPP	methyl *p*-methoxyphenyl phosphate
MPP	methyl phenyl phosphate
MS	mass spectrometry
NLLSQ	non-linear least squares
NMR	nuclear magnetic resonance

NPP	nucleotide pyrophosphatase/phosphodiesterase
$^{-}$OTf	trifluoromethane sulfonate (triflate)
PLC	phospholipase C
PTFE	polytetrafluoroethylene
RNA	ribonucleic acid
S	phosphodiester substrate
Ser	serine
T	thymine
TREN	1,4,7,10-tetraazacyclodecane
Tris	tris(hydroxymethyl)aminomethane
U	uracil
2’-UMP	uridine 2’-monophosphate
3’-UMP	uridine 3’-monophosphate
2’:3’-cUMP	uridine cyclic (2’:3’)-monophosphate
UpA	uridyl(3’→5’)adenine
UpPNP	uridine 3’-*p*-nitrophenyl phosphate
UpU	uridy(3’→5’)uridine
UV	ultra-violet
Vis	visible

Chapter 1. Introduction

Much research effort has been invested into understanding the mechanisms by which metalloenzymes cleave DNA and RNA. Small molecule metal ion complexes have been designed with the intent of mimicking natural phosphoryl transfer reactions.[1] The stability of DNA and RNA and their resistance to hydrolysis at physiological temperature and pH make these biopolymers difficult to study in practice. DNA and RNA models with activated leaving groups have been explored to assist in the elucidation of mechanistic information and to better design catalysts that will accelerate the cleavage of phosphates with unactivated groups. 2-Hydroxylpropyl aryl phosphodiesters (**1**), such as the most widely used 2-hydroxylpropyl *p*-nitrophenyl phosphate (HPNPP, **1**a), are commonly investigated RNA models. Dimethyl phosphate (DMP, **2**) serves as an excellent DNA model, although due to its unreactivity, bis *p*-nitrophenyl phosphate (BNP, **3**) and methyl aryl phosphates (**4**) have received more attention.[1(a)] The methanolyses of these DNA and RNA models were investigated in the study below.

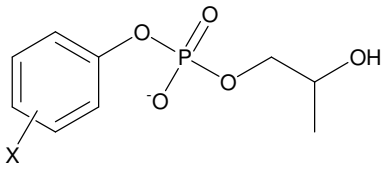

1 (a) X = 4-nitro
(b) X = 3-methyl, 4-nitro
(c) X = 3-nitro
(d) X = 4-chloro
(e) X = 3-methoxy
(f) X = H
(g) X = 4-methoxy

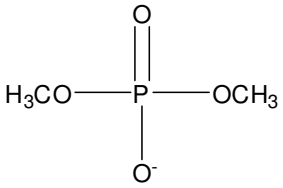

DMP, **2**

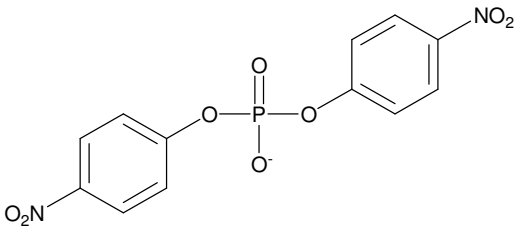

BNP, **3**

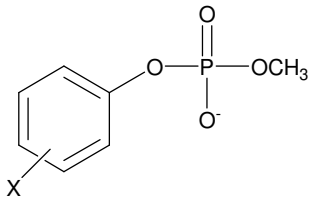

4 (a) X = 2-chloro-4-nitro
(b) X = 2, 4, 5-trichloro
(c) X = 4-nitro
(d) X = 3-nitro
(e) X = 4-chloro
(f) X = 3-methoxy
(g) X = H
(h) X = 4-methoxy

1.1 Monoanionic phosphate diesters

Phosphate esters comprise a class of compounds crucial to life. Monoanionic phosphate diesters are particularly interesting as they form the backbone of the biopolymers DNA (**5**) and RNA (**6**) as depicted in Figure 1. These phosphodiesters are inherently stable; the half-time for hydrolysis of RNA is estimated to be 110 years at pH 7, 25 ^{o}C[2] and is about 20 million years for DNA at pH 14, 25 ^{o}C.[3] The higher reactivity of RNA over DNA is attributable to the presence of a ribose 2'-OH group, which serves as an intramolecular nucleophile in phosphoryl transfer reactions. If the overall reaction is concerted, attack by the 2'-OH group occurs simultaneously with the departure of the

leaving group sugar. Alternatively, the two-step hydrolysis of RNA, as depicted in Scheme 1, where the high effective molarity of the 2'-OH group means that intramolecular attack is the only observable reaction[2] leading to a pentacoordinate phosphorane intermediate, followed by release of the leaving group alcohol to give a cyclic phosphate. Alternatively, the phosphorane intermediate may undergo pseudorotation resulting in the isomerization of the starting material. This will be discussed later.

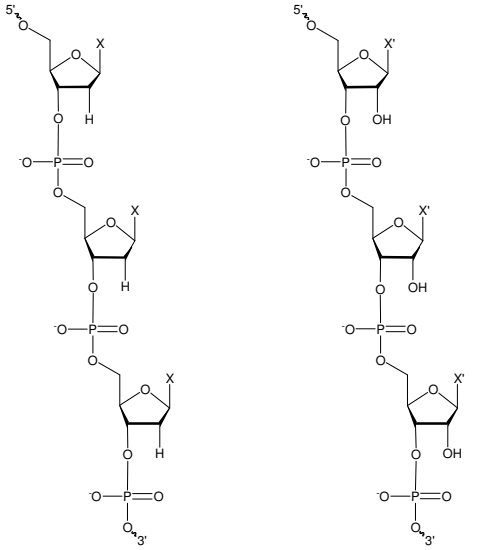

5 (X = A, C, G, T) **6** (X' = A, C, G, U)

Purines (A, G) **Pyrimidines** (C, T, U)

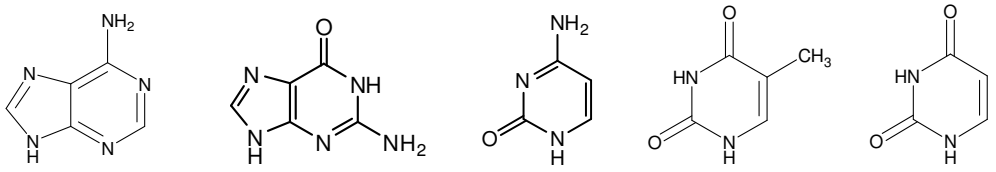

A = adenine G = guanine C = cytosine T = thymine U = uracil

Figure 1. The single-stranded fragment of DNA (**5**) and RNA (**6**) showing the polyanionic phosphodiester backbone and purine and pyrimidine bases.

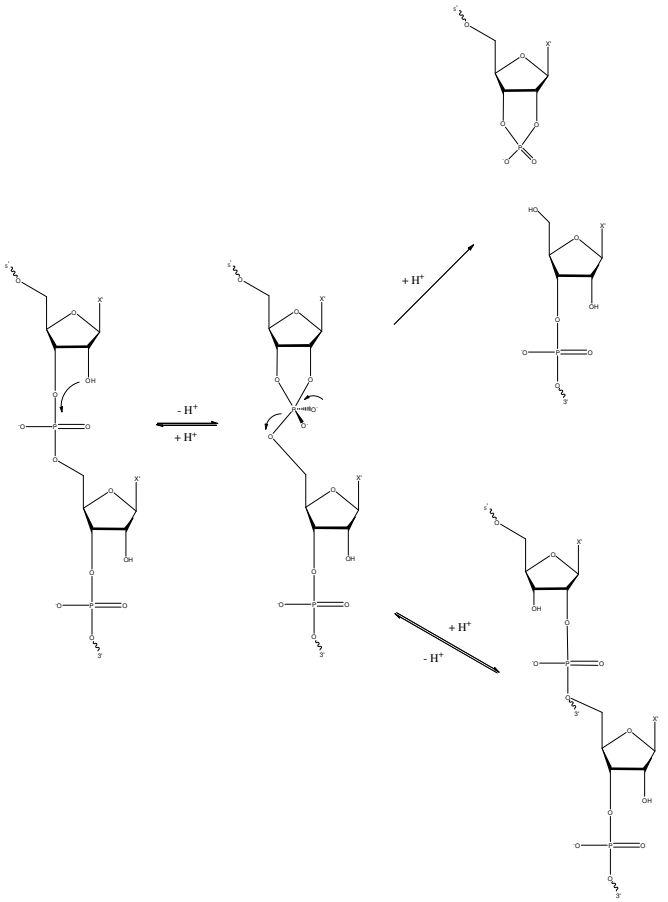

Scheme 1. The two-step isomerization and transesterification of RNA, where X' = A, C, G, or U.

1.2 Phosphodiesterases

The conservation of genetic material is an insufficient necessity to the proliferation of life. Repair and mutation of the genetic code are essential processes that the cell must also be able to accommodate. Thus, phosphoryl transfer is essential to normal cell functioning and this class of reactions is responsible for nucleic acid replication and repair, gene expression, and additional reactions unrelated to genetic material. Although indispensable, in the absence of catalytic activity these reactions are exceptionally slow and ineffective from a biological standpoint; the spontaneous

hydrolysis of an alkyl phosphate monoester dianion proceeds with a half-time of 1.1 x 10^{12} years ($k_{obs} \approx 10^{-20}$ s^{-1}) while a phosphodiester anion, such as the phosphodiester backbone of the nucleic acids, hydrolyzes with a half-time of approximately 1.4 x 10^5 years at 25 ^{o}C.[4] These reactions are pH dependent and are faster at more basic pH as the abundance of hydroxide and phosphate anion increase. To overcome the inherent stability of such compounds Nature has designed a class of enzymes responsible for the hydrolysis of highly stable phosphate esters.[5] Many of the enzymes responsible for the cleavage of phosphodiesters are referred to as phosphotransferases or phosphodiesterases and are bi- or tri-metallic using metal ions (Mg(II), Ca(II), Zn(II), Co(II), Fe(II), Fe(III), Mn(II), Cd(II)) for catalytic activity.[6, 7, 8]

It is essential that the phosphoryl transfer reactions performed within the enzyme's active site be highly efficient and specific. Substrate specificity and orientation are governed by the geometry of the active site, which is dictated by the tertiary structure afforded by an enzyme's amino acid sequence and by coordination to auxiliary metal ions. Metal ions coordinated within the active site act to position and bind the substrate such that the enzyme is able to cleave phosphate diesters with a rate accelerated 10^{15} to 10^{17}-fold relative to the uncatalyzed reactions.[9]

Examples of metal-containing phosphotransferases include alkaline phosphatase, a non-specific phosphate monoesterase,[10, 11] and zinc-dependent phospholipase C, which is responsible for hydrolyzing phospholipids (Figure 2).[1b]

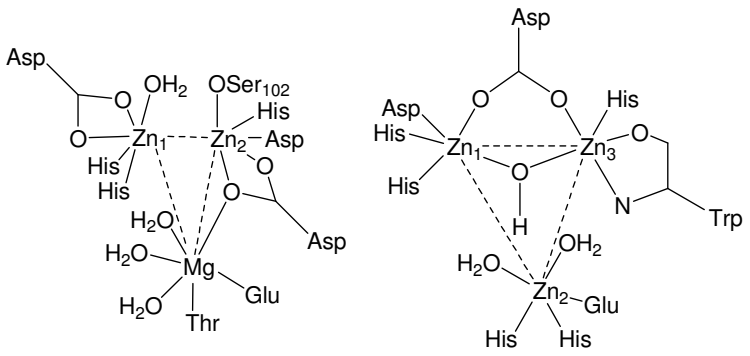

alkaline phosphatase **phospholipase C**

Figure 2. Representation of the metal-coordinated active sites of alkaline phosphatase and phospholipase C. (Reference 1b)

It is thought that alkaline phosphatase (AP) is responsible for the harvesting of inorganic phosphate from phosphate monoesters in phosphate-poor environments at alkaline pH.[6] Although it was once considered to be exclusively a monoesterase, AP has been discovered to retain lower, but still substantial levels of phosphodiesterase activity, presumably as a result of a distant evolutionary relationship to nucleotide pyrophosphatase/phosphodiesterase (NPP).[11] Non-specificity may arise from the shallow active site of AP, which does not accommodate the alkyl moiety of the phosphate and thus recognizes only the PO_4 portion of the substrate.[12]

Eukaryotic and prokaryotic APs share only 25-30% homology, however the majority of similarity is in the active site structure. Owing to the ease with which it is isolated and due to the structural similarity that it shares with the active site of mammalian phosphatases,[6] the most extensively studied form of this metalloenzyme is that from *Escherichia coli*. Structural X-ray crystallographic[13] and NMR[14] studies of *E. coli* AP have demonstrated a nucleophilic role of a deprotonated serine (102) residue

within the active site. The phosphoseryl intermediate that results is then intramolecularly attacked by a Zn(II)-bound hydroxide and the hydrolysis product is then released with retention of configuration around the phosphorus atom.[15] In the active region of each AP subunit there are three metal binding centres conventionally labeled M1, M2, and M3. In the wild-type enzyme the M1 and M2 sites are occupied by Zn(II) ions, while the M3 site contains an Mg(II) ion. The Zn(II) ions are involved in binding and orientating the substrate in the active site, are Lewis acidic and electrophilically activate the phosphate through coordination to bridging phorphoryl oxygen atoms, stabilize developing negative charge in the transition state, and mediate the release of the leaving group alkoxide.[16] The role of the Mg(II) ion has yet to be elucidated, but is thought to make its contribution to the structure of the enzyme's active site. The metal-ligand constellation that is observed for AP is similar to other phosphate cleaving enzymes. One such example is phospholipase C (PLC) whose trimetal centre reflects that of APs in both metal-metal distances and ligand orientations.[8]

PLC isolated from *Bacillus cereus*[16] is a metallolipase which hydrolyzes the phosphodiesters phosphatidylinositol and phosphatidylcholine to generate secondary messengers such as diacylglycerol (DAG) and inositol triphosphate.[17] The active site of this zinc-dependent phosphodiesterase is found at the N-terminus where three Zn(II) ions have an adopted trigonal bipyramidal configuration and each binds to the phosphate diester oxygen atoms.[18, 19] Hydrolysis has been proposed to proceed through an in-line displacement step with the assisted delivery of a Zn1-Zn3 bridging water molecule and

breakdown to products. All three metal ions are thought to be involved in the stabilization of the transition state and assisted departure of the leaving group alkoxide.[16]

Through the assembly of information regarding Zn(II)-dependent phosphoesterases and other related metalloenzymes the design of artificial catalysts mimicking the efficiency of Nature is becoming increasingly feasible. While the design and exploration of artificial enzymes is a relatively new field, evolving only within the past 20 years, much attention has been paid by the scientific community towards the hydrolysis of phosphodiesters promoted by metal ions.[6, 9-11]

1.3 Base-promoted hydrolysis of biologically relevant phosphodiesters

The base-promoted decomposition of phosphodiesters serves as a reference point in determining the effectiveness of synthetic catalysts and in providing information regarding the factors that contribute to efficient catalysis, such as stabilization of the transition state.[9, 20, 21] Complications arise in the determination of the rates of hydrolysis of DNA and RNA as their inherent stability makes base-promoted cleavage reactions very slow even in the presence of excessive amounts of base. Additionally, phosphorus is not the most reactive site within DNA and this complicates the direct measurement of hydrolysis at phosphorus.[22]

Often model substrates and extreme reaction conditions, such as high temperatures, are employed and rates are then extrapolated from an Arrhenius plot to physiological temperature.[23] Even with the use of model substrates complications are inevitable. For instance, dimethyl phosphate (DMP, **2**) is a convenient DNA model and early studies performed by Westheimer *et al.*[24] used this substrate to estimate the rate of

DNA hydrolysis. Shortly thereafter, Bunton *et al.*[3(d)] used ^{18}O-label studies to show that most of the reaction proceeded with nucleophilic attack at carbon with C-O cleavage as opposed to the desired P-O cleavage. Taking C-O cleavage into consideration, Westheimer and Haake[3(b)] proposed a corrected second order rate constant of 6.8×10^{-12} $M^{-1}s^{-1}$ for the hydroxide-promoted hydrolysis of DNA at 25 ^{o}C. The accuracy of this number has been of keen interest and under experimental probe ever since the original Westheimer report.[24] Thirty years later, Wolfenden and Radzicka[23] used high temperature kinetic data to extrapolate a half-life of 130, 000 years for the hydrolysis of DNA at 25 ^{o}C, pH 6.8. This number served as an upper limit for DNA hydrolysis as only C-O cleavage was occurring in the explored reaction.

More recently, the rate of hydrolysis of dineopentyl phosphate (**7**) was studied to eliminate C-O cleavage without hindering the attack at the phosphorus centre.[3(a)] The steric effect conferred by γ branching of the leaving group alcohol makes the P-O bond the only site of cleavage and allows for a more reliable prediction for the half-life of DNA. At 25 ^{o}C and a pH of 14 the estimated half-life of DNA is 20 million years.[3(a)] If hydroxide catalysis is the dominant reaction, at pH 7 and 25 ^{o}C the rate constant for the hydrolysis of dialkyl phosphodiesters is 10^{-22} s^{-1}.[3(a)]

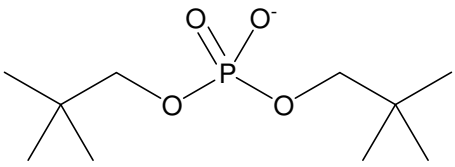

7

The stability of DNA and its models which complicates the determination of the rates of cleavage are not as problematic in determining the reaction rates of RNA and its models. C-O cleavage is not observed for this class of phosphodiesters due to an increased steric hindrance at carbon. The requirement for an external nucleophile is also alleviated by the presence of the ribose 2'-OH group of RNA. Hydrolysis involves an intramolecular attack of a 2'-OH group on the phosphorus centre and decomposition yields a cyclic phosphate intermediate (Scheme 1). Comparing the rate of hydrolysis of simple dialkyl phosphodiesters with ethylene phosphate (**8**), the cyclic phosphodiester achieved a 10^{11}-fold rate enhancement over its acyclic counterpart.[23] Rate enhancements of this magnitude can be attributed to the strain of the five-membered ring.

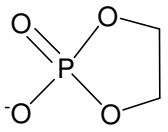

8

DNA and RNA models with aryloxy substituents (**1** and **4**, respectively) have also been studied to decipher mechanisms of phosphoryl transfer. In addition to the increased rates of reaction, C-O bond cleavage is suppressed and hydrolytic reaction rates can be directly determined for nucleophilic attack at phosphorus and P-O cleavage.[23] It should be noted that the results obtained using activated DNA and RNA models can not be directly applied to the extrapolation of rate constants for the cleavage of natural unactivated substrates.[25] Phosphodiesters with highly labile, activated leaving groups, such as *p*-nitrophenyl, likely have a different mechanism of transesterification than DNA and RNA, which have unactivated departing groups. Nucleophilic attack and formation

of a phosphorane intermediate or a phosphorane-like transition state[26] tends to be rate limiting for activated phosphate esters, while the breakdown of the phosphorane is rate limiting for unactivated phosphate esters. [27]

1.4 Modes of catalysis in phosphoryl transfer reactions

The hydrolysis of DNA and RNA is largely hindered by the large negative charge of the polyanionic backbone which repels nucleophilic attack by hydroxide. The use of metal ions to complex and nullify the negative charge associated with these biopolymers is a mechanism used by many natural nucleases.[27] Complexation of anionic phosphates by metal ions is performed by Nature in the active sites of enzymes and has been applied to the development of synthetic P-O cleaving catalysts.

Metal ions act as Lewis acids by coordinating to phosphoryl oxygen atoms and activating the phosphate group towards nucleophilic attack. The generation of the nucleophile is also facilitated by metal ions which effectively lower the pK_a of solvent molecules and promote deprotonation at physiological pH. Metal ions also serve to minimize electrostatic repulsion between the anionic substrate and nucleophile, to stabilize developing negative charge in the transition state, and to assist in the departure of the leaving group.[1a]

Selection of the metal ion for the cleavage of phosphates is not trivial. The metal must be strongly Lewis acidic, undergo rapid ligand exchange, and be redox inactive so as to avoid the activation of oxidative cleavage reactions with nucleic acids.[28] Nature commonly uses the bioaccessible and prevalent Mg(II), Zn(II), Ca(II) ions and the redox active Fe(II) ion for the decomposition of phosphates.[1a] Artificial systems typically

employ metal ions that are better Lewis acids than those chosen by Nature (La(III)) and metals that are spectroscopically active (Cu(II) and Co(III)).[1a, 29]

While Mg(II) is the metal Nature most often selects for phosphate hydrolysis,[30] much research has focused on Zn(II) ions as the active metal in phosphate cleavage reactions. Zn(II) is a good Lewis acid, exchanges ligands quickly in solution, and is non-toxic.[31] This d^{10} transition metal is redox inactive and is unsusceptible to ligand field stabilization energy and can therefore adopt the coordination geometry that best suits the structural requirements of a given reaction. [31]

In the absence of an active site, or a metal-coordinating ligand, metal ion salts have been observed to catalyze the cleavage of phosphate diesters.[25, 31] However, cleavage does not approach the rates seen for natural enzymes, occurs without substrate isomerization, and does not involve the formation of pentacoordinate phosphorane intermediates.[32] Thus, the decomposition of RNA does not proceed step-wise as depicted in Scheme 1, but rather by a concerted mechanism as illustrated below in Scheme 2.

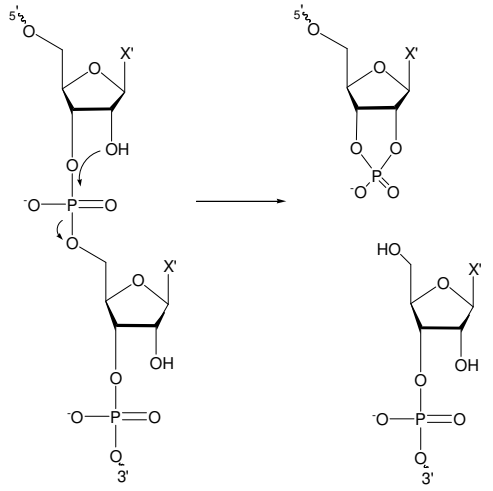

Scheme 2. The concerted transesterification of RNA, where X' = A, C, G, or U.

Additionally, substrate reactivity and the range of pH over which reactions may be followed are limited by the speciation of the metal ions and their solubility in solution. The development of metal-coordinating ligand complexes that eliminate these complications and that are capable of inducing rates of phosphate decomposition that approach those seen for natural enzymes and that better mimic the mechanism of phosphate cleavage mediated by enzymes has received much attention recently.[1b]

1.5 Mononuclear catalysis of DNA and DNA models

To compensate for the inherent stability of natural DNA, DNA models such as **2-4** are employed to test the catalytic effectiveness of synthetic metallo-organic complexes. The most commonly used model is bis *p*-nitrophenol phosphate (BNP, **3**) which is hydrolyzed in water with an estimated half-life of more than 1300 years at pH 7, 25 ^{o}C (k_{obs} = 1.6 x 10^{-11} s^{-1}).[33, 34]

In 1990, the hydrolysis of BNP catalyzed by a mononuclear Zn(II) complex was first explored by Trögler and de Rosch.[35] By following the initial rate of *p*-nitrophenoxide production at pH 7.0 and 75 ^{o}C, 1 mM of the Zn(II)-coordinated TREN (**9**) and Bpy (**10**) complexes achieved 2 and 53-fold rate accelerations over the background reaction towards the hydrolysis of BNP in 0.1 M $NaNO_3$. The strong binding of amines to transition metals, such as Zn(II), was further explored by Kimura and Koike[36] and nitrogen atom containing macrocycles were designed to catalyze the cleavage of BNP. Zn(II)-coordinated 1,4,7,10-tetraazacyclododecane ([12]aneN_4, **11**) and 1,5,9-triazacyclododecane ([12]aneN_3, **12**) complexes catalyzed the cleavage of BNP at pH 7, 35 ^{o}C (0.2 M $NaClO_4$) with pseudo-first order rate constants of 2.8 x 10^{-9} s^{-1} and

3.3×10^{-8} s^{-1}. Rate constants were determined using an initial slope method. The greater activity of the mononuclear Zn(II) complex of **12** is attributable to its ability to ionize a metal-bound water molecule at physiological pH. The suppressed activity of the tetradentate ligand was due to the saturation of the binding sites of the metal ion by ligand atoms.[33, 34] To capitalize on the effectiveness seen with the Zn(II) complex of **12** focus has since been paid on the design of tridentate ligands for phosphate cleavage.

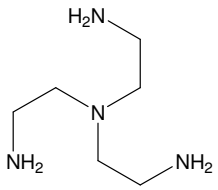

TREN, **9**

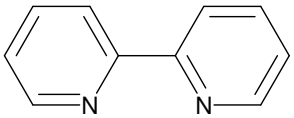

Bpy, **10**

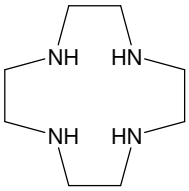

[12]aneN_4, **11**

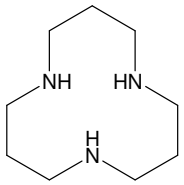

[12]aneN_3, **12**

A series tridentate ligands (**13**-**18**) were investigated by Tonellato, *et al.*[37] at 25 ^{o}C, pH 11.0 in CAPS buffer to investigate the effects of the nucleophilicity of a metal-coordinated water molecule on the rate of BNP hydrolysis. The absorption of *p*-nitrophenoxide was followed to 1% of substrate hydrolysis and pseudo-first order rate constants were determined from the slope of the absorbance vs time data and divided by the absorbance of *p*-nitrophenoxide and the concentration of BNP. The logarithms of the catalytic second order rate constants were plotted against the pK_a of the metal-bound water nucleophile to establish the correlation between the acidity of the coordinated water and the reactivity of the complex. The tripod ligands (**13**-**15**) offered larger rate enhancements over the linear ligand systems (**16-18**). For complexes which bound tightest to the substrate a greater reactivity was seen as was an increase in nucleophile acidity (ie. a decrease in nucleophile pKa). However, by enhancing the acidity of a

metal-bound water molecule its nucleophilicity is reduced. For the complexes examined, the reactivity of the complex had a greater impact on the rate of reaction over the lowered acidity of the nucleophile and the rate of reaction was enhanced by complexes which were able to strongly bind to the substrate and enhance its electrophilicity.

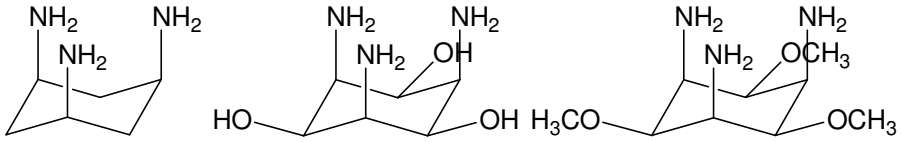

13 **14** **15**

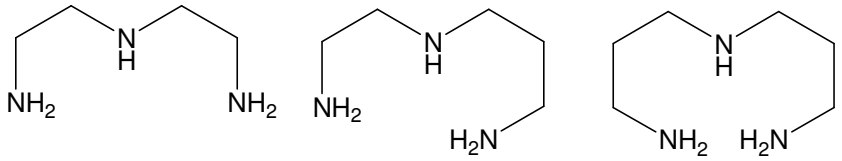

16 **17** **18**

Catalysis was seen by Ichikawa and co-workers[38] who examined the reactivity of a Zn(II) complex of a histidine-containing pseudopeptide ligand (3.6 mM) towards the hydrolysis of BNP (0.04 mM) at 50 ^{o}C, pH 6 to 9. The bell-shaped pH-k_{obs} profile maximized around pH 7 with a pseudo-first order rate constant of 1.1 x 10^{-5} s^{-1}. The Zn(II)-coordinated complex exerted a 36,000-fold rate enhancement over the background hydrolysis reaction. A pH titration of the complex suggested that the active species was a monohydroxo species (**19**, pK_a 6.1), however the accuracy of this identification is complicated by the possible deprotonation of the amino groups at this low pH.

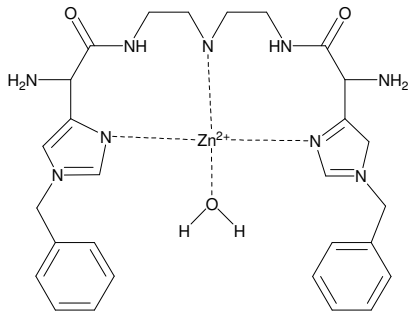

19

Metal ions coordinated to tridentate complexes offer the greatest enhancement of reactivity of BNP seen to date. These complexes offer free binding sites to coordinate substrates and nucleophiles and are also capable of reducing the acidity of the nucleophile such that its reactivity is optimized. However, the rate accelerations achieved with these systems does not equate to those seen with phosphoesterases and improvements to these systems are required. Complex activity can be enhanced by employing two or more metal ions that act cooperatively to cleave phosphates.

1.6 The role of metal ion cooperativity in phosphate cleaving reactions

The active sites of many enzymes rely on two or more metal ions for efficacious cleavage of phosphates.[1a] The intermetallic distance is approximately 4 Å within the active site of phosphoesterases[1b, 6, 17, 39] and ligands which achieve a similar metal ion constellation to that found naturally are desirable for cooperativity.[26] For a system to be considered to behave truly cooperatively the rate constant of the catalyzed reaction must be greater than the sum of the individual rate constants for the reaction catalyzed by individual mononuclear counterparts. Generally, multinuclear complexes that accelerate the rate of reaction by at least 10-fold relative to the mononuclear case may be regarded

to perform cooperatively. Metal ions that act truly cooperatively can effectively increase the Lewis acid catalysis exerted on the substrate, assist in the deprotonation of the attacking nucleophile, enhance the stabilization of the transition state, and assist in leaving group departure.[1d] The design of bimetallic small molecule catalysts has been exploited for the acceleration of phosphoryltransfer reactions.[37] $Zn(II)_2$, $Cu(II)_2$, and $Co(III)_2$ complexes have received much attention.

Many ligand systems have been designed and tested against the RNA model HPNPP with the intent of optimizing metal ion cooperativity and the rate of phosphate cleavage. Williams and co-workers[1d, 7, 40] have explored a *bis*[1,4,7-triazacyclononane:Co(III)($^{-}$OH)]$_2$ complex (**20**) which has an intermetallic distance of 2.9 Å. In water at 25 ^{o}C, 50 mM $NaClO_4$ a pH-k_{obs} profile was obtained for the transesterification and dissociation of HPNPP (0.2 mM). The curve at pH > 8 could be fit to a linear regression from which a second order rate constant of 430 $M^{-1}s^{-1}$ was determined for the hydroxide-catalyzed decomposition of HPNPP. At the corresponding hydroxide concentration a 4 x 10^5-fold rate acceleration over the background reaction was observed.

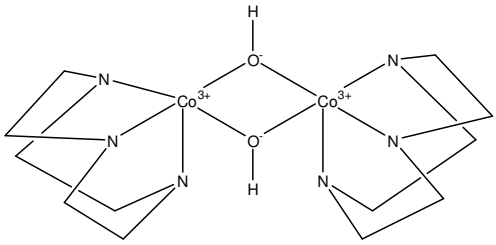

20

Dinuclear Zn(II) and Cu(II) complexes have also been witnessed to accelerate the cleavage of HPNPP (**1**a) with rates that are one to two orders of magnitude larger than their mononuclear counterparts. Of these complexes, those that are capable of bridging a nucleophilic hydroxide or alkoxide achieve rates that are up to 100-fold faster than those that are incapable of bridging a nucleophile.[21b, 41, 42] To date, multinuclear complexes have afforded the largest rate accelerations observed. While this phenomenon is not universal for every multinuclear complex studied, the design of complexes capable of binding two or more metal ions with a bridging nucleophile is desirable for phosphate ester cleavage.

1.7 Dinuclear catalysis of DNA and DNA models

Nature relies on the cooperative action of metal ions to cleave phosphate esters. Metal ions acting in concert enhance the Lewis acid catalysis exerted on substrates, promote the stabilization of the transition state, and assist in the departure of the leaving group.[1d] Cooperativity was first explored by Breslow and Chapman, Jr.[43] for the cleavage of phosphate esters and BNP in 1995. The rigidity of the linker between monometallic ligands was explored and it was found that the activity of the monometallic counterpart towards phosphate cleavage was not enhanced to any significant extent by dinuclear complexes with rigid spacers. Pseudo-first order rate constants were determined for the initial 5% of substrate hydrolysis from the initial slope of the absorbance vs time curve. At 55 ^{o}C, pH 8.36 in 20% DMSO the bimetallic Zn(II) complex of **21** (50 mM) was observed to catalyze BNP (50 mM) with a k_{obs} of 6.4 x 10^{-6} s^{-1}. This is only five times greater than that of its monometallic counterpart (**22**). The

enhanced activity of **21** with respect to **22** was later attributed to a hydrophobic interaction between the substrate aryl moiety and the aromatic spacer and was not due to cooperativity between metal centres.

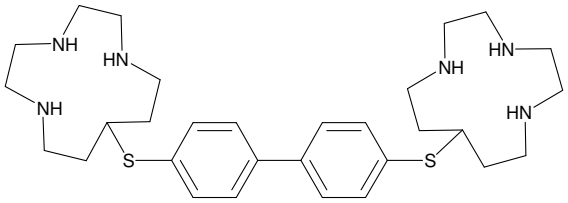

21

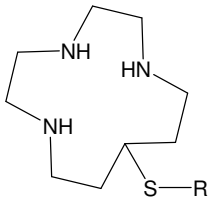

22

A dinuclear Zn(II) complex of [30]aneN_6O_4 (**23**) was soon after explored by Bencini, *et al.* [44] where each metal ion is coordinated to a triamine subunit and a hydroxide anion. The oxygen atoms are weakly involved in Zn(II) ion coordination. The reactivity of this dinuclear Zn(II) complex was accelerated by 10-fold over its mononuclear counterpart (**24**) towards the cleavage of BNP and can be considered to have achieved cooperativity between metal ions. This complex was considered to mimic the activity of alkaline phosphatase where the hydrolysis of a phosphate monoester proceeds through a phosphoseryl intermediate.

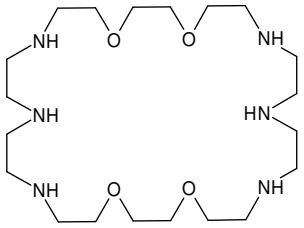

[30]aneN_6O_4, **23**

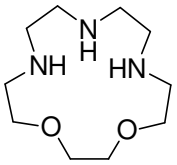

24

In 2000, Lippard[45] introduced a ligand containing pyridine rings, namely 2,7-bis[(2-pyridylethyl)aminomethyl]-1,8-naphthyridine (BPAN, **25**), and investigated it at

pH 7, 40 ^{o}C. The dinuclear Zn(II) complex of **25** accelerated the rate of BNP hydrolysis by 9,200-fold (k_{obs} = 3.7 x 10^{-7} s^{-1}) over the background base-promoted reaction. This correlates with a 1.8-fold reactivity increase over its monometallic counterpart and thus, the metal ions of this bimetallic system cannot be considered to behave cooperatively. Interestingly, despite the small binding constant for the interaction between the dinuclear Zn(II) complex of **25** and substrate (K_a = 86 M^{-1}) the initial rate of BNP hydrolysis was observed to diminish with increasing substrate concentration. This gave support for saturation behaviour between this complex and substrate. While the reactivity of this system was poor, its substrate binding behaviour stimulated others to incorporate pyridine moieties into bimetallic systems.

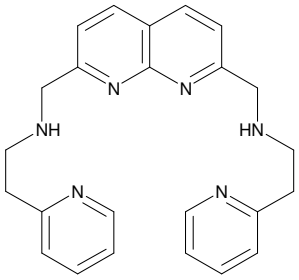

BPAN, **25**

Meyer *et al* [46] investigated ligands with a pyrazolate bridge connecting four pyridine rings (**26** and **27**). The intermetallic distance of complexing Zn(II) ions was tuned and respective pseudo-first order rate constants were determined from the initial rate of the hydrolysis of 2 mM of BNP by the catalyst at a narrow range of concentrations (0 to ~ 1.2 mM). The k_{obs} obtained were 2.6 x 10^{-7} and 8.5 x 10^{-7} s^{-1} for the dinuclear Zn(II) complexes of **26** and **27** in DMSO/HEPES buffer (1:1) at pH 8.26, 50 ^{o}C. The dependence of initial rates on substrate concentration indicated that these reactions were

first order in BNP. At higher concentrations of substrate, a reduction in the initial rate was observed suggesting saturation of both complexes over the range of catalyst and substrate concentrations used.

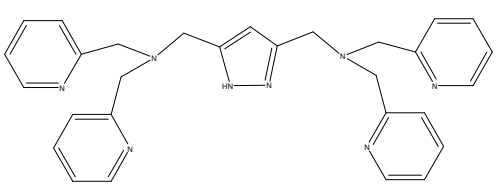

26

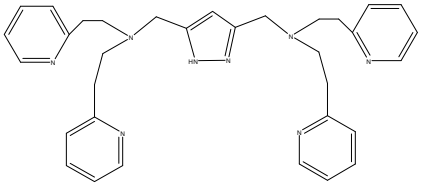

27

The reactivity of monometallic cyclam complexes was examined by Kaden, Vichard, and co-workers[47] and a pyrazolate bridge was incorporated into a diligand containing two [9]aneN_3 units (**28**). A pseudo-first order rate constant of 1.2 x 10^{-8} s^{-1} was obtained from the initial rate of BNP hydrolysis for the first 1-2% of the catalyzed reaction. Catalysis was unimpressive corresponding to only a 200-fold rate acceleration over the background reaction at pH 7, 25 ^{o}C. The complex exhibited a linear dependence on substrate at low BNP concentrations. At higher substrate concentrations, Michaelis-Menten behaviour was observed.

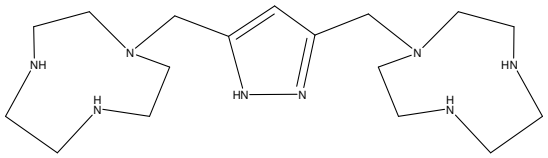

28

The flexibility of **28** was modified by Bencini and co-workers[48] who employed semi-rigid 2,2'-dimethylbipyridine-1,10-dimethylphenanthroline, and 2,3-dimethylquinoxaline spacers to link together two [9]aneN_3 units (**29-31**). The dinuclear Zn(II) complex of **31** was most active towards BNP hydrolysis at pH 7, 35 ^{o}C. Using an

initial slope method, 1 mM of the dinuclear Zn(II) complex of **31** cleaved BNP (1-10 mM) with a pseudo-first order rate constant of 3.9 x 10^{-8} s^{-1}. Different from the other dinuclear complexes described above, the active form of the dinuclear Zn(II) complex of **31** is the trihydroxo species where one hydroxide ion is bridged by the two metal centres and each metal coordinates an independent hydroxide ion. The binding of a third hydroxide ion is believed to weaken one of the μ-OH bridging bonds and to enhance its nucleophilicity. This five-coordinate system does not have a site available to bind the substrate and so it likely achieves BNP hydrolysis by functioning to deprotonate the nucleophile. The mono- and dihydroxo complexes are inactive as the metal-coordinated hydroxide ions bridge the metal centres and are unreactive nucleophiles.

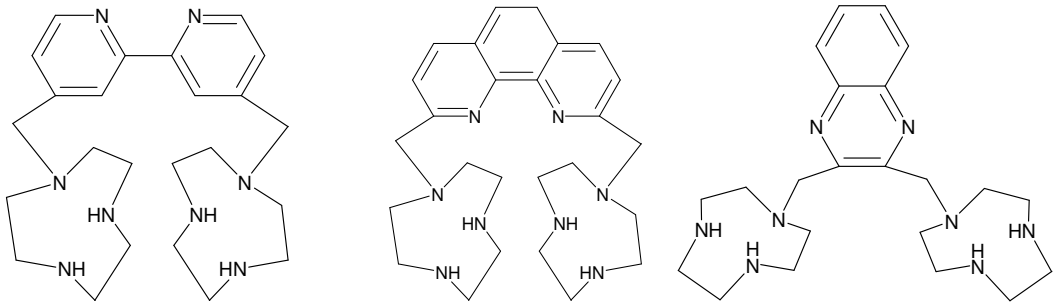

29 **30** **31**

The dinuclear Zn(II) complexes outlined above achieved less than impressive improvements to the rate of BNP hydrolysis over the background reaction. To boost the efficacy of synthetic complexes a new approach was needed. Strategies included functionalizing ligands with moieties that would enhance nucleophilicity, activate the substrate, and stabilize the transition state and/or the leaving group through hydrogen bond or electrostatic interactions.

A mononuclear ligand with an intramolecular nucleophile was developed by Kimura and co-workers[49] who attached a benzyl alcohol moiety to [12]aneN_4 (**32**). The transesterification of BNP occurred 125-fold faster than its hydrolysis promoted by the Zn(II) ion-coordinated [12]aneN_4. Bencini, Bianchi, Paoletti, *et al.*[50] appended a hydroxyethyl arm to their dinuclear Zn(II) complex of [30]aneN_6O_4 (**23**) and witnessed a similar trend in BNP transesterification activity; a seven-fold rate enhancement was observed with the addition of the intramolecular nucleophile. Hydrolysis of the transesterification product was not seen for both systems, and thus they are not truly catalytic.

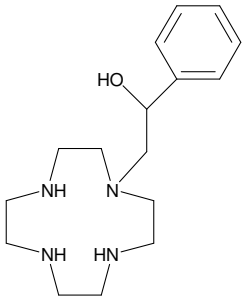

32

Attaching more than one nucleophilic unit to a bimetallic ligand was examined by Guo and co-workers[51] who designed a phenolate bridging ligand with two pyridylmethyl amine binding moieties and two hydroxylethyl arms (**33**). The alcohol moieties function as intramolecular nucleophiles towards the transesterification of BNP. The dinuclear Zn(II) complex of **33** is the only bimetallic ligand with a phenolate bridge that is capable of cleaving BNP. The pseudo-first order rate constants for the cleavage of 0.20 mM of BNP promoteded by the dinuclear Zn(II) complex of **33** at concentrations ranging from 0-0.05 mM were determined from the initial rates of the reaction up to 5% of substate

cleavage at pH 7.2 (50 mM Tris-HCl buffer), 50 ^{o}C. The obtained k_{obs} values were plotted as a function of complex concentration and a second order rate constant of 6.34 x 10^{-2} $M^{-1}s^{-1}$ was obtained for BNP transesterification. The complex accelerated the reaction by 2,500-fold over the background hydroxide-promoted reaction and saturation kinetics were observed for this system at higher substrate concentrations. This system is not truly catalytic and hydrolysis of the transesterification product was not observed.

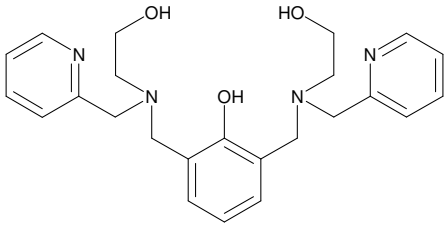

33

The reactivity of a ligand with variable functional groups has been explored and recently a monometallic Zn(II) complex with an internal nucleophile and two hydrogen bond-donating amino groups was reacted with BNP at pH 7, 25 ^{o}C.[52] The bis(pyridylmethyl)amine derivative (**34**) was able to hydrogen-bond to the substrate and enhance the stabilization of the transition state. The reactivity toward BNP cleavage was accelerated by almost one million-fold over the background reaction. As with the mono- and bimetallic complexes of **32** and **33**, the phosphorylated transesterification product was non-reactive and the system was not truly catalytic. In the absence of a hydroxylalkyl arm to act as an internal nucleophile the mononuclear Zn(II) complex of **35** was able to hydrolyze BNP catalytically and achieve a 230-fold reactivity increase over the background reaction. Initial rates methods, as described above, were used to monitor the cleavage of BNP catalyzed by the bimetallic complexes of **34** and **35**. The

contribution of both functional groups accomplished impressive rate accelerations and better mimic the mechanism of some natural enzymes, such as AP which invokes a Ser residue as an intermolecular nucleophile in the cleavage of phosphomonoesters and phosphodiesters.

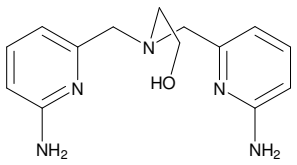

34

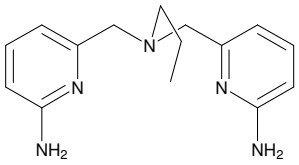

35

The reactivity of BNP makes this a desirable substrate for use in developing an understanding of DNA hydrolysis. However, results obtained with activated substrates can not be interpreted to parallel the reactivity of unactivated DNA towards cleavage. Methyl aryl phosphates (**4**) have an intrinsic stability that is a better mimic of DNA than BNP and these also have activated leaving groups which make them a practical model for studying the cleavage reaction. A series of methyl aryl phosphates (**4**a-h) have been recently studied by our group[53] and their rates of decomposition catalyzed by the dinuclear Zn(II) complex of 1,3-bis[N_1,N_1'-(1,5,9-triazacyclododecyl)]propane (([12]aneN_3)$_2$, **36**) in methanol achieved remarkable acceleration (4 x 10^{11}- to 3 x 10^{13}-fold) over the background methoxide-promoted reaction at $^{s}_{s}$pH 9.8, 25 ^{o}C. Interestingly, this complex was reported to be ineffective towards the binding of two metal ions and is only active as the mononuclear Zn(II) complex towards the hydrolysis of BNP in water.[54] Obviously, a medium effect is exerted by methanol which enhances the reactivity of this complex towards phosphate diester cleavage. This effect will be discussed later.

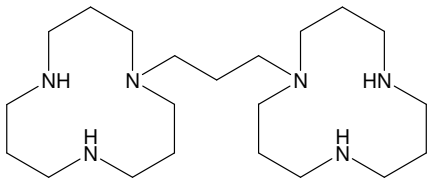

([12]aneN$_3$)$_2$, **36**

Dinuclear complexes coordinating Cu(II), Co(III), or Ln(III) have also been studied and found to give rates of phosphodiester hydrolysis that are generally higher than those observed with Zn(II).[1a] The enhanced reactivity of these complexes reflects the improved Lewis acidity of these other metals. These metals are not used in phosphoester cleavage and will not be the focus of this study. Synthetic systems with oligonucleotide conjugation, peptide linked macrocyclic ligands, and association with nanoparticles have also been designed and may be the future direction for the study of DNA and DNA model cleavage.[1a] This study will focus on the cleavage of highly stable DNA models catalyzed by ligands with two [12]aneN$_3$ Zn(II) ion-binding units linked by alkane spacers in methanol.

1.8 Mononuclear catalysis of RNA and RNA models

RNA is less resistant towards cleavage than DNA due to the presence of a ribose 2'-OH group that acts as an internal nucleophile. The modeling of RNA cleavage has most commonly been explored using the model substrate HPNPP, which has an UV-active *p*-nitrophenol leaving group moiety and displays high reactivity at ambient temperature. As 2-hydroxylpropyl aryl phosphates (**1**) are inherently more reactive than DNA and its models are towards hydrolysis, the investigation of these RNA models has been more actively pursued.[1a] The ambiguity surrounding the mechanism by which

metals catalyze the cleavage reaction and the existence of a putative phosphorane intermediate has been the focus of much attention. Monometallic systems have been explored in hopes of elucidating the unknown.

Two mechanisms have been proposed for the metal-catalyzed transesterification of RNA and its models.[1b] The first involves a general base catalyzed reaction in which a metal-bound hydroxide deprotonates the substrate 2'-OH group to generate the active intramolecular nucleophile (Figure 3A).[1b] The second proposed mechanism involves the coordination of the substrate 2'-OH moiety to a metal ion and a subsequent attack of the coordinated alkoxide due to its enhanced nucleophilicity (Figure 3B).[1b] Whether metal-ion catalyzed cleavage of RNA and its models involves the formation of a pentacoordinate phosphorane transition state or intermediate is dependent upon reaction conditions. This will be explored below.

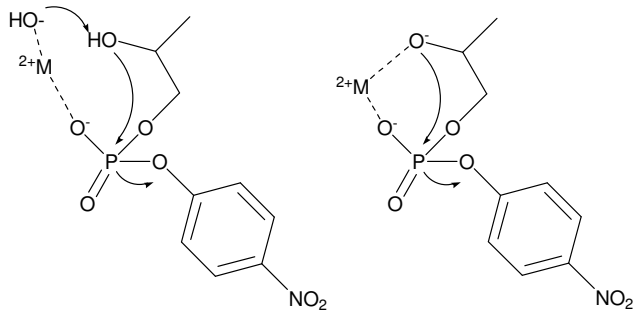

A **B**

Figure 3. The proposed metal-promoted cleavage of HPNPP (Reference 1b).

In 1965, RNA cleavage by free Zn(II) ions in solution was observed by Butzow and Eichorn.[55] It wasn't until over 20 years later that Breslow and co-workers[56] explored the effect of metal-coordinating ligands in the Zn(II)-ion catalyzed cleavage of

diribonucleotides and HPNPP. At pH 7 (10 mM Hepes buffer in water) and 37 ^{o}C a 24:1 imidazole/Zn(II) mixture (0.5 mM) resulted in a 850-fold rate enhancement for the cleavage of HPNPP (0.19 mM) over the background reaction (k_{obs} = 0.27 s^{-1}). Pseudo-first order rate constants were determined by monitoring the release of product phenol via UV/Vis methods. In the absence of imidazole the Zn(II)-ions afforded only a 150-fold acceleration. Similarly, for the cleavage of UpU the imidazole/Zn(II) mixture afforded a thousand-fold rate acceleration whereas Zn(II) alone mediated only a 32-fold reactivity increase over the background hydrolysis. The enhanced reactivity of these substrates is attributable to the Lewis acidity of the Zn(II)-ions and the role of imidazole as a base to deprotonate the substrate 2'-OH group. The intramolecular nucleophile generated has enhanced nucleophilicity over a metal-coordinated hydroxyl group leading to reactivity increases.

Monometallic complexes have since been designed and their activity towards HPNPP explored under physiological conditions. As with BNP, the most active complexes possessed ligands with three donor atoms. The tridentate Zn(II)-coordinating ligands [12]aneN_3 (**12**) (pH 7, 37 ^{o}C)[57] and **22** (R = CH_3, pH 8.36, 30 ^{o}C)[43] achieved 403- and 194-fold rate accelerations, respectively, over the background hydrolysis reaction of HPNPP.

Recent research efforts have employed di- and tri-metallic complexes to promote the cleavage of RNA and its models with rates that better resemble those achieved by enzymes.

1.9 Di- and trinuclear catalysis of RNA and RNA models

Enhancing the reactivity of monometallic systems towards the cleavage of RNA and RNA models was the inspiration behind exploiting the cooperativity between two or more complexed metal ions. Monometallic systems linked together by spacers which optimized the distance between metal centres and that were capable of enhancing the interaction between the substrate and ligand have been explored. As with the synthetic DNA cleaving systems macrocyclic ligands which are tridentate are optimal for phosphate cleaving activity. Within these complexes the metal ions are capable of binding the substrate and nucleophile and are also able to lower the pK_a of the metal-bound solvent and enhance its concentration at physiological pH.

A 4,4'-biphenyl spacer between two Zn(II)-coordinating macrocycles was noted by Breslow and Chapman, Jr.[43] to increase the π-stacking interactions between the aromatic linker and aromatic substituents. The dinuclear Zn(II) complex of **21** offered 1,072-fold and 39-fold rate acceleration towards the cleavage of HPNPP and UpU, respectively, over the background reactions. These rates are 5-fold more reactive than those seen with the respective monometallic counterpart and thus the Zn(II) ions of these bimetallic complexes cannot be concluded to act cooperatively.

A similar rate acceleration of a bimetallic complex over its monometallic complement has been observed with Lippard's BPAN complex (**25**), which cleaved HPNPP with 6.4-fold higher activity.[58] While this system was noncooperative between metal ions, the active dinuclear Zn(II) complex with a bridging hydroxide nucleophile afforded a 2,900-fold reactivity increase towards the cleavage of HPNPP over the

background reaction at pH 7, 25 °C. Komiyama and co-workers[59] have explored mono-, di-, and trinuclear ligand systems (**37-39**) with methyl pyridine groups and found that the tridentate ligand (**39**) offered three times the reactivity of the bimetallic complex (**38**) towards the cleavage of diribonucleotides at pH 7, 50 °C. Rate accelerations over the background reactions were not reported and support for cooperativity between metal ions of the bi- and trimetallic systems was not convincing.

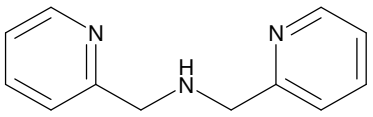

37

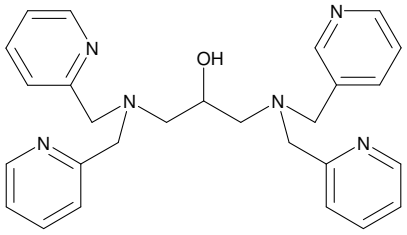

38

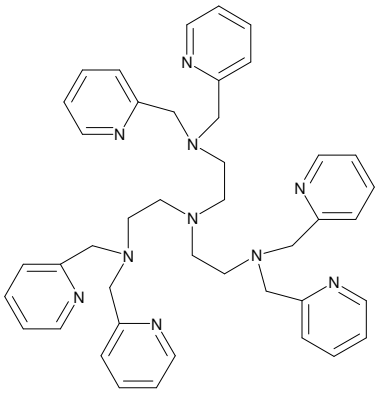

39

Calix[4]arene ligands with an upper rim substituted with one, two, or three 2,6-bis(aminomethyl)pyridine units (**40**) have been developed by Engbertsen, Reinhoudt, and co-workers[60] and the trimetallic system was regarded to be most active towards HPNPP hydrolysis. At pH 7, 25 °C in a 50% H_2O/CH_3CN solution it was 35 times more reactive than its monometallic counterpart and offered 32,000-fold rate acceleration over the

background reaction. This significant rate enhancement was attributed to the enhanced substrate-ligand interactions between the hydrophobic pocket of the calixarene scaffold and the *p*-nitrophenol moiety of the substrate and also the optimal intermetallic distance provided by the flexible bridge of the lower rim.[60(b)] This system was also active towards the hydrolysis of UpU, GpG, and ApA, although the reactivity of ApA was low. At pH 8, 50 ^{o}C in 35% EtOH/H_2O, the trinuclear Zn(II) complex was 8,600-fold more reactive towards the hydrolysis of UpU over the background reaction.[60(c)] The third metal was speculated to bind to the acidic N3 amine of uridine and enhance substrate to ligand complexation and thus enhance substrate reactivity.

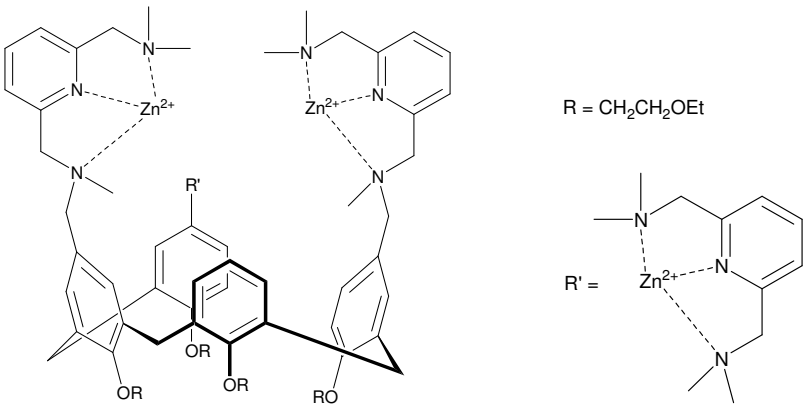

40

Calix[4]arene ligands appended with [12]aneN_3 units were inefficient HPNPP cleaving Zn(II)-coordinating complexes.[61] However, the di- and trinuclear Zn(II) complexes of [12]aneN_3 with spacers of variable lengths explored by Wang and Lönnberg[26] (**41-46**) were active towards the cleavage of some diribonucleotides. Interestingly, the dinuclear complexes offered sequence selectivity and cleaved ApU and UpA 100-fold faster than ApA and UpU. The trinuclear complex (**46**) cleaved UpU,

ApU, and UpA without selectivity and was less active than the bimetallic system towards ApA cleavage.

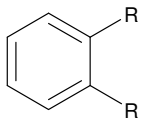

41

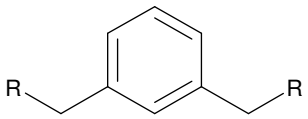

42

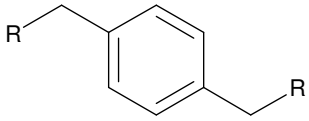

43

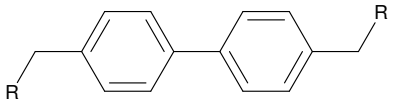

44

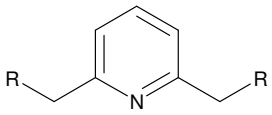

45

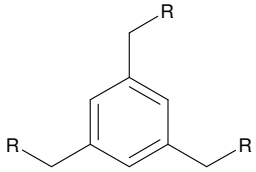

46

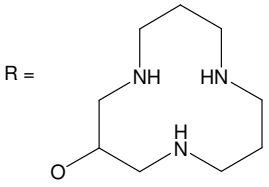

A bimetallic system comprised of two [9]aneN_3 units with a 2-propanol spacer (**47**) was studied by Richard, Morrow, *et al.*[42, 62] Remarkable acceleration that approached the reactivities of calixarene-based complexes was seen for the catalyzed cleavage of HPNPP (19,000-fold)[60(d)] and UpPNP (**48**, 60-fold)[60(e)] over the background reactions. The intermetallic distance of the two Zn(II) ions (3.66 Å) was optimal and promoted cooperativity between metal ions and double Lewis acid activation of the substrate. In addition, the bridging alkoxide keeps the metal centres at the correct distance preventing the formation of an inactive μ-hydroxo-bridged nucleophile and contributing to the efficaciousness of the system. This dinuclear Zn(II) complex is unique and was observed to more actively cleave UpU over the activated RNA

models.[60(c)] It was speculated that the stabilization of the transition state by way of interactions between the metal complex and the leaving group oxyanion are more strongly favoured for the more basic alkoxy leaving group of the nucleoside.[60(a)]

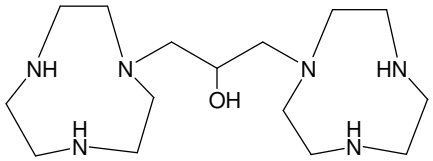

47

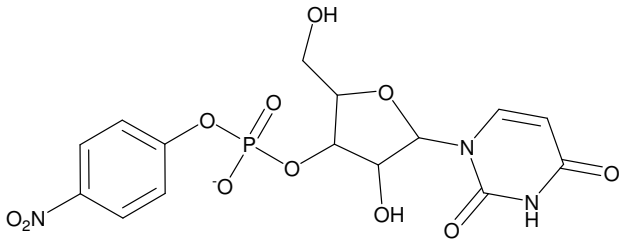

UpPNP, **48**

Bi- and trimetallic systems with more exotic spacers and complexes that are allosterically regulated by metal ions have been explored,[63, 64, 65, 66] however these complexes do not offer the significant rate enhancements seen with the dinuclear Zn(II) complex of **47** towards both unactivated substrates with alkoxy leaving groups and activated substrates with aryloxy leaving groups. Allosteric regulation is a phenomenon seen in natural systems and additional research on this category of small molecule catalysts further assist in the development of a system that cleaves natural substrates with rates comparable to those seen in Nature.

Our group has explored a dinuclear Zn(II) complex (**36**) and examined the reactivity of this complex towards RNA models (**1**a-g) in methanol at 25.0 ± 0.1 ^{o}C ,

$^{s}_{s}$pH 9.8 ± 0.1.[67] Accelerations of 10^{12}-fold relative to the background methoxide-promoted reactions were witnessed thus proving **36**:Zn(II)$_2$:($^{-}$OCH$_3$) to be the most efficacious system towards the cleavage of this series of RNA models.

The most active dinuclear complexes have not been applied to the cleavage of RNA nor have they been used to study the decomposition of DNA and its models. These two areas are interesting avenues worthy of exploration. The application of dinuclear Zn(II) complexes consisting of two [12]aneN$_3$ binding units and alkane bridges of variable length to the cleavage of activated and unactivated RNA models and diribonucleotides in methanol is the focus of this study.

1.10 The putative pentacoordinate phosphorane intermediate

In 1942, the isomerization of 2-phosphoglycerol to 1-phosphoglycerol was first observed and was the first reported acid-catalyzed rearrangement reaction where the rate of isomerization exceeded that of hydrolysis.[3b] Over a decade later, the acid-catalyzed hydrolysis of hydrogen ethylene phosphate was explored in ^{18}O-labeled water and heavy atom incorporation in the absence of hydrolysis was seen (Scheme 3).[3b] Similarly, the hydrolysis of methyl ethylene phosphate under acidic conditions was noted to yield 30% of the hydrolysis product without ring opening (Scheme 4).[68] Hydrolysis external to the ring was speculated to proceed through the formation of a trigonal bipyramidal phosphorane intermediate capable of Berry pseudorotation (Figure 4).[69]

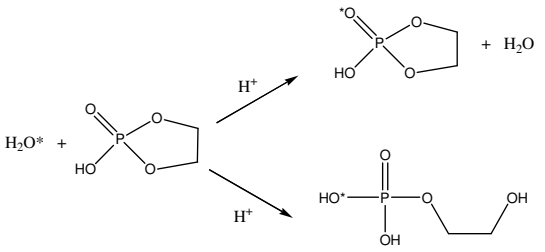

Scheme 3. The acid catalyzed cleavage of ethylene phosphate. (Reference 3b)

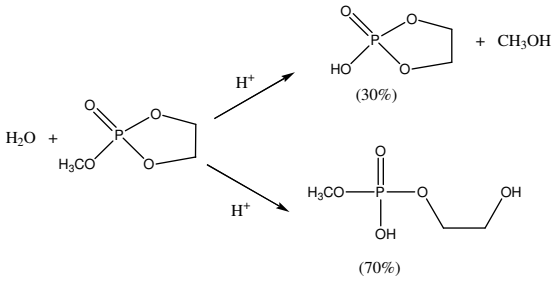

Scheme 4. The acid catalyzed hydrolysis of methyl ethylene phosphate. (Reference 68)

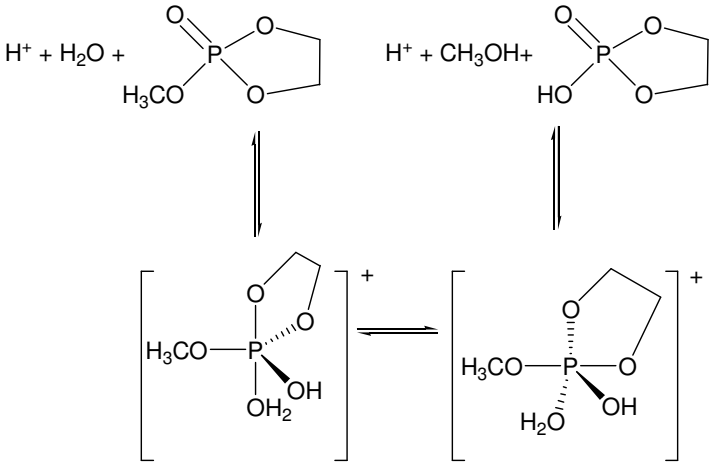

Figure 4. Berry pseudorotation of a trigonal bipyramidal phosphorane intermediate. (Reference 69)

Pseudorotation of pentacoordinate phosphoranes is an intramolecular process whereby the bonds in a trigonal bipyramidal molecule are distorted such that the molecule appears to have been rotated by 90^{o} about a fixed substituent (Figure 5). In

other words, two ligands in equatorial positions are exchanged for two in axial positions with an equatorial ligand held stationary as a pivot.[27]

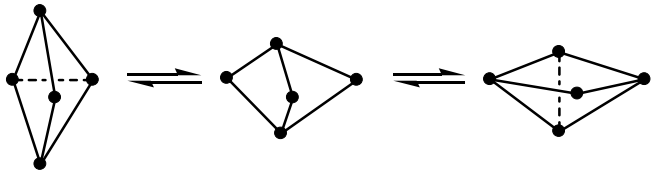

Figure 5. Pseudorotation of a trigonal bipyramidal molecule. (Reference 27)

The hydrolysis of phosphates involves the nucleophilic attack at a phosphorus centre in one of three ways. The first is classified as a dissociative pathway[70] in which a monomeric metaphosphate is intermediate and can become symmetrically solvated to give a racemic mixture of products. The second pathway is "in-line associative"[70] or a concerted replacement of the leaving group by an attacking nucleophile. The transition state is trigonal bipyramidal with the entering and leaving groups in apical positions. The product is inverted with respect to the starting phosphate. The third process can be termed an "adjacent associative"[70] and nucleophilic attack on phosphorus results in the formation of a pentacoordinate phosphorane intermediate which is capable of at least one Berry pseudorotation[71] before the expulsion of the leaving group from an apical position. Inversion or retention of configuration in the product is observed and product distribution is dependent upon the number of pseudorotations the intermediate experiences which is dependent upon reaction conditions.

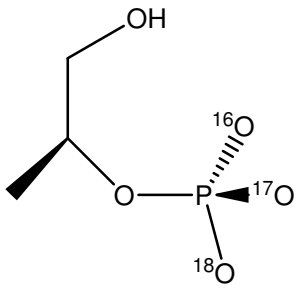

49

In the mid 1960's, Westheimer proposed a set of predictive rules governing the formation and breakdown of pentacoordinate phosphorane intermediates.[69] Pseudorotation was predicted to be under the following constraints: the alkyl groups must preferentially occupy equatorial positions and five-membered rings were linked through one equatorial and one axial position in the trigonal bipyramid.[69] In 1984, Knowles and co-workers[70] obtained the first evidence for pseudorotation in a reaction with a phosphoric monoester, 2-[(*R*)-^{16}O,^{17}O,^{18}O]phospho-(*S*)-propane-1,2-diol (**49**). It was observed that under acidic conditions (0.5 N $HClO_4$) 36% of the 1-phosphopropane-1,2-diol (**50**) formed from 2-phosphopropane-1,2-diol (**51**) came from the direct route without the formation of the cyclic phosphate intermediate (Scheme 5). The phospho group transfer occurred with retention of configuration at the phosphorus centre and proceeded through the pseudorotation of a pentacoordinate phosphorane intermediate as depicted in Scheme 6.

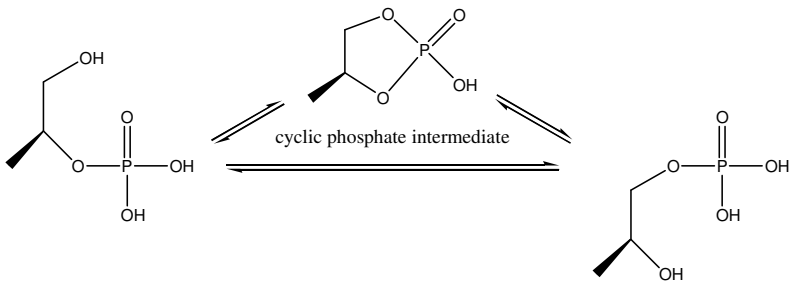

50 **51**

Scheme 5. The isomerization of 1-phospho-(S)-propane-1,2-diol (**50**) and 2-phospho-(S)-propane-1,2-diol (**51**).

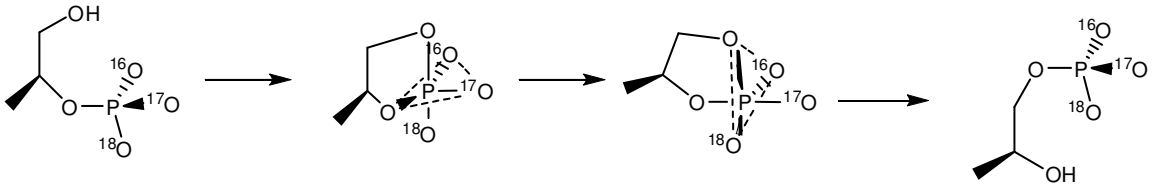

49

Scheme 6. The retention of configuration at the phosphorus centre of 2-phosphopropane-1,2-diol (**49**). (Reference 70)

The existence of phosphorane intermediates in reactions with phosphate diesters and triesters has been speculated and until only recently[72] the dianionic phosphorane intermediate was assumed to be kinetically indistinguishable from a phosphorane transition state as it did not exist long enough for most diffusion-controlled processes to occur, let alone protonation.[73, 74] Moreover, it was held that the lifetime of a dianionic phosphorane intermediate was too short to allow for pseudorotation in basic solution. The hydronium and hydroxide ion catalyzed reactions of a series of uridine 3'-phosphate esters was studied by Lönnberg and co-workers[74] in the late 1990's. Under acidic conditions, both the cleavage and isomerization products were seen, however in aqueous base only the cyclic phosphate was observed. In 2004, support for a phosphorane formed

under basic conditions was established when the isomerization of ApA and GpG was achieved by a dinuclear Ni(II) complex of **28** at pH 9.80.[75]

Hybrid density functional theory (DFT) methods performed on a series of pseudorotation reactions of oxyphosphoranes and of PF_5 by York *et al.*[27] examined the factors governing the lifetime of phosphorane intermediates.[75] Pseudorotation of phosphorane intermediates is governed by the nature of the acyclic and cyclic ligands around the phosphorus centre (apicophilicity), its protonation state, and its interaction with solvent molecules, metal ions, and the functional groups of coordinating catalyst complexes. With respect to the existence of a dianionic phosphorane intermediate, Taira and co-workers[76, 77] performed *ab initio* calculations which supported its stability in aqueous solution to be sufficient for it to be considered an intermediate. These theoretical calculations were supported experimentally in 2008 by Williams *et al.*[72] who observed isomerization products in the transesterification of UpU catalyzed by a dinuclear complex of **52**. These findings have been complemented by the findings herein reported in this study and together support the existence of dianionic phosphorane intermediates.

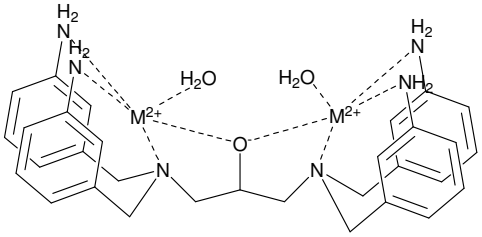

52

Chapter 2. Proposed research

To date, the catalyzed decomposition of DNA and RNA models afforded by synthetic mono- and dinuclear Zn(II) complexes has been less than spectacular. In fact, most of the complexes in the literature report reaction rates that are not much better than those reported for Zn(II):(¯OH) or hydroxide in water. Nature has proven that it is vital to employ enzymes to assist the achievement of rates of phosphate decomposition that are compliant with life processes on a biological timescale. Although a synthetic challenge, a complex which is capable of effectively mimicking the enzyme active site would appear to be a desirable path in promoting efficient phosphate cleavage reaction rates. While many of the dinuclear complexes reported do not offer much rate enhancement over their mononuclear counterparts, cooperativity between metal centres is crucial to the functioning of many enzymes. Unfortunately, designing ligands with multiple metal binding sites adds to the hydrophobic bulk of the ligand and results in solubility problems in water. Often, phosphate cleavage achieved using bulky multinuclear complexes is examined in a mixture of water and an organic solvent, such as DMSO, acetonitrile, or alcohols. Reactions performed in DMSO are unfavorable as this solvent has a high affinity towards binding metal ions in solution. Acetonitrile also less resembles the actual environment of an enzyme as this solvent is not hydrogen bonding. However, the active site of an enzyme is hydrophobic and using a solvent that is less polar than water and one that has hydrogen bonding capability may effectively model an enzymatic active site. The use of such a solvent, such as an alcohol, may assist synthetic catalysts to

obtain rates of phosphate decomposition that would resemble those obtained naturally by enzymes.

2.1 Hydrophobic nature of the enzyme active site

The mechanistic information achieved using synthetic metal complexes and DNA and RNA model phosphate diesters may provide insight into the workings of hydrolytic enzymes.[78] While phosphate ester cleavage is biologically a hydrolytic process, to better mimic the nature of an enzyme active site a reduced polarity medium, such as methanol, can be employed. The selection of this medium is based upon the belief that "active sites of enzymes are nonaqueous, and the effective dielectric constants resemble those in organic solvents rather than that in water."[79] A medium of low polarity confers several advantages. First, the solvation of charges is reduced by a solvent with a depressed dielectric constant (ε is 31.5 for methanol and 78 for water),[80] and thus the electrostatic forces between charged species are enhanced. This can influence the extent of interaction between a negatively charged substrate, such as a monoanionic phosphodiester, and positively charged residues such as metal ions. Substituting an aqueous medium for one with lower polarity also increases the pH range over which metal-catalyzed phosphoryl transfer reactions can be studied. Under basic conditions many transition metal complexes precipitate from aqueous solution.

These advantages prompted our study of the cleavage of DNA and RNA models and diribonucleotides by small-molecule Zn(II) complexes in methanol. The initial cleavage of the phosphate ester bonds in RNA and RNA models is mediated by an

intramolecular transesterification, which is achieved through the participation of a 2'-hydroxyl group; this event occurs regardless of the solvent medium.[81]

For the designation of pH in non-aqueous solvents we use the forms recommended by the IUPAC, *Compendium of Analytical Nomenclature. Definitive Rules 1997* 3rd ed., Blackwell, Oxford, U. K. 1998. If one calibrates the measuring electrode with aqueous buffers and then measures the pH of an aqueous buffer solution, the term ${}^{w}_{w}\mathrm{pH}$ is used; if the electrode is calibrated in water and the 'pH' of the neat buffered methanol solution then measured, the term ${}^{s}_{w}\mathrm{pH}$ is used; and if the electrode is calibrated in the same solvent that the 'pH' reading is made, then the term ${}^{s}_{s}\mathrm{pH}$ is used. In practice, one standardizes the electrode in water, takes the meter reading in methanol, and subtracts a correction factor of -2.24 from the reading to obtain the ${}^{s}_{s}\mathrm{pH}$. Since the autoprotolysis constant of methanol is $10^{-16.77}$, neutral ${}^{s}_{s}\mathrm{pH}$ is 8.4.

2.2 The cleavage of highly stable phosphate diesters by dinuclear Zn(II) complexes in methanol

The design of a metallic system capable of efficaciously cleaving phosphate diesters is not trivial. Much work has been done to highlight the factors contributing to efficient catalysis. The rate accelerations seen with systems coordinating two or more metal ions capable of acting cooperatively makes the complexation of multiple metal ions mandatory. The flexibility of the spacer used to link metal-binding units plays a fundamental role in achieving optimal intermetallic distances that resemble those seen in natural enzymes. Additionally, substrate binding and stabilizing interactions may also be

mediated by the spacer and its design may be crucial to designing better mimics of the activity of natural phosphodiesterases. The design of the metal-binding moiety of the ligand is essential and tridentate ligands are optimal.

The literature available for the background hydrolysis and metal-catalyzed cleavage of DNA and RNA models is extensive. The results reported for the cleavage of DNA models are much less impressive than the factors of rate acceleration reported for the cleavage of RNA models. At physiological pH, the rate accelerations recorded for catalyzed BNP cleavage are on the order of 1,000 to 10,000-fold and recently little improvement has been made.[1a] Perhaps not so surprisingly, the majority of studies have been executed on either DNA or RNA models, but rarely both. Either the catalytic systems employed to accelerate solvolysis are active towards one class of phosphodiester and not the other, or quite simply the study has not been applied to both classes.[1b]

The focus of the research reported herein is on the use of synthetic agents to cleave DNA and RNA models and diribonucleotides. The activity of a dinuclear Zn(II) complex of **53** towards the cleavage of RNA models, namely 2-hydroxylpropyl aryl phosphates (**1**a-g), were studied in methanol (Chapter 3). The remarkable decomposition of the series of RNA models studied catalyzed by this dinuclear Zn(II) complex stimulated an interest in applying this complex and the dinuclear Zn(II) complex of **36** to the transesterification of diribonucleotides, uridyl(3'→5')uridine (UpU) and adenylyl(3'→5')cytidine (ApC) (Chapter 4). Additionally, the reactivity of these diribonucleotides was cursorily explored using Zn(II) ions in ethanol. Remarkable catalysis towards the cleavage of DNA and RNA models had been achieved by our group

using the dinuclear Zn(II) complex of **36** in methanol.[53, 67] This finding made this bimetallic system a suitable candidate for cleaving the more resilient P-O bonds of highly stable RNA and DNA models such as 2-hydroxylpropyl methyl phosphate (**54**), its cyclic analog (Chapter 5), and dimethyl phosphate (**2**) (Chapter 6). All reactions were studied in CH_3OH and/or CD_3OD.

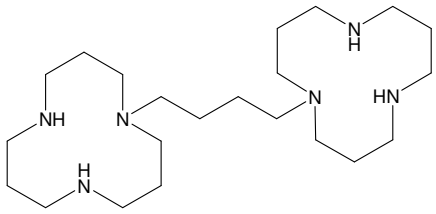

53

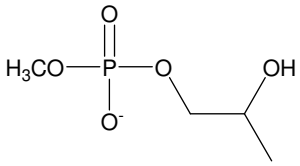

54

Chapter 3. Cleavage of a series of RNA models by a dinuclear Zn(II) complex 53:Zn(II)$_2$:($^-$OCH$_3$) in methanol

The cyclization of a series of 2-hydroxylpropyl aryl phosphates (**1**a-g) catalyzed by a dinuclear Zn(II) complex of **53** was studied in methanol at 25.0 ± 0.1^{o}C, ^s_spH 9.47 ± 0.17 (Scheme 7). The reactivity of these substrates in the presence of a structurally related dinuclear Zn(II) complex (**36**:Zn(II)$_2$:($^-$OCH$_3$)) has been examined previously by our group in methanol. Coordination of the phosphodiester to **36** occurs through a single metal ion which is followed by a rearrangement step and double activation of **1** as depicted in Scheme 8. It is reasonable to assume that coordination of substrate to the dinuclear Zn(II) complex of **53** occurs through the same mechanism as ligands **53** and **36** differ structurally by only one methylene unit within the spacer. The chemical step for both the **53**:Zn(II)$_2$:($^-$OCH$_3$)- and **36**:Zn(II)$_2$:($^-$OCH$_3$)-catalyzed decomposition of substrate occurred with a release of product phenol which was monitored by UV/Vis methods.[67] The catalyzed reactions had a progressive change in the observed kinetics from Michaelis-Menten saturation kinetics for the substrates with poor leaving groups (**1**e-g) to second order kinetics (linear in **53**:Zn(II)$_2$:($^-$OCH$_3$)) for the substrates with better leaving groups (**1**a-d). To determine the amount of charge development in the rate determining transition state a Brønsted relationship according to $k_2 = 10^{(\beta lg \cdot {}^s_s pKa + C)}$ was plotted for **1**a-g and fitting the data to a linear regression gives β_{lg} = (-0.32 ± 0.06).

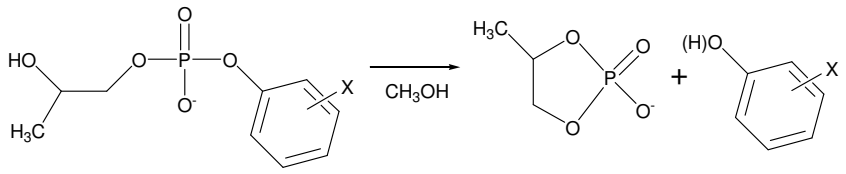

1 (a) X = 4-nitro
(b) X = 3-methyl, 4-nitro
(c) X = 3-nitro
(d) X = 4-chloro
(e) X = 3-methoxy
(f) X = H
(g) X = 4-methoxy

Scheme 7. The cyclization of a series of 2-hydroxylpropyl aryl phosphates (**1**a-g) catalyzed by **53**:$Zn(II)_2$:($^-OCH_3$) in methanol.

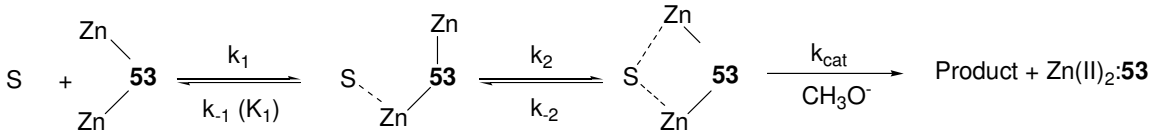

Scheme 8. The proposed coordination of a phosphodiester to the dinuclear Zn(II) complex of **53** based upon earlier findings of the **36**:$Zn(II)_2$:($^-OCH_3$)-catalyzed decomposition of substrates **1**a-g.[67] The corresponding rate constants are also given. S = phosphodiester substrate, charges omitted for simplicity. (Reference 67)

3.1 Experimental

3.1.1 Materials

Methanol (99.8% anhydrous), sodium methoxide (0.50 M solution in methanol), zinc trifluoromethanesulfonate, and ammonium triflouromethanesulfonate (99%) were obtained from Aldrich and used without further purification. $HClO_4$ (70% aqueous solution, titrated to be 11.40 M) was used as supplied from Acros Organics. Paraoxon (99.5%) was supplied by Chem Service and used as supplied. Methanol-d4 (D, 99.8%) was used as received from Cambridge Isotope Laboratories, Inc. The sodium salts of all

the 2-hydroxylpropyl aryl phosphates (**1**a-g) were prepared by Tony Liu by a procedure[82] modified from that reported prior.[83] 1,3-Bis[N_1,N_1'-(1,5,9-triazacyclododecyl)]butane (**53**) was prepared by Chaomin Liu from a procedure reported previously.[84] The lithium salts of the methyl aryl phosphates (**4**f and **4**g) were prepared by Tony Liu in accordance with a known procedure[85] and converted to their corresponding acids as previously published.[53]

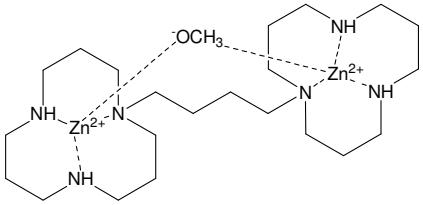

53:$Zn(II)_2$:($^-OCH_3$)

Stock solutions of $NaOCH_3$, **53**, $Zn(CF_3SO_3)_2$, $HClO_4$, $NH_4(CF_3SO_3)$, and paraoxon (**55**) were independently prepared to 50 mM in anhydrous methanol. Stock solutions of phosphates **1**a-g, **4**f, and **4**g were prepared at various concentrations in anhydrous methanol and stored at ~ 4 ^oC.

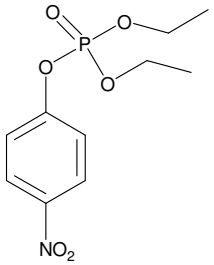

55

3.1.2 Methods

Anhydrous methanol was used as received and found to contain 16 ± 1 mM H_2O.[67]

The stopped-flow kinetic experiments were performed using an Applied Photophysics SX-17MV reaction analyzer thermostated at 25.0 ± 0.1°C with a 0.2 cm path length. The ${}^{s}_{s}$pH values for the stopped-flow kinetic experiments were found to be within 9.47 ± 0.17 at the **53**:$Zn(II)_2$:($^{-}OCH_3$) and phosphate diester concentrations employed in methanol and were determined by subtracting a corrective constant of –2.24 from the readings obtained using a combination glass electrode (Radiometer model # XC100-111-120-161) calibrated with certified standard aqueous buffers (pH = 4.00 and 10.00) as described in previous papers.[86] The autoprotolysis constant of methanol was taken to be $10^{-16.77}$ M^2.[87] The use of buffers to control ${}^{s}_{s}$pH was found to inhibit the catalytic activity of **36**:$Zn(II)_2$:($^{-}OCH_3$), likely due to associated counterions binding to the catalyst,[67] and so was avoided. The first and second macroscopic ${}^{s}_{s}pK_a$ values for **53**:$Zn(II)_2$:($HOCH_3$) and **53**:$Zn(II)_2$:($HOCH_3$)($^{-}OCH_3$) were determined to be 9.67 ± 0.01 and 10.14 ± 0.01 from duplicate measurements of the ${}^{s}_{s}$pH at half neutralization, where the [**53**:$Zn(II)_2$:($^{-}OCH_3$)]/[**53**:$Zn(II)_2$:($HOCH_3$)] or [**53**:$Zn(II)_2$:($^{-}OCH_3)_2$]/[**53**:$Zn(II)_2$:($^{-}OCH_3$)] ratios were 1.0 as depicted in Scheme 9. The half neutralization involved treating a 1.0 mM methanol solution of **53**:$Zn(II)_2$:($^{-}OCH_3$), prepared as described in the stopped-flow kinetics in methanol section below, with ½ eq. of $HClO_4$ or $NaOCH_3$ and measuring the ${}^{s}_{s}$pH.

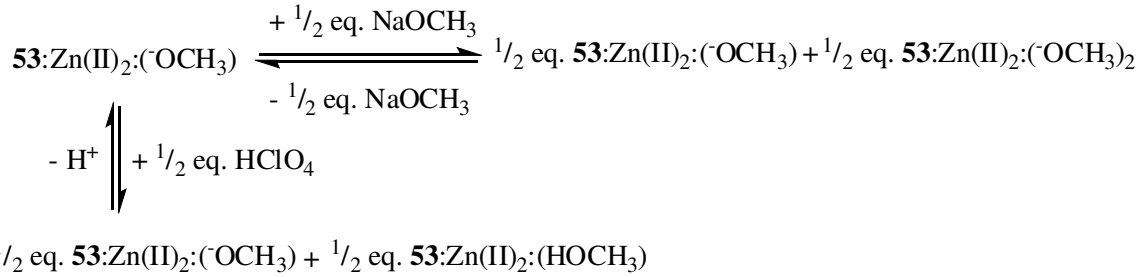

Scheme 9. The first and second macroscopic ${}^{s}_{s}pK_a$ values for **53**:$Zn(II)_2$:($HOCH_3$) and **53**:$Zn(II)_2$:($^{-}OCH_3$).

A triflate inhibition correction factor for **53**:$Zn(II)_2$:($^{-}OCH_3$) was established to determine [**53**:$Zn(II)_2$:($^{-}OCH_3$)]$_{free}$ using a Cary 100 UV-visible spectrophotometer thermostated at 25.0 ± 0.1°C with a 1.0 cm path length. The reduction in the catalytic activity of the **53**:$Zn(II)_2$:($^{-}OCH_3$) complex (0.50 mM) towards paraoxon (**55**, 0.05 mM) was monitored in the presence of increasing amounts of ammonium triflate ($0 < [NH_4^+$ ($^{-}$OTf)] < 6.0 mM) through the rate of appearance of the phenol product at 320 nm. Final triflate ion concentrations ranged from 2.0 - 8.0 mM, taking into account the four triflate counterions associated with the zinc triflate consumed by the catalyst complex.

The ${}^{s}_{s}pK_a$ values of leaving group phenols of **1**a, **1**c, **1**d, **1**f, and **1**g were determined in previous work in methanol.[88] These values were plotted against the known pK_a values of the corresponding phenols in water; the relationship fit a linear regression which can be expressed as ${}^{s}_{s}pK_a^{MeOH} = (1.09 \pm 0.06)pK_a^{HOH} + (3.40 \pm 0.50)$.[67] Using this expression, the ${}^{s}_{s}pK_a$ values of the leaving group phenols of **1**b and **1**e were interpolated.

The rates of the methoxide-promoted cyclization of substrates **1**a-g have been previously determined by our group (Appendix I, Table 1S).[67]

3.1.3 Stopped-flow kinetics in methanol

Dinuclear Zn(II) complexes were prepared in duplicate at 0.4 < [**53**:$Zn(II)_2$:($^-OCH_3$)] < 2.0 mM in anhydrous methanol at ambient temperature by sequential addition of aliquots of stock solutions of $NaOCH_3$, **53**, and $Zn(CF_3SO_3)_2$ such that the relative ratios were 1:1:2. This order of addition is essential for the formation of the catalyst complex, which takes approximately 25 minutes in methanol. The **53**:$Zn(II)_2$:($^-OCH_3$) solutions in methanol were loaded into one syringe of the stopped-flow reaction analyzer and 0.10 mM solutions of **1**a-g in methanol were loaded into the other syringe such that the final concentrations reaching the detector were 0.2 < [**53**:$Zn(II)_2$:($^-OCH_3$)] < 1.0 mM and [**1**a-g] = 0.05 mM. Two kinetic runs were recorded for each catalyst concentration and average k_{obs} values were determined for the appearance of phenol product and plotted against [**53**:$Zn(II)_2$:($^-OCH_3$)]$_{free}$. The rate of change in absorbance was followed at the λ_{max} for the appearance of product phenol: **1**a, 320nm; **1**b, 323 nm; **1**c, 340 nm; **1**d, 287 nm; **1**e, 281 nm; **1**f, 280 nm; **1**g, 295 nm.[67]

The amount of time required to reach maximal catalytic activity and the stability of the **53**:$Zn(II)_2$:($^-OCH_3$) catalyst over time in methanol solution were determined by examining the rate constants for the transesterification of **1**a at ^s_spH 9.47 ± 0.17, 25.0 ± 0.1°C. The **53**:$Zn(II)_2$:($^-OCH_3$) complex (1.0 mM) was allowed to sit at ambient temperature in a sealed vial and the observed first-order rate constants for the catalyzed methanolysis of **1**a (0.05mM) were determined at various times over 75 hours from the rate of appearance of product phenol at 320nm. The rate constants for the reaction were then plotted as a function of time and from which the time required for the complex to

reach maximal catalytic activity and the kinetic stability constant (k_s) for the active **53**:$Zn(II)_2$:($^-OCH_3$) catalyst could be determined.

The base dependence of the **53**:$Zn(II)_2$ catalyzed cyclization of **1**e was determined by monitoring the rate of production of product phenol as a function of [$NaOCH_3$]. Varied amounts of $HClO_4$ or $NaOCH_3$ were added to the vial containing **1**e (0.10 mM) such that when mixed with **53**:$Zn(II)_2$:($^-OCH_3$) (1.0 mM) the final concentration of the complex was 0.50 mM, that of **1**e was 0.05 mM, and the [CH_3O^-]/[**53**:$Zn(II)_2$] ratio varied from 0 to 2.0.

Phosphate inhibition constants were independently determined for the **53**:$Zn(II)_2$:($^-OCH_3$) (0.50 mM) catalyzed cyclization of **1**a (0.05 mM) in the presence of increasing amounts of slow reacting phosphates **4**f or **4**g. Varied amounts of **4**f or **4**g were added to the vial containing **1**a (0.10 mM) such that when mixed with **53**:$Zn(II)_2$: ($^-OCH_3$) (1.0 mM) the final concentration of the catalyst complex was 0.50 mM, that of **1**a was 0.05 mM, and 0 < [**4**f or **4**g] < 0.5 mM.

3.2 Results

3.2.1 Methoxide promoted cyclization of **1**a-g.

The extent of rate acceleration afforded by **53**:$Zn(II)_2$:($^-OCH_3$) for the cleavage of phosphodiesters **1**a-g was determined by comparing the rates of catalyzed cleavage to the background, methoxide-promoted reactions. The second order rate constants for the base-promoted methanolysis of the substrates (**1**a-g) were determined in previous work from this group (Appendix I, Table 1S).[67] A Brønsted plot of the log k_2^{-OMe} vs $^{s}_{s}pK_a$ fit a

linear regression of log k_2^{-OMe} = (-0.72 ± 0.08) $^{s}_{s}pK_a$ + (5.36 ± 1.08), r^2 = 0.939 (Appendix I, Figure 1S).[67]

3.2.2 Cyclization reaction of 1a-g promoted by 53:Zn(II)$_2$:($^-$OCH$_3$) in methanol.

The stability of **53**:Zn(II)$_2$:($^-$OCH$_3$) as a function of time was examined to maximize catalyst activity and minimize the depression of observed rate constants due to complex decomposition as a function of time (Figure 6). Maximal activity was achieved when the complex was allotted 25 minutes for formation since the rate constant for the catalyzed decomposition of **1**a is maximized when the catalyst is allowed this amount of time for formation prior to the introduction of substrate. A fit of the observed catalytic first order rate constant (k_{obs}) for promoting the cleavage of **1**a vs time reveals a decrease in activity that can be fit to a first order decay, giving a kinetic stability constant (k_s) of (1.26 ± 0.10) x 10^{-5} s^{-1} ($t_{1/2}$ of 15.3 h). The obtainment of observed rate constants for the **53**:Zn(II)$_2$:($^-$OCH$_3$)-catalyzed decomposition of substrates **1**a-g over the concentration range of catalyst investigated took no longer than 60 minutes for each substrate. Thus, the catalyst can be assumed to retain its level of maximal activity during the completion of the independent experiments and a correction for the decomposition of the catalyst over time is not required.

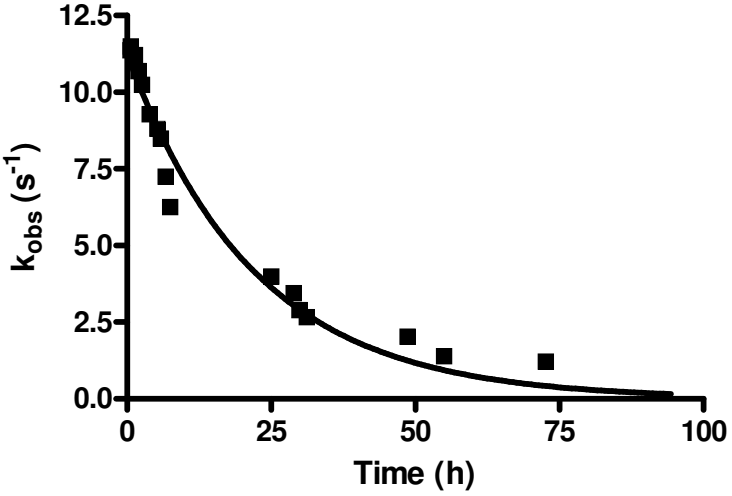

Figure 6. Plot of the observed first order rate constants for the methanolysis of 0.05 mM **1**a catalyzed by 0.5 mM [**53**:$Zn(II)_2$:($^-OCH_3$)]$_{total}$ (allotted 25 minutes for formation) as a function of time determined from the rate of appearance of product phenol at 320nm, ^s_spH 9.47 ± 0.17, and 25.0 ± 0.1°C. Fitting of the data to a first-order exponential decay equation ($k_{obs}(t) = k_{obs}(0)e^{-ks*t} + A$, where at A is the plateau and is assumed to be 0) gives a stability constant, k_s, of (1.26 ± 0.10) x 10^{-5} s^{-1} ($t_{1/2}$ = 5.52 x 10^4 s) for **53**:$Zn(II)_2$:($^-OCH_3$), r^2 = 0.970.

Upon first inspection, plots of [**53**:$Zn(II)_2$:($^-OCH_3$)] vs k_{obs} showed obvious downward curvature for substrates **1**e-g. To distinguish between this being an effect of saturation substrate binding or inhibitory binding of $^-$OTf an independent experiment was performed. The quantitative effect of triflate ions on the activity of the catalyst was determined by monitoring the catalyzed methanolysis of a weak binding substrate **55**. The activity of **53**:$Zn(II)_2$:($^-OCH_3$) towards the cleavage of **55** was observed to decrease with the addition of increasing amounts of NH_4^+($^-$OTf) (Figure 7). The suppressed observed rate constants were plotted as a function of [NH_4^+($^-$OTf)] and fit to a one-site binding model given in Eq. (1):[67]

(1) $k_{obs} = k_{cat}^{max}K_{inhib}/([NH_4^+(^-OTf)] + K_{inhib})$

where an inhibition constant (K_{inhib}) of 7.20 ± 0.88 mM was determined. This constant

can then be used to determine the amount of free catalyst in solution and used to correct the kinetic data for the catalyzed methanolyses of substrates **1**a-g.

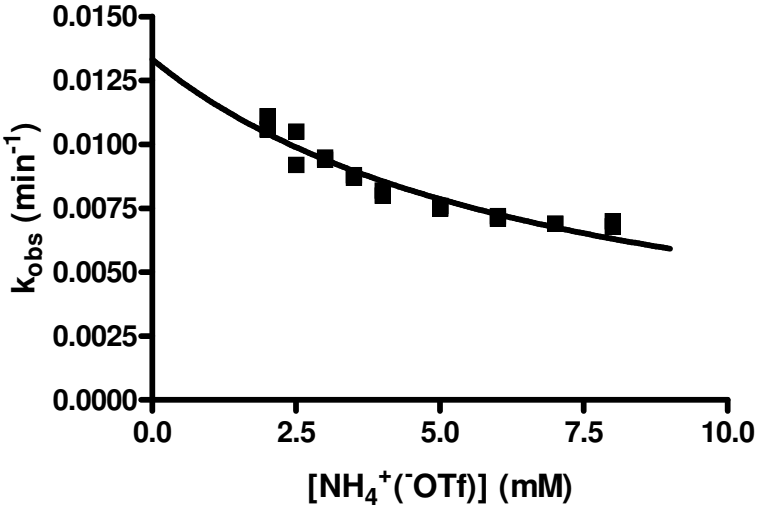

Figure 7. Plot of the observed first order rate constants for the methanolysis of **55** (0.05 mM) catalyzed by [**53**:$Zn(II)_2$:($^-OCH_3$)]$_{total}$ (0.50 mM) as a function of increasing amounts of [$NH_4^+(^-OTf)$] at 25.0 ± 0.1°C. Fitting of the data to the inhibition Eq. (1) gives a triflate ion inhibition constant, K_{inhib}, of 7.20 ± 0.88 mM for **53**:$Zn(II)_2$:($^-OCH_3$), $r^2 = 0.914$.

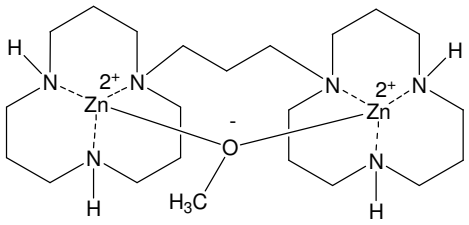

36:$Zn(II)_2$:($^-OCH_3$)

It should be noted that the K_{inhib} observed for **53**:$Zn(II)_2$:($^-OCH_3$) is significantly different from that seen for the structurally analogous complex **36**:$Zn(II)_2$:($^-OCH_3$) (14.9 mM).[67] Since the maximum [**53**:$Zn(II)_2$:($^-OCH_3$)] achievable in methanol is ~ 2.5 mM, the inhibition constant has a significant effect on reducing the [**53**:$Zn(II)_2$:($^-OCH_3$)]$_{free}$ over the range of concentrations studied. The low solubility of the complex taken in combination with the elevated K_{inhib} makes the examinable catalyst concentration range

narrow and makes determination of saturation kinetics for the faster reacting substrates (**1**a-d) more difficult. Applying the correction for triflate inhibition, saturation kinetics were not observed for substrates **1**a-c, and arguably **1**d. The plots of k_{obs} vs [**53**:$Zn(II)_2$:($^{-}OCH_3$)]$_{free}$ were linear for these faster reacting substrates. Shown in Figure 8 is a plot of k_{obs} vs [**53**:$Zn(II)_2$:($^{-}OCH_3$)]$_{free}$ for the catalyzed decomposition of substrate **1**a. Application of the triflate inhibition constant to the data produces a fit that is linear and no longer depicts curvature over the concentration range of **53**:$Zn(II)_2$:($^{-}OCH_3$) examined. Fitting the k_{obs} vs [**53**:$Zn(II)_2$:($^{-}OCH_3$)]$_{free}$ data to a linear regression was achieved for substrates **1**b and **1**c (Appendix I, Figures 1S and 2S).

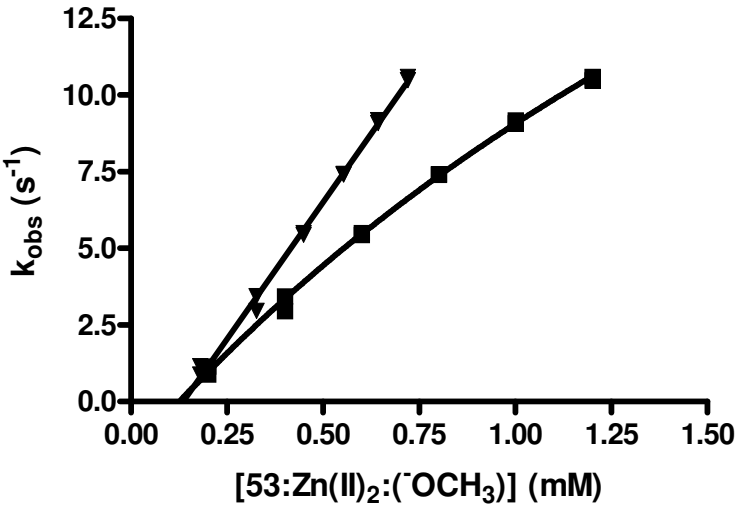

Figure 8. A plot of k_{obs} vs [**53**:$Zn(II)_2$:($^{-}OCH_3$)] for the catalyzed methanolysis of **1**a (5×10^{-5} M) determined from the rate of appearance of product phenol at 320 nm, $^{s}_{s}$pH 9.47 ± 0.17, and 25.0 ± 0.1°C. The data (■) show slight curvature that is an artifact of inhibition by triflate anions. This curve was fit to a first order association equation ($k_{obs}(t) = k_{obs}(\infty)(1-e^{-k1*t})$). When corrected for triflate inhibition, linear regression of the data (▼) give $k_2 = (2.08 \pm 0.04) \times 10^4\ M^{-1}s^{-1}$ with an intercept of A = 0.12 ± 0.02 mM, r^2 = 0.998.

It was difficult to distinguish if saturation kinetics were evident for substrate **1**d as the data displayed mild curvature and the k_{obs} vs [**53**:$Zn(II)_2$:($^{-}OCH_3$)]$_{free}$ could be fit to

both a universal binding Eq. (2)[67] or a linear regression (Figure 9). Fitting the data to Eq. (2) provided values for k_{cat}^{max} and K_M. However, the error associated with the value for K_M was larger than that of K_M and a reasonable fit of the data could not be achieved. The k_{obs} vs [**53**:Zn(II)$_2$:($^-$OCH$_3$)]$_{free}$ data for substrate **1**d were electively fit to a linear regression which afforded a value for k_2 of (2.63 ± 0.12) x 10^3 $M^{-1}s^{-1}$.

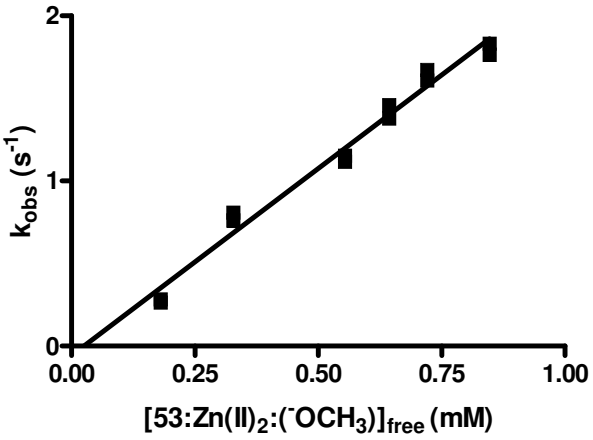

Figure 9. A plot of k_{obs} vs [**53**:Zn(II)$_2$:($^-$OCH$_3$)]$_{free}$ for the catalyzed methanolysis of **1**d (5 x 10^{-5} M) determined from the rate of appearance of product phenol at 287 nm, ^s_spH 9.47 ± 0.17, and 25.0 ± 0.1°C. Linear regression of the data gives k_2 = (2.63 ± 0.12) x 10^3 $M^{-1}s^{-1}$ and an intercept X = 0.02 ± 0.05 mM, r^2 = 0.979.

Saturation binding was apparent for substrates **1**e-g following application of the correction for triflate inhibition and a plot of the k_{obs} vs [**53**:Zn(II)$_2$:($^-$OCH$_3$)]$_{free}$ data determined for the catalyzed decomposition of **1**g is shown in Figure 10.

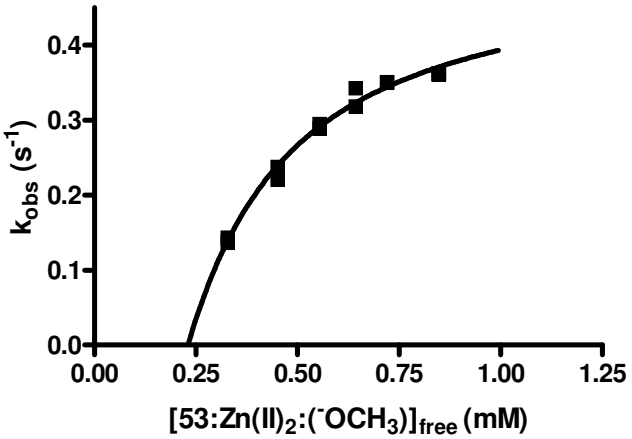

Figure 10. A plot of k_{obs} vs [**53**:Zn(II)$_2$:($^-$OCH$_3$)]$_{free}$ for the catalyzed methanolysis of **1**g (5 x 10^{-5} M) determined from the rate of appearance of product phenol at 295nm, $^{s}_{s}$pH 9.47 ± 0.17, and 25.0 ± 0.1°C. Fitting the data to the expression given in Eq. (2) gives k_{cat}^{max} = (5.15 ± 0.40) x 10^{-1} s^{-1}, K_M = (1.92 ± 0.30) x 10^{-4} M, and an intercept X = 0.20 ± 0.01 mM, r^2 = 0.986.

The k_{obs} vs [**53**:Zn(II)$_2$:($^-$OCH$_3$)]$_{free}$ data for substrates **1**e-g were fit to a universal binding Eq. (2)[67, 89] that is applicable to both strong and weak binding situations (Appendix I, Figures 3S and 4S).

$$(2) \qquad k_{obs} = k_{cat}(1 + K_B * [S] + [Cat] * K_B - X)/(2K_B)/[S]$$

where:

$$X = (1 + 2K_B * [S] + 2 * [Cat] * K_B + K_B^{\,2} * [S]^2 - 2 * K_B^{\,2} * [Cat][S] + [Cat]^2 * K_B^{\,2})^{0.5}$$

and K_B refers to the binding constant (units of M^{-1}) for the association of **53**:Zn(II)$_2$:($^-$OCH$_3$) with each phosphate diester, the reciprocal is defined here as the Michaelis-Menten constant, K_M, with units of M. The [S] term refers to the concentration of the substrate and the [Cat] term corresponds to [**53**:Zn(II)$_2$:($^-$OCH$_3$)]$_{free}$ which is derived according to an expression of the form [Cat] = ([Zn^{2+}]$_{total}$ – A), where A is an independently fitted parameter generally having the value of ~ 0.16-0.23 mM that

corresponds to the observed X-intercept for substrates **1**a-c and **1**e-g. The same approach in determining the concentration of active catalyst in solution has been used by our group for the La^{3+}-catalyzed methanolysis of carboxylate esters and neutral phosphate triesters, where only the catalytically active La^{3+}-containing dimer was considered for the determination of second-order rate constants.[90]

The data for each substrate showed a significant X-intercept that is attributable to the incomplete formation of catalyst at low concentrations. The X-intercept for substrate **1**d yielded a low value of 0.02 ± 0.05 mM, which within two standard deviations experimentally agrees with the average X-intercept determined for substrates **1**a-c and **1**e-g ($A_{ave.}$ = 0.18 ± 0.04) .

Given in Table 1 are the best fit K_M and k_{cat}^{max} constants for the **53**:$Zn(II)_2$:($^-OCH_3$)-catalyzed methanolysis of substrates **1**e-g, along with the experimentally observed second order rate constants for substrates **1**a-d.

Table 1. Kinetic constants (maximum rate constants (k_{cat}^{max}), Michaelis-Menten constants (K_M), and second-order rate constants (k_2 or k_{cat}^{max}/K_M)) for the cleavage of **1**a-g mediated by [**53**:Zn(II)$_2$:($^-$OCH$_3$)]$_{free}$ in anhydrous methanol at ^s_spH 9.47 ± 0.17 and 25.0 ± 0.1°C.

X	phenol $^s_s pK_a$	k_2 ($M^{-1}s^{-1}$)	k_{cat}^{max} (s^{-1})	K_M (M)	Acceleration by catalyst at ^s_spH 9.47
4-NO_2[a]	11.30	(2.08 ± 0.04) x 10^4	*NA*	*NA*	1.60 x 10^{11}[d]
3-CH_3, 4-NO_2[a]	11.50	(1.51 ± 0.07) x 10^4	*NA*	*NA*	5.69 x 10^{11}[d]
3-NO_2[a]	12.49	(1.38 ± 0.08) x 10^4	*NA*	*NA*	4.11 x 10^{11}[d]
4-Cl[a]	13.59	(2.63 ± 0.12) x 10^3	*NA*	*NA*	1.01 x 10^{12}[c]
3-OCH_3	13.93	*(2.34 ± 1.35) x 10^3*[b]	(9.50 ± 1.93) x 10^{-1}	(4.78 ± 3.14) x 10^{-4}	1.13 x 10^{12}[c]
H	14.33	*(3.98 ±0.99) x 10^3*[b]	(7.20 ± 0.72) x 10^{-1}	(1.81 ±0.41) x 10^{-4}	1.19 x 10^{12}[c]
4-OCH_3	14.77	*(2.68± 0.47) x 10^3*[b]	(5.15 ± 0.40) x 10^{-1}	(1.92 ± 0.30) x 10^{-4}	1.74 x 10^{12}[c]

a. K_M and k_{cat}^{max} values were not determined for the faster reacting substrates **1**a-d.

b. The k_2 values for **1**a-d are the experimentally observed values from the slopes of the k_{obs} vs [**53**:Zn(II)$_2$:($^-$OCH$_3$)]$_{free}$ plots. The k_2 values in italics are computed from k_{cat}^{max}/K_M.

c. Acceleration in terms of k_{cat}^{max} relative to the methoxide reaction at ^s_spH 9.47 where [$^-$OCH$_3$] = 5.01 x 10^{-8} M.[67]

d. Acceleration in terms of 1 mM catalyst reacting with the observed second order rate constant relative to the methoxide reaction at ^s_spH 9.47.[67]

For the slower reacting substrates (**1**e-g), for which saturation kinetics were observed, k_2 values can be computed from k_{cat}^{max}/K_M. These values can be used in combination with the experimentally determined k_2 values for the more reactive substrates **1**a-d. The log k_2 vs $^s_s pK_a$ of the product phenol resulting from the **53**:Zn(II)$_2$:

($^-OCH_3$)-catalyzed decomposition of **1**a-g can be plotted to fit the Brønsted relationship $k_2 = 10^{(\beta lg \cdot {}^{s}_{s}pKa + C)}$ (Figure 11). A linear regression of the data gives $\beta_{lg} = (-0.32 \pm 0.06)$.

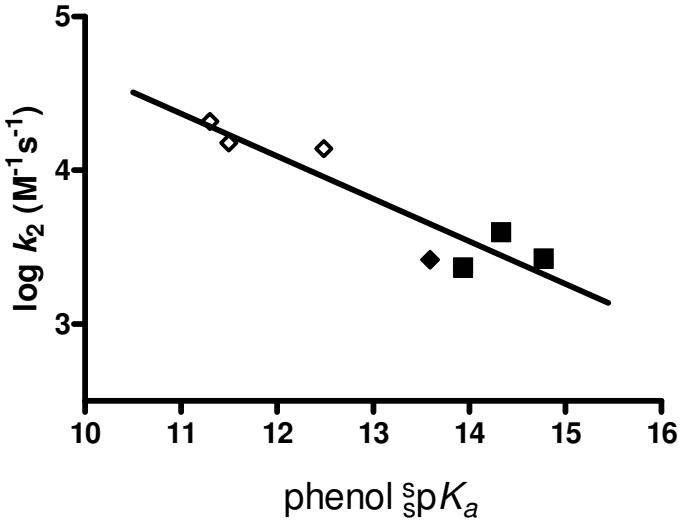

Figure 11. A Brønsted plot for the **53**:$Zn(II)_2$:($^-OCH_3$)-catalyzed methanolyses of phosphates (**1**a-g). The seven data points (**1**a-c (◊), **1**d (♦), and **1**e-g (■)) were fit to a standard linear regression of log $k_2 = (-0.318 \pm 0.060)\ {}^{s}_{s}pK_a + (7.86 \pm 0.79)$, $r^2 = 0.851$.

A plot of the observed rate constants of **53**:$Zn(II)_2$:($^-OCH_3$) (0.50 mM) promoted cyclization of substrate **1**e (5×10^{-5} M) as a function of $[CH_3O^-]/[$**53**$:Zn(II)_2]$ (0 - 2.0 mM) is shown in Figure 12. The maximum rate constant observed for **1**e is obtained when $[CH_3O^-]/[$**53**$:Zn(II)_2]$ is unity, which is consistent with a rate limiting product releasing transition state containing one methoxide, one **53**:$Zn(II)_2$ complex, and one substrate. The catalytic activity of the dinuclear Zn(II) complex of **53** is lost upon the introduction of 0.6 mM of $HClO_4$. The consequence of this phenomenon on determining the first macroscopic ${}^{s}_{s}pK_a$ will be discussed below.

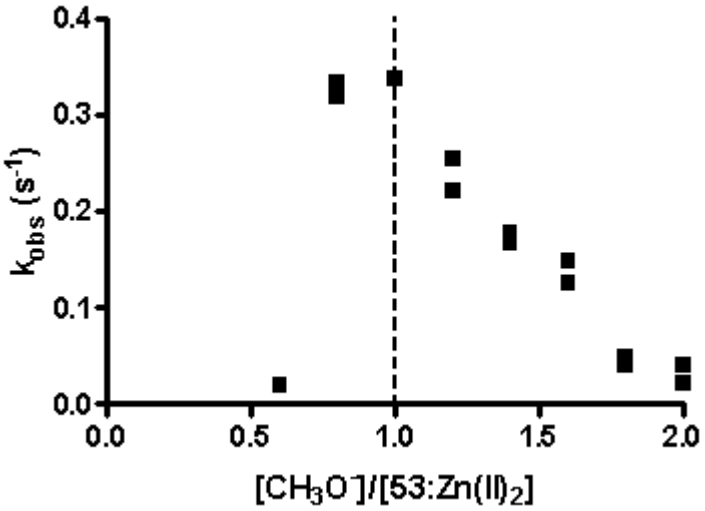

Figure 12. Plot of the observed first order rate constants for the methanolysis of **1**e (0.05 mM) catalyzed by [**53**:$Zn(II)_2$:($^-OCH_3$)]$_{total}$ (0.50 mM) as a function of the [CH_3O^-]/[**53**:$Zn(II)_2$] ratio at 25.0 ± 0.1°C.

3.3 Discussion

3.3.1 Methoxide-promoted cyclization of **1**a-g

It has been contended that the nucleophilic displacement of good leaving groups from neutral or monoanionic phosphates is a concerted process with the formation of a phosphorane-like transition state. The phosphorane species could only be considered an intermediate if it existed in an extremely shallow energy well at the top of a barrier and had a lifetime greater than one bond vibration.[91, 92] For the hydroxide-promoted cleavage of 2-hydroxylpropyl aryl phosphates and methyl aryl phosphates β_{lg} values of –0.62 and –0.58 have been reported,[1d] which are comparable to the respective β_{lg} values in methanol.[53, 67] The β_{lg} for the methoxide-promoted cyclization of substrates **1**a-g[67] is –0.72 and for the cleavage of a series of methyl aryl phosphates[53] is –0.57. Similar β_{lg} values have also been reported for the hydrolysis of uridine 3'-phosphate esters and for the attack of aryloxy anions on methyl aryl phosphate diesters (-0.54 and –0.64,

respectively).[73] Recently, the support for a concerted mechanism for the hydrolysis of 2-hydroxylpropyl aryl and alkyl phosphodiesters obtained by Brown and Usher[83] has been reinterpreted to support hydrolysis occurring via a stepwise process. An investigation[26] of the base-promoted cyclization of a series of uridine 3'-phosphate diesters with leaving groups spanning a pK_a range of 5-17 units produced a break in the Brønsted plot of log k_2 vs pK_a and gave support for the existence of a stable intermediate. For substrates with good leaving groups ($\beta_{lg} = -0.52$) the formation of the intermediate is rate limiting and for substrates with poorer leaving groups ($\beta_{lg} = -1.34$) the breakdown of the phosphorane becomes rate determining. These findings are consistent with a stepwise process and formation of a pentacoordiante phosphorane intermediate.

The β_{lg} value reported herein for the methoxide-promoted cleavage of substrates **1**a-g supports a single rate determining step over the ${}^{s}_{s}pK_a$ range examined. The process is indeterminable between being concerted or stepwise, where aryloxy substituents are good leaving groups and the formation of the phosphorane intermediate would be rate limiting with the fast departure of the leaving group. The Leffler parameter (α) can be used to measure the extent of P-OAr bond cleavage. It takes into account the change in the Brønsted β_{lg} value for the transition state relative to the β_{eq} value for the transfer of the phosphoryl group between oxyanion nucleophiles. With respect to the transfer of $(RO)P(=O)O^-$,[93] the O-Ar oxygen has a net effective charge of +0.74 in the starting material and of -1.0 in the product phenolate. This gives the β_{eq} an overall value of -1.74. When methoxide is the nucleophile the Leffler parameter is $\beta_{lg}/\beta_{eq} = 0.43$, which can be

interpreted to mean that P-OAr cleavage is 43% of the way from starting material to product in the transition state.

3.3.2 Cyclization reaction of **1**a-g catalyzed by **53**:Zn(II)$_2$:($^-$OCH$_3$)

The observed rate constants of cyclization of substrates **1**a-d catalyzed by **53**:Zn(II)$_2$:($^-$OCH$_3$) were fit to a linear relationship over the range of catalyst concentration employed (0.2 – 1.0 mM) as demonstrated in Figures 8 and 9 and in Appendix I, Figures 1S and 2S. Linear regression gives k_2 values for each substrate. Michaelis-Menten saturation kinetics were observed for substrates **1**e-g (Figure 10 and Appendix I, Figures 3S and 4S) and K_M and k_{cat}^{max} values were obtained from a fitting of the k_{obs} vs [**53**:Zn(II)$_2$:($^-$OCH$_3$)]$_{free}$ data to Eq. (2). These values can be found in Table 1 along with k_2 values determined for substrates **1**e-g from the relationship $k_2 = k_{cat}^{max}/K_M$.

3.3.3 Catalysis and mechanistic questions

It is possible to rule out certain mechanisms taking into consideration the ^s_spKa of the the 2-OH group of substrate **1**a and the operative ^s_spH of **53**:Zn(II)$_2$:($^-$OCH$_3$) in methanol. The ^s_spKa for the deprotonation of the 2-OH group of the anionic **1**a in methanol should be at least as large, if not greater, than the ^s_spKa of methanol (K_W/[MeOH] = ($10^{-16.77}$/30M) or ^s_spKa $\geq$ 18.2. One part in $10^{8.7}$ ($10^{(18.2-9.47)}$) of the dianionic form of **1**a would be present at ^s_spH 9.47 where **53**:Zn(II)$_2$:($^-$OCH$_3$) is operative. The second order rate constants for the cleavage of **1**a-c by **53**:Zn(II)$_2$:($^-$OCH$_3$) are 20,800, 15,100, and 13,800 $M^{-1}s^{-1}$, respectively, which would require that these reactions exceed the diffusion limit of 10^{10} $M^{-1}s^{-1}$ by ~ 275 to 400-fold if the dianionic

form of the substrate was the required form for binding. This acceleration was determined from the k_{obs} for **1**a-c at 1 mM of complex (k_{obs}*(1/$10^{8.7}$)) and would be magnified taking into consideration that at $^{s}_{s}$pH 9.47 the complex is essentially fully bound as **53**:Zn(II)$_2$:($^{-}$OCH$_3$) with only a small proportion in the **53**:Zn(II)$_2$:(HOCH$_3$) form required to bind the dianionic substrate. These considerations are not in compliance with the proposed mechanism for the cleavage of uridine 3'-*p*-nitrophenyl phosphate and some RNA models by a dinuclear Zn(II) complex of **47** and other metallic complexes.[94, 95] Shown in Scheme 10 is the proposed substrate-binding step involving the deprotonated 2-OH form of substrate **1** and the protonated form of the catalyst (**47**:Zn(II)$_2$:(OH$_2$)), rather than the protonated form of the substrate and deprotonated catalyst. For the reasons iterated above, this mechanism can be excluded. Alternatively, transient binding of **53**:Zn(II)$_2$:($^{-}$OCH$_3$) and **1** followed by a fast formation of **53**:Zn(II)$_2$:**1**$^{-}$ with subsequent or simultaneous double Lewis acid activation and cyclization cannot be rejected.

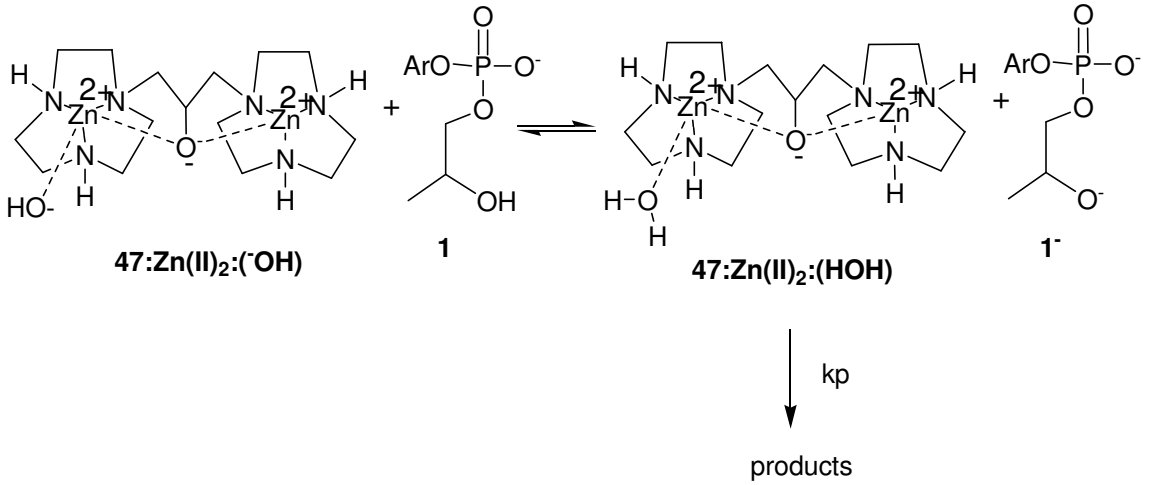

Scheme 10. The **47**:Zn(II)$_2$:(OH$_2$)-catalyzed decomposition of 2-hydroxylpropyl aryl phosphates, **1**. (Reference 67)

A detailed schematic for the **53**:$Zn(II)_2$:($^-OCH_3$)-catalyzed decomposition of substrates **1**a-g is presented in Scheme 11.[67] Pictorially represented are the possible species involved in the **53**:$Zn(II)_2$:($^-OCH_3$)-catalyzed cleavage of **1**a-g. Upon inspection of the k_{obs} vs [**53**:$Zn(II)_2$:($^-OCH_3$)]$_{free}$ data for substrate **1**g Michaelis-Menten kinetics is observed and the catalyst complex is fully bound and saturated when [**53**:$Zn(II)_2$:($^-OCH_3$)]$_{free}$ is ≥ 1 mM (Figure 10). In Figure 12, the observed rate constant for the production of product phenol from the **53**:$Zn(II)_2$:($^-OCH_3$)-catalyzed cleavage of **1**e maximizes at one equivalent of methoxide per equivalent of **53**:$Zn(II)_2$. This stopped-flow experiment was performed by inoculating the fully formed **53**:$Zn(II)_2$:($^-OCH_3$) catalyst with **1**e and an appropriate amount of $HClO_4$ or $NaOCH_3$. Taken together, these observations for the catalyzed cleavage of **1**e and **1**g suggest a transition state consisting of one methoxide, one substrate, and **53**:$Zn(II)_2$, assuming that the metal ion does not dissociate from the complex over the course of the reaction and that substrate binding and acid/base reactions are fast.

Interestingly, at lower [$^-OCH_3$]/[**53**:$Zn(II)_2$] ratios the k_{obs} for the catalyzed decomposition of **1**e drops of dramatically. This would be consistent with a reduction in the amount of methoxide available which is required for the deprotonation of substrate and subsequent production of phenol, however the experimentally observed ${}^{s}_{s}pH$ has been observed to increase with the introduction of 0.5 equivalents of $HClO_4$ (${}^{s}_{s}pH$ increases from 9.47 ± 0.17 to 9.67 ± 0.01).

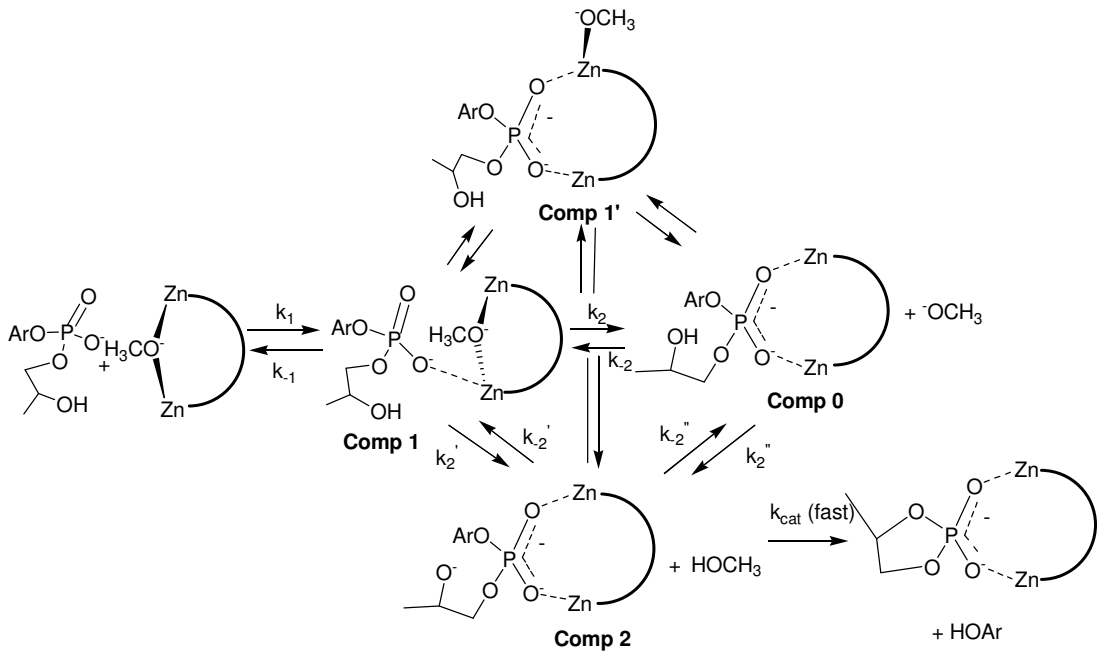

Scheme 11. The possible candidates involved in the **53**:$Zn(II)_2$:($^-OCH_3$)-catalyzed cleavage of 2-hydroxylpropyl aryl phosphates **1**a-g. (Reference 67)

The findings mentioned above are consistent with the ([$^-OCH_3$]/[$Zn(II)_2$:**36**])-rate constant profile determined for the **36**:$Zn(II)_2$:($^-OCH_3$)-catalyzed cleavage of substrate **1**f[67] which also maximizes at 1.0. However, the activity of **36**:$Zn(II)_2$:($^-OCH_3$) was not as compromised upon the addition of $HClO_4$ as was seen for **53**:$Zn(II)_2$:($^-OCH_3$). A comparison of the contradictive first macroscopic ${}^{s}_{s}pK_a$ of 1.0 mM of **53**:$Zn(II)_2$:($^-OCH_3$) measured by half neutralization in methanol (9.67 ± 0.01) and the operative ${}^{s}_{s}pH$ of the **53**:$Zn(II)_2$:($^-OCH_3$) complex (9.47 ± 0.17) may assist in reconciling the reduced activity of the dinuclear Zn(II) complex of **53** with respect to that of **36** upon the introduction of acid.

The reduced activity observed for **53**:$Zn(II)_2$:($^-OCH_3$)-catalyzed cleavage of **1**e upon the introduction of acid proves that catalytic activity requires at least one equivalent

of methoxide. It is reasonable to assume that the complex is unstable with the introduction of acid and its instability is manifested in the first macroscopic ${}^{s}_{s}pK_a$ value of the dinuclear complex of **53** in methanol. A first half neutralization ${}^{s}_{s}pK_a$ value that is greater than the operative ${}^{s}_{s}pH$ of the complex suggests that the addition of acid destroys the complex, protonating the highly basic amines which then buffer the solution at the measured ${}^{s}_{s}pH$ value.

The mechanism suggested in Scheme 11 depicts the binding of **53**:$Zn(II)_2$:($^{-}OCH_3$) to the 2-hydroxylpropyl aryl phosphate, first through one metal ion (Comp 1), with subsequent rearrangement and binding to the second metal ion.[67] Support for a methoxide bridged by two metal ions comes from the X-ray diffraction structure of the closely related **36**:$Zn(II)_2$:(^{-}OH) complex showing a hydroxide anion bridged by the two Zn(II) ions.[96] It is a reasonable assumption that this structure is conserved for the methoxide complex prior to substrate binding. The nucleophilicity of a methoxide bridged by two Zn(II) ions would be less than that of an external methoxide and is thus difficult to envision as the active nucleophile.[53] In Scheme 11 one of the bridging methoxide-Zn(II) bonds of Comp 1 is broken during a rearrangement that doubly activates the substrate via binding to the second Zn(II) ion as in Comp 1' or with deprotonation of the 2-OH group and the loss of CH_3OH as depicted in Comp 2.[67] If the deprotonation of the substrate 2-OH group by a departing methoxide is reversible it is equivalent to specific base deprotonation by an external methoxide as in Comp 0 ↔

Comp 2. In compliance with the kinetic data presented here, a specific base role for methoxide is feasible if the rate of deprotonation approaches the diffusion limit (~10^{10} $M^{-1}s^{-1}$). For substrate **1**e which exhibits Michaelis-Menten behaviour, the k_{cat}^{max} value is 0.95 s^{-1}. At $^{s}_{s}$pH 9.47 the concentration of external methoxide would be 5.0 x 10^{-8} M and the k_{cat}^{max} would have an upper limit of 500 s^{-1}, which encompasses the observed value of this substrate. Simlar findings are found for substrates **1**f and **1**g using this approach.

3.3.4 Catalytic acceleration of the cyclization of 1 and energetic considerations

Given in Table 1 are the accelerations provided by **53**:$Zn(II)_2$:($^{-}OCH_3$) for the cleavage of **1**a-g in comparison with the background methoxide-promoted reaction at $^{s}_{s}$pH 9.47. With respect to k_{cat}^{max}, the accelerations lie within a range of 1.1 to 1.7 x 10^{12}-fold. The catalytic efficiency of **53**:$Zn(II)_2$:($^{-}OCH_3$) can be quantified by comparing the differences in energy of a methoxide-promoted transition state comprised of $[CH_3O^{-}$:**1**$]^{\ddagger}$ to one including a bound catalyst ([**53**:$Zn(II)_2$:($^{-}OCH_3$):**1**]‡ or its kinetic equivalent). A thermodynamic cycle is presented in Scheme 12, where the methoxide-promoted and **53**:$Zn(II)_2$:($^{-}OCH_3$)-catalyzed reaction with substrates **1**a-g are depicted.

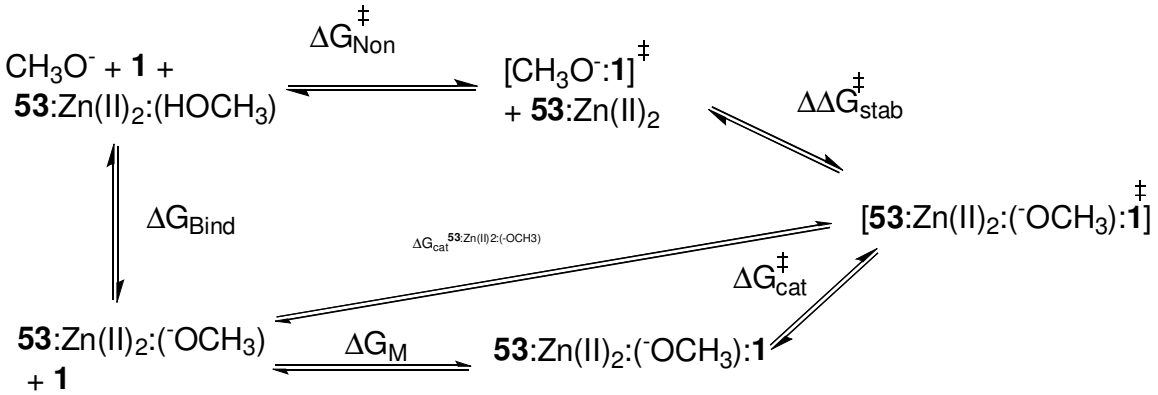

Scheme 12. The free energy of activation for the reaction of **1** with methoxide and with **53**:$Zn(II)_2$:($^{-}OCH_3$). (Reference 67)

Depicted in Scheme 12 is ΔG_{Bind}, $\Delta G^{\ddagger}_{cat}$, and $\Delta G^{\ddagger}_{Non}$ which are, respectively, free energies for the binding of methoxide to **53**:Zn(II)$_2$, for the activation energy for the unimolecular reaction of **53**:Zn(II)$_2$:($^{-}$OCH$_3$):**1**, and the free energy of activation for the reaction of methoxide with **1**. The free energy of association of substrate **1** with **53**:Zn(II)$_2$:($^{-}$OCH$_3$) is given by ΔG_M which is determined from the Michaelis constant K_M of the corresponding substrate.[67] The free energy difference ($\Delta\Delta G^{\ddagger}_{stab}$) between [$CH_3O^-$:**1**]‡ and [**53**:Zn(II)$_2$:($^{-}$OCH$_3$):**1**]‡ is given by Eq. (3) for substrates **1**e-g.[67] For substrates displaying first order dependence on [**53**:Zn(II)$_2$:($^{-}$OCH$_3$)]$_{free}$ throughout the catalyst concentration range investigated (**1**a-d), Eq. (4) gives the free energy calculation.[67]

(3) $$\Delta\Delta G^{\neq}_{stab} = (\Delta G_{Bind} - \Delta G_M + \Delta G^{\neq}_{cat}) - \Delta G^{\neq}_{Non} = -RT \ln\left[\frac{(k_{cat\,max}/K_M)(K_a/K_w)}{k_2^{-OMe}}\right]$$

(4) $$\Delta\Delta \mathbf{G}^{\neq}_{\mathbf{stab}} = (\Delta \mathbf{G}_{\mathbf{Bind}} + \Delta \mathbf{G}_{\mathbf{cat}}^{\mathbf{53{:}Zn(II)2{:}(OCH3)}}) - \Delta \mathbf{G}^{\neq}_{\mathbf{Non}} = -\mathbf{RT} \ln\left[\frac{(\mathbf{k}_2)(\mathbf{K_a}/\mathbf{K_w})}{\mathbf{k}_2^{-OMe}}\right]$$

The k_{cat}^{max}/K_M values for substrates **1**e-g and the equivalent k_2 values for substrates **1**a-d are given in Table 1. The second order rate constants for the methoxide promoted cyclization of **1** (k_2^{-OMe}) have been previously determined by our group and can be found in Appendix I, Table 1S.[67] K_a/K_w may be considered equivalent to the binding constant of methoxide to the diZn(II)$_2$-complex to form **53**:Zn(II)$_2$:($^{-}$OCH$_3$), where K_w is the autoprotolysis constant of methanol ($10^{-16.77}$) and K_a is determined as follows. As previously discussed, the first half neutralization $^{s}_{s}pK_a$ determined from the addition of a ½ equivalent of $HClO_4$ to 1.0 mM of **53**:Zn(II)$_2$:($^{-}$OCH$_3$) in methanol resulted in the loss of catalytic activity of this complex. Thus, an accurate first macroscopic $^{s}_{s}pK_a$ could not

be experimentally determined. As the dinuclear $Zn(II)_2$ complexes of **53** and **36** are structurally very similar and differ only by one methylene unit in the alkane spacer an assumed first acid dissociation constant can be determined for **53**:$Zn(II)_2$:($HOCH_3$) from the difference between the operative ${}^{s}_{s}pH$ of 9.8 ± 0.1 of **36**:$Zn(II)_2$:($^{-}OCH_3$) and the first acid dissociation constant of **36**:$Zn(II)_2$:($HOCH_3$) of 9.41 ± 0.1.[67, 97] This difference can be subtracted from the operative ${}^{s}_{s}pH$ of **53**:$Zn(II)_2$:($HOCH_3$) to yield a theoretical first neutralization ${}^{s}_{s}pK_a$ of ~ 9.0 – 9.1. Using a value of 9.08 for the energetics calculations below results in $\Delta\Delta G^{\ddagger}_{stab}$ values for substrates **1**a-g that differ by only 0.8 kcal/mol from those determined using the measured half neutralization ${}^{s}_{s}pK_a$. This difference is negligible and energetics calculations determined using the assumed half neutralization ${}^{s}_{s}pK_a$ will be discussed below.

Given in Table 2 are the $(k_{cat}/K_M)/k_2^{-OMe}$, $(k_{cat}/K_M)(K_a/K_w)$, ΔG_{Bind}-ΔG_M, $\Delta G^{\ddagger}_{cat}$, and $\Delta\Delta G^{\ddagger}_{stab}$ values computed for the catalyzed reactions of substrates **1**a-g at standard state. For substrates **1**a-d, saturation kinetics were not observable and thus the experimentally determined k_2 value was used in place of k_{cat}^{max}/K_M. Comparison of k_2 values (defined as k_{cat}^{max}/K_M for substrates **1**e-g) for the catalyzed and the base-promoted reactions with **1**a-g at ${}^{s}_{s}pH$ 9.47 ± 0.17 provide rate accelerations within the range of 1.6 to 10.1 x 10^{11}-fold for the more reactive substrates **1**a-d and a range of 2.8 to 9.1 x 10^{12}-fold for the less reactive substrates **1**e-g. The structurally similar **36**:$Zn(II)_2$:($^{-}OCH_3$) complex achieved rate accelerations of 10^{12}-fold throughout the series of substrates **1**a-g with respect to the background methoxide-promoted reaction.[67] The computed $\Delta\Delta G^{\ddagger}_{stab}$

values are within a range of –20 to –22 kcal/mol for the **53**:$Zn(II)_2$:($^-OCH_3$)-catalyzed cleavage of substrates **1**a-g, which are approximately equivalent to those seen with **36**:$Zn(II)_2$:($^-OCH_3$) (-21 to –23 kcal/mol).[67] For the series the K_a/K_w term contributes –10.5 kcal/mol to $\Delta\Delta G^{\ddagger}_{stab}$ and the $(k_{cat}^{max}/K_M)/k_2^{-OMe}$ term contributes –10.4 to –11.6 kcal/mol for substrates **1**e-g. The k_2/k_2^{-OMe} term contributes –9.4 to –10.1 kcal/mol for substrates **1**a-d. For substrates **1**a-d which do not show saturation kinetics the computed energies of activation for the second order rate constants for the reactions of **53**:$Zn(II)_2$:($^-OCH_3$) and **1**a-d are 11.5, 11.7, 11.8, and 12.8 kcal/mol, respectively.

Table 2. The $(k_{cat}^{max}/K_M)/k_2^{-OMe}$ and $(k_{cat}^{max}/K_M)(K_a/K_w)$ constants, computed free energies of formation of Michaelis complexes (ΔG_{Bind}-ΔG_M), free energies of activation ($\Delta G^{\ddagger}_{cat}$), and the free energies of stabilization of the methoxide transition state through binding to **53**:Zn(II)$_2$ ($\Delta\Delta G^{\ddagger}_{stab}$)[a] for the reaction of **53**:Zn(II)$_2$:($^-OCH_3$) with substrates **1**a-g at 25 ^oC in methanol.

Substrate	$(k_{cat}^{max}/K_M)/(k_2^{-OMe})$[a,b]	$(k_{cat}^{max}/K_M)(K_a/K_w)$ $(M^{-2}s^{-1})$[a,c]	ΔG_{Bind}-ΔG_M (kcal/mol)[d,e]	$\Delta G^{\ddagger}_{cat}$ (kcal/mol)[f]	$\Delta\Delta G^{\ddagger}_{stab}$ (kcal/mol)[g]
1a	8.0×10^6	1.0×10^{12}	*NA*	11.5	-19.9
1b	2.8×10^7	7.4×10^{11}	*NA*	11.7	-20.6
1c	2.1×10^7	6.8×10^{11}	*NA*	11.8	-20.5
1d	5.1×10^7	1.3×10^{11}	*NA*	12.8	-21.0
1e	1.2×10^7	9.7×10^{10}	-15.0	17.4	-21.5
1f	3.3×10^7	1.9×10^{11}	-15.6	17.6	-22.1
1g	4.5×10^7	1.3×10^{11}	-15.5	17.8	-20.9

a. k_2 from Table 1 were used in place of k_{cat}^{max}/K_M for the faster reacting substrates **1**a-d
b. k_{cat}^{max}/K_M from Table 1.
c. K_a was determined from the half-neutralization ${}^{s}_{s}pK_a$ to be $10^{-9.08}$ as described in the text; $K_w = 10^{-16.77}$; $K_a/K_w = 4.9 \times 10^7$.
d. Computed as $(\Delta G_{Bind}-\Delta G_M) = -RTln((K_a/K_w)/K_M)$.
e. K_M values were indeterminable for substrates **1**a-d and were unavailable for use in energetics calculations.
f. Computed from the Eyring equation $\Delta G^{\ddagger}_{cat} = -RTln(k_{cat}^{max}/(kT/h))$, where $(kT/h) = 6 \times 10^{12}$ s^{-1} at 298K for substrates **1**e-g and from $\Delta G^{\ddagger}_{cat} = -RTln(k_2/(kT/h))$ for substrates **1**a-d.
g. $\Delta G^{\ddagger}_{stab}$ computed from application of kinetic and equilibrium constants to Eq. (3) and Eq. (4); k_2^{-OMe} constants determined previously by our group.[67]

The binding constants given in Table 2 are pictorially represented in Figure 13 for the base-promoted and **53**:Zn(II)$_2$:($^-OCH_3$)-catalyzed reaction with substrate **1**e, where the ground state is considered to be CH_3O^-, **53**:Zn(II)$_2$, and **1**e ($\Delta G^o = 0$). In the absence of catalyst, the $\Delta G^{\ddagger}_{non}$ for the methoxide reaction with **1**e is 23.9 kcal/mol with respect to

the ground state. The formation of the **53**:Zn(II)$_2$:($^-$OCH$_3$)-complex and its coordination to **1**e is exothermic by –15.0 kcal/mol. The activation energy associated with the k_{cat}^{max} term for the catalyzed reaction with **1**e is 17.4 kcal/mol, which was calculated from the Eyring equation $\Delta G^{\ddagger} = - RTln(k_{cat}^{max}/(kT/h))$.

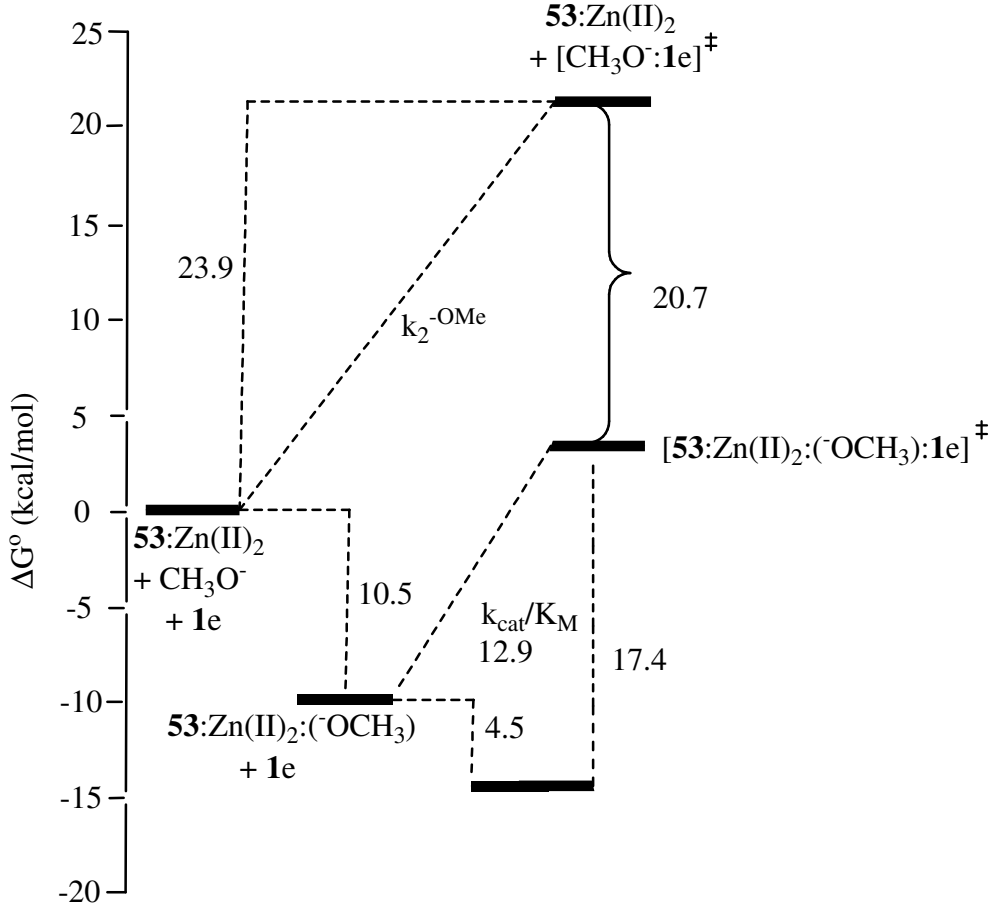

Figure 13. An activation energy diagram for the reaction of substrate **1**e with CH_3O^- and **53**:Zn(II):($^-$OCH$_3$) at standard state conditions (1 M, 25 ^{o}C). The calculated energies of binding methoxide to **53**:Zn(II)$_2$ and of binding the substrate to **53**:Zn(II)$_2$:($^-$OCH$_3$) as well as the calculated activation energies associated with k_{cat}^{max} and k_2^{-OMe} are displayed. (Reference 67)

The ternary complex composed of catalyst and substrate (**1**e-g) is stabilized by –15.0 to –15.6 kcal/mol (ΔG_{Bind}-ΔG_M) relative to its constituents. For the cyclization

reaction, this thermodynamic well is offset by the larger stabilization of the transition state afforded by the dinuclear $Zn(II)_2$ complex. The energies of activation ($\Delta G^{\ddagger}_{cat}$) for the catalyzed cyclization of the bound substrates **1**a-g are endothermic, ranging from 11.5 - 17.8 kcal/mol, and thus the binding of **53**:$Zn(II)_2$ to $[CH_3O^-$:**1**$]^{\ddagger}$ provides stabilizing energies of –17.4 to –22.1 kcal/mol with respect to the methoxide-promoted reaction ($\Delta G^{\ddagger}_{non}$ = 23.2 – 24.1 kcal/mol). The energy of [**53**:$Zn(II)_2$:($^-OCH_3$):**1**e-g]‡ is brought within 2.0-2.4 kcal/mol of the ground state. The $\Delta\Delta G^{\ddagger}_{stab}$ values reported herein are suppressed slightly from those observed for the cyclization of **1**a-g catalyzed by **36**:$Zn(II)_2$:($^-OCH_3$) previously determined by our group (-21 to –23 kcal/mol).[67] Also, with respect to the ground state the free energy of [**53**:$Zn(II)_2$:($^-OCH_3$):**1**]‡ is higher than that reported for [**36**:$Zn(II)_2$:($^-OCH_3$):**1**]‡ (1.1-1.7 kcal/mol).[67] The additional flexibility provided by the butane linker apparently reduces the degree of stabilization of the transition state. A weaker association between the substrate and more flexible catalyst complex is reflected in the ΔG_{Bind}-ΔG_M values for substrates **1**e-g, which are less negative than those reported for the complex with a less flexible propane spacer (-15.5 to –15.6 kcal/mol).[67]

3.4 Conclusions and future directions

The catalyst complex reported herein achieves remarkable rates of catalysis for the cyclization of a series of 2-hydroxylpropyl aryl phosphates that are noteworthy with respect to those reported for the hydrolysis of this class of substrates by other catalytic systems. The medium effect introduced by methanol enhances the reactivity of this complex as seen likewise for the more rigid **36**:$Zn(II)_2$:($^-OCH_3$).[67] The flexibility added

by the butane spacer of **53** over the propane space of **36** does not add to the acceleration afforded by the catalyst with respect to the methoxide-promoted cyclization of **1**a-g. The dinuclear Zn(II) complex of **53** does provide ~10^{11} to 10^{12}-fold rate acceleration while that of **36** offers 10^{12}-fold rate acceleration over the background methoxide-promoted reaction. However, the flexibility in **53**:$Zn(II)_2$ seems to make this a more fragile catalyst as it is sensitive to acidic conditions such that a first $^{s}_{s}$pKa cannot be experimentally determined.

In water, **36**:$Zn(II)_2$ is a poor catalyst towards the hydrolysis of BNP[54] and it is reasonable that the rates of reaction seen with the structurally analogous **53**:$Zn(II)_2$ can also be wholly or in part attributed to the reduced polarity of a solvent with a lower dielectric constant. The ways by which methanol possibly enhances catalysis include desolvating ionic reaction constituents, enhancing the energy of interaction of oppositely charged reactants, and stabilizing a transition state with a dispersed charge relative to the starting materials and products. Considering that the two systems operate in different media, through the binding of **53**:$Zn(II)_2$ to a transition state comprising CH_3O^-:**1**, the catalyzed reaction in methanol provides ~ 20 kcal/mol of stabilization energy which is comparable to the degree of stabilization provided by enzymes that assist the cleavage of phosphate diesters.[98]

Currently, research is being performed by our group to attempt to enhance the activity of the dinuclear Zn(II) complex of **53** by improving its binding to 2-hydroxylpropyl aryl phosphates **1**a-g. The binding of phosphate diesters to **53**:$Zn(II)_2$:($^-OCH_3$) is weaker than that reported for **36**:$Zn(II)_2$:($^-OCH_3$) in methanol and potentially an

ethanol medium can be employed to improve complexation. It has been previously reported by our group that Zn(II) ions tightly bind to HPNPP in ethanol, efficiently cleave HPNPP, and show Michaelis-Menten kinetics.[99] A comparison of the medium effect of solvents of reduced polarity can then be made for the **53**:$Zn(II)_2$:($^-OCH_3$)-catalyzed transesterification of these RNA models.

An investigation of the catalytic activity of the dinuclear Zn(II) complexes **53** and **36** towards diribonucleotides would be interesting as it would test the applicability and reactivity of these zinc-containing catalysts toward the decomposition of biologically relevant substrates. This may ultimately lead to the design of artifical enzymes that could potentially replace restriction enzymes for use in molecular biology.

Chapter 4. Cleavage of a dinucleotide by dinuclear Zn(II) complexes 36:$Zn(II)_2$:($^-OCH_3$) and 53:$Zn(II)_2$:($^-OCH_3$) in methanol

To overcome the inherent stability of phosphodiester P-O bonds many natural enzymes use two or more metal ions to promote hydrolysis. The study of synthetic systems to mimic the activity of enzymes that cleave phosphate diesters may ultimately lead to the development of artificial nucleases which could compete with the efficiency and selectivity of natural enzymes, thereby replacing restriction enzymes for use in molecular biology.

Until recently,[72] Zn(II)-promoted cleavage of ribonucleotides was maintained to be a one-step reaction where intramolecular attack of the 2'-OH group was concerted with departure of the leaving group (Chapter 1, Scheme 1).[1a] A bimetallic complex of **52** has recently been studied by Williams and co-workers[72] for its ability to promote the cleavage of uridyl(3'→5')uridine (UpU) in water at pH 6.5, 25 ^oC. The rate of isomerization to form uridyl(2'→5')uridine ((2'→5')UpU) was found to exceed that of hydrolysis. This work provided the first evidence for pentacoordinate phosphorane intermediate stabilized by a dinuclear metal ion complex and a proposed reaction mechanism is depicted in Scheme 13.

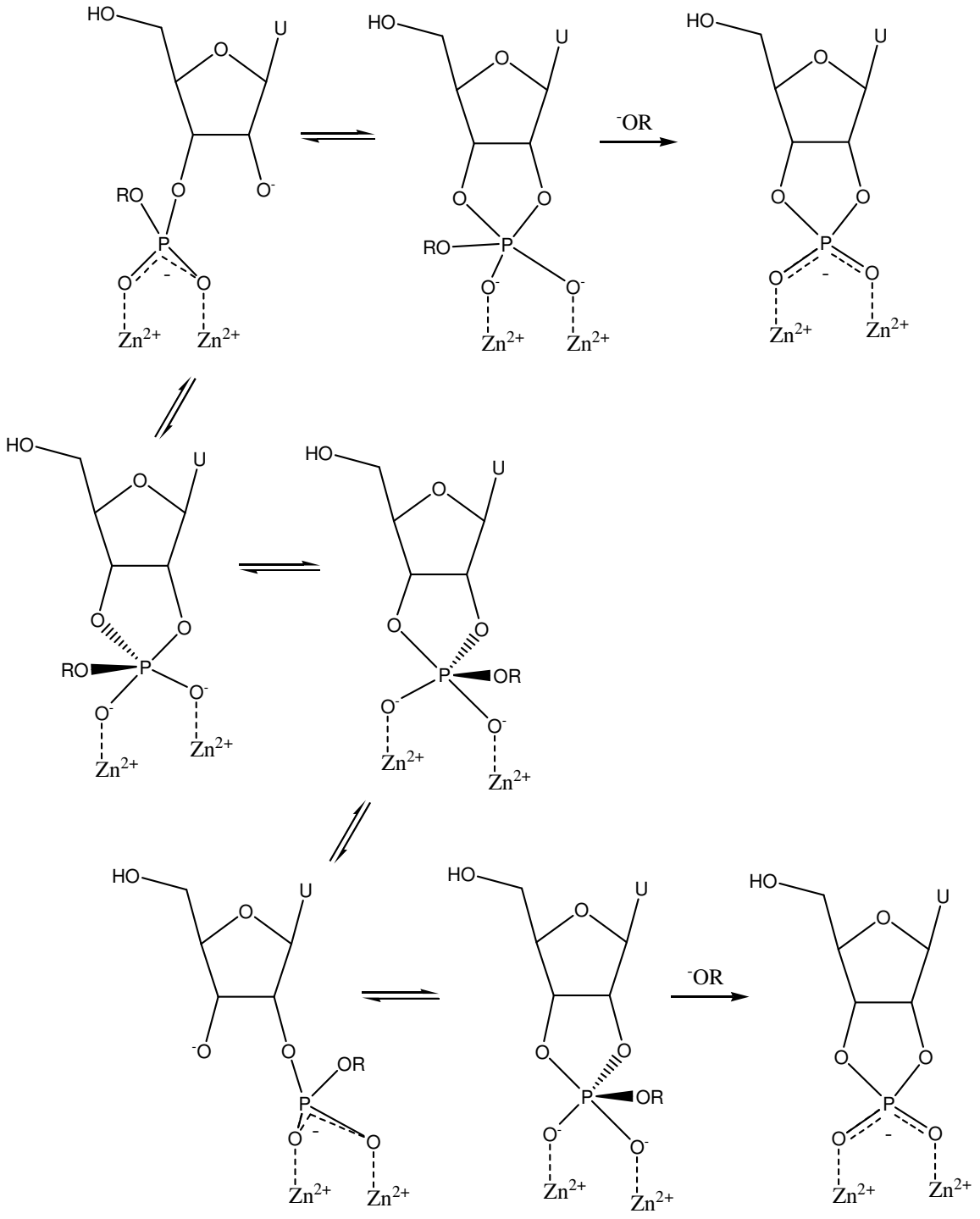

Scheme 13. The proposed mechanism for the cleavage and isomerization of UpU catalyzed by the dinuclear Zn(II) complex of **52** in water. The metal-binding complex and nucleobases are excluded for simplicity. (Reference 72)

In the work reported here the cleavage and isomerization of UpU and adenyly(3'→5')cytidine (ApC) promoted by Zn(II) ions was explored in media of reduced polarity in the presence and absence of metal-binding small molecule complexes **36** and **53**.

4.1 Experimental

4.1.1 Materials

Uridyl(3'→5')uridine ammonium salt, uridine (≥ 99%), HPLC marker (1:2:3:4 uridine, uridine 2'-monophosphate, uridine 3'-monophosphate, uridine 2':3'-cyclic monophosphate), uridine 2'-monophosphate lithium salt (~98%), adenylyl(3'→5')cytidine (≥ 98%), cytosine, adenosine 2'-monophosphate (from yeast), and adenosine 3'-monophosphate sodium salt (from yeast) were obtained and used as supplied from Sigma. Methanol (99.8% anhydrous), sodium methoxide (0.50 M solution in methanol), zinc(II) trifluoromethanesulfonate (98%), sodium ethoxide (21 wt. % solution in denatured ethanol), and *p*-nitrophenol (reagent grade, 98%) were obtained from Aldrich and used without further purification. Potassium phosphate monobasic (HPLC grade) and methanol (HPLC grade) were obtained from Fisher Scientific and used as supplied. Absolute ethanol was purchased from Commercial Alcohols Inc. and was de-gassed by bubbling argon gas through it for 1h and then stored under $Ar_{(g)}$. Freshly dispensed ethanol was used for all kinetic experiments. The concentration of water in the freshly dispensed de-gassed ethanol was found to be ~ 0.028 ± 0.007 M based on 5 titrations using a Mettler Toledo DL32 Karl Fischer Coulometer. Zhong-Lin Lu

synthesized ([12]aneN$_3$)$_2$ (**36**) as previously described from a published methodology[52] and **53** was prepared by Chaomin Liu from a procedure reported previously.[84]

Stock solutions of Zn(CF$_3$SO$_3$)$_2$, NaOCH$_3$, and *p*-nitrophenol were independently prepared to 50 mM in anhydrous CH$_3$OH. A 25 mM stock solution of **36** and a 50 mM stock solution of **53** were prepared in anhydrous methanol. In anhydrous methanol a 10 mM stock solution of UpU was prepared. A 5 mM stock solution of ApC was prepared in a 1:1 ddH$_2$O-anhydrous methanol mixture. In doubly deionized H$_2$O (ddH$_2$O), a 14.72 mM adenosine stock solution and a 50 mM cytosine stock solution were prepared. Stock solutions of Zn(CF$_3$SO$_3$)$_2$, NaOCH$_2$CH$_3$, and *p*-nitrophenol were prepared to 50 mM in ethanol. A pH 2.8 phosphate buffer (25 mM) was prepared in ddH$_2$O with monobasic potassium phosphate.

4.1.2 Stopped-flow reaction kinetics

4.1.2.1 Uridine inhibition of the catalytic activity of 36:Zn(II)$_2$:($^-$OCH$_3$) and 53:Zn(II)$_2$:($^-$OCH$_3$) in methanol

Uridine inhibition constants were independently determined for the **53**:Zn(II)$_2$:($^-$OCH$_3$) (1.0 mM, ^s_spH 9.47 ± 0.17) and the **36**:Zn(II)$_2$:($^-$OCH$_3$) (1.0 mM, ^s_spH 9.8 ± 0.1) catalyzed cyclization of HPNPP (0.05 mM) at 25.0 ± 0.1 ^{o}C. Two experiments were executed wherein independent vials containing 2.0 mM of the **53**:Zn(II)$_2$:($^-$OCH$_3$) complex and 2.0 mM of the **36**:Zn(II)$_2$:($^-$OCH$_3$) complex were prepared in methanol and allotted their required time for formation. Varied amounts of uridine (0 < [uridine] < 8.0 mM) were added to a separate vial containing HPNPP (0.10 mM) in methanol. The contents of the vials containing substrate/uridine and catalyst were loaded into separate

syringes for analysis by stopped-flow reaction kinetics. The catalyst was introduced to the substrate/uridine solution such that the final concentration of **53**:$Zn(II)_2$:($^-OCH_3$) was 0.5 mM, of **36**:$Zn(II)_2$:($^-OCH_3$) was 0.5 mM, of **1**a was 0.05 mM, and 0 < [uridine] < 4.0 mM.

4.1.2.2 The stability of 36:$Zn(II)_2$:($^-OCH_3$) in methanol

The stability of the **36**:$Zn(II)_2$:($^-OCH_3$) catalyst over time in methanol solution was determined by examining the rate constants for the transesterification of **1**a at ^s_spH 9.8 ± 0.1, 25.0 ± 0.1°C. The **36**:$Zn(II)_2$:($^-OCH_3$) complex (1.0 mM) and **1**a (0.10 mM) were allowed to sit at ambient temperature in individual, sealed vials. The observed first-order rate constants for the catalyzed methanolysis of **1**a (0.05mM) by **36**:$Zn(II)_2$:($^-OCH_3$) (0.5 mM) were determined at various times over 145 hours from the rate of appearance of product phenol at 320nm by stopped-flow reaction kinetics. Analysis of the rate constants vs time plot was used to determine a kinetic stability constant for the active **36**:$Zn(II)_2$:($^-OCH_3$) catalyst.

4.1.3 Methods

High resolution exact MS spectra were obtained in ESI$^-$ mode with N_2 carrier gas and direct syringe injection using an Applied Biosystems/MDS Sciex QSTAR XL QqTOF mass spectrometer.

4.1.3.1 HPLC analysis

The rate of the catalyzed transesterification of UpU and ApC was followed by HPLC using a Varian 9100 Autosampler, a Varian 9010 Solvent Delivery System, a Varian 9050 Variable λ UV-VIS Detector (λ = 260 nm), and a Waters Spherisorb 5 μm

C18 reverse phase analytical column (4.6 x 250 mm). The phosphate buffer (pH 2.8, 25 mM):methanol gradient outlined in Table 3 was employed to elute target analytes from the column using a flow rate of 1.0 mL/min.

Table 3. The phosphate buffer (pH 2.8, 25 mM):methanol gradient used to elute the products resulting from the catalyzed decomposition of UpU and ApC from a C18 reverse phase column at ambient temperature.

Run Time (min.)	**% pH 2.8 phosphate buffer (25 mM)**	**% HPLC grade methanol**
0.00	96	4
1.00	96	4
7.00	90	10
10.00	80	20
15.00	20	80
20.00	20	80
21.00	96	4
23.00	96	4

The rates of UpU transesterification catalyzed by **36**:$Zn(II)_2$:($^-OCH_3$) and **53**:$Zn(II)_2$:($^-OCH_3$) in methanol were determined by monitoring the appearance of product peaks corresponding to uridine, methyl uridine 2′-monophosphate (methyl 2′-UMP), methyl uridine-3′-monophosphate (methyl 3′-UMP), and 2':3'-cyclic uridine monophosphate (2':3'-cUMP) by reverse phase HPLC (λ = 260 nm) at ambient temperature. Product peaks were confirmed by comparison of the retention time of authentic uridine, 2′:3′-cUMP, uridine-2′-monophosphate (2′-UMP), uridine 3′-monophosphate (3′-UMP), and UpU using identical HPLC conditions as those used to monitor catalyzed substrate cleavage. Retention times of substrate and products are given in Table 4 and pseudo-first order rate constants (k_{obs}) were obtained from the plot of relative product peak area vs time. *p*-Nitrophenol was used as an internal standard to

determine the relative product peak areas. A linear regression analysis of the k_{obs} vs $[catalyst]_{free}$ provided the second order rate constant (k_2) for the reaction.

Table 4. The retention times of authentic analytes eluted from a reverse phase analytical column at ambient temperature using the phosphate buffer (pH 2.8, 25 mM): methanol gradient outlined in Table 3.

Analyte	Retention Time (min.)
2':3'-cUMP	5.2
2'-UMP	5.9
3'-UMP	6.8
Uridine	9.9
UpU	14.9
p-nitrophenol	19.0

In Figure 14 is an HPLC chromatogram displaying the peaks and corresponding retention times of uridine, 2'-UMP, 3'-UMP, 2':3'-cUMP, and UPU eluted from a reverse phase analytical column at ambient temperature using the phosphate buffer:methanol gradient outlined in Table 3.

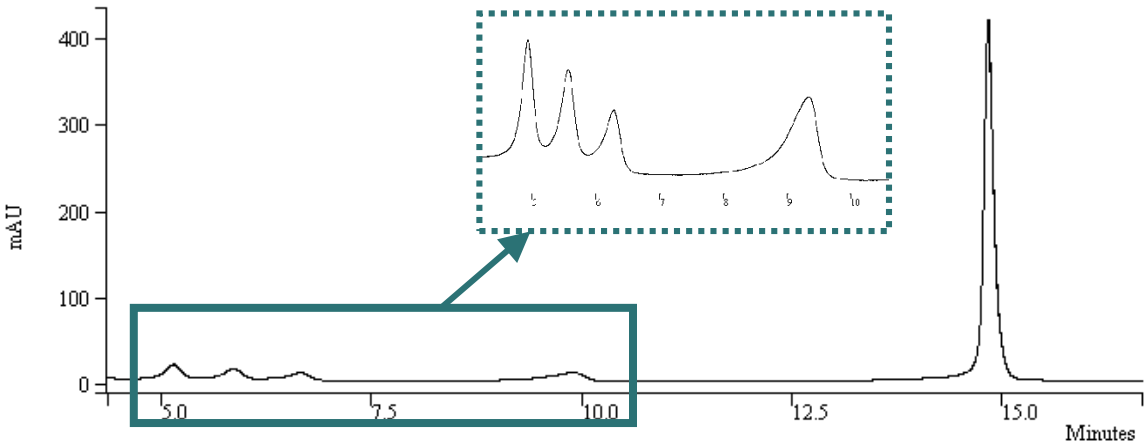

Figure 14. An HPLC chromatogram depicting the retention times of, from left to right, 2':3'-cUMP, 2'-UMP, 3'-UMP, uridine, and UpU eluted from a reverse phase analytical column using a phosphate buffer (pH 2.8, 25 mM):methanol gradient.

A cursorary examinination of the **53**:$Zn(II)_2$:($^{-}OCH_3$)-catalyzed transesterification of ApC was investigated in methanol at ambient temperature by HPLC (λ = 260 nm). The appearance of peaks belonging to products cytosine, methyl adenosine 2'-monophopshate (methyl 2'-AMP), methyl adenosine 3'-monophosphate (methyl 3'-AMP), and 2':3'-cyclic adenosine monophosphate (2':3'-cAMP) were monitored and their elution from a reverse phase analytical column was accomplished using the phosphate buffer (pH 2.8, 25 mM):methanol gradient described in Table 3. *p*-Nitrophenol was used as an internal standard and reaction products were identified by comparison with authentic cytosine, 3′-AMP, and ApC. Retention times of substrate and products are given in Table 5.

Table 5. The retention times of authentic analytes eluted from a reverse phase analytical column at ambient temperature using the phosphate buffer (pH 2.8, 25 mM): methanol gradient outlined in Table 3.

Analyte	**Retention Time (min.)**
Cytosine	7.6
3'-AMP	11.0
(3'→5')ApC	15.2
p-nitrophenol	19.0

The Zn(II) ion catalyzed transesterification of UpU and ApC were cursorily examined in ethanol and monitored by reverse phase HPLC (λ = 260 nm) at ambient temperature. The cleavage of UpU was observed by following the production of peaks corresponding to products uridine, ethyl uridine 2′-monophosphate (ethyl 2′-UMP), ethyl uridine-3′-monophosphate (ethyl 3′-UMP), and 2':3'-cUMP. The transesterification of ApC was followed by monitoring the appearance of product peaks cytosine, ethyl adenosine 2'-monophosphate (ethyl 2'-AMP), ethyl adenosine 3'-monophosphate (ethyl

3'-AMP), and adenyl 2':3'-cyclic monophosphate (2':3'-cAMP). The isomerization of ApC promoted by Zn(II):($^-$OEt) in ethanol was studied by following the appearance of a peak corresponding to (2'→5')ApC. *p*-Nitrophenol was used as an internal standard and reaction products were identified by comparison with authentic uridine, 2′:3′-cUMP, 2′-UMP, 3′-UMP, UpU, cytosine, 3'-AMP, and ApC.

4.1.3.2 Transesterification of 2':3'-cUMP promoted by 36:Zn(II)$_2$:($^-$OCH$_3$) in methanol

The cleavage of 2':3'-cUMP catalyzed by **36**:Zn(II)$_2$:($^-$OCH$_3$) (1.0 mM) was monitored by preparing the complex in anhydrous CH_3OH in a PTFE/silicone septa capped vial. The complex was formed by the sequential addition of 1:1:2 parts of $NaOCH_3$, **36**, $Zn(CF_3SO_3)_2$ and was allotted 45 min. for formation before inoculating it with 5 mM of *p*-nitrophenol and 0.25 mM of the HPLC marker (1:2:3:4 uridine, 2'-UMP, 3'-UMP, 2':3'-cUMP) at ambient temperature. A 15 μL aliquot of the reaction solution was immediately injected into the HPLC instrument.

4.1.3.3 Transesterification of UpU promoted by 36:Zn(II)$_2$:($^-$OCH$_3$) and 53:Zn(II)$_2$:($^-$OCH$_3$) in methanol

The **53**:Zn(II)$_2$:($^-$OCH$_3$) and **36**:Zn(II)$_2$:($^-$OCH$_3$) solutions were prepared in anhydrous CH_3OH in PTFE/silicone septa capped vials by the sequential addition of 1:1:2 parts of $NaOCH_3$, **53** or **36**, $Zn(CF_3SO_3)_2$ such that the final [**53**:Zn(II)$_2$:($^-$OCH$_3$)] ranged from 0.67 – 1.72 mM and the final [**36**:Zn(II)$_2$:($^-$OCH$_3$)] ranged from 0.5 – 1.5 mM. The dinuclear Zn(II) complex of **53** was allotted 25 minutes for formation (as described in Chapter 3) and **36**:Zn(II)$_2$:($^-$OCH$_3$) was allotted 45 minutes for formation.

After the allotted time for formation, each catalyst was introduced to the internal standard (5 mM of *p*-nitrophenol) and substrate (0.25 mM of UpU). The reactions were performed in duplicate at ambient temperature. At various times 15 μL aliquots were withdrawn and injected into the HPLC instrument for analysis.

The stability of the **53**:$Zn(II)_2$:($^-OCH_3$) complex was explored in Chapter 3 (Figure 6). The stability of the **36**:$Zn(II)_2$:($^-OCH_3$) complex in methanol was determined by examining the change in the rate of the catalyzed transesterification of HPNPP as a function of time at ^s_spH 9.8 ± 0.1, 25.0 ± 0.1 ^oC by stopped-flow reaction kinetics. The **36**:$Zn(II)_2$:($^-OCH_3$) complex (1.0 mM) was allowed to sit at ambient temperature in a sealed vial and the observed first order rate constants for the catalyzed methanolysis of HPNPP (0.05mM) were determined at various times over 145 hours by fitting the absorbance vs time data to a first order exponential model.

4.1.3.4 Transesterification of UpU and ApC promoted by Zn(II):($^-$OEt) in ethanol

The transesterification of UpU and ApC catalyzed by Zn(II):($^-$OEt) (1.0 mM) was examined in ethanol at ambient temperature. In a PTFE/silicone septa capped vial, 1 equivalent of each $Zn(CF_3SO_3)_2$ and NaOEt were combined in anhydrous ethanol. The vial was then introduced to the internal standard (5 mM of *p*-nitrophenol) and substrate (0.25 mM of UpU or ApC). At various times 15 μL aliquots were withdrawn and injected into the HPLC instrument for analysis.

4.2 Results

4.2.1 Uridine inhibition of the catalytic activity of 36:Zn(II)$_2$:($^-$OCH$_3$) and 53:Zn(II)$_2$:($^-$OCH$_3$) in methanol

The catalytic activity of **36**:Zn(II)$_2$:($^-$OCH$_3$) and **53**:Zn(II)$_2$:($^-$OCH$_3$) towards the cleavage of HPNPP were independently examined in the presence of increasing amounts of uridine at 25.0 ± 0.1 ^{o}C. Both complexes exhibited an appreciable reduction in HPNPP cleaving activity upon the introduction of uridine. Inhibition constants (K_{inhib}) for the **53**:Zn(II)$_2$:($^-$OCH$_3$)- and **36**:Zn(II)$_2$:($^-$OCH$_3$)-catalyzed cleavage of HPNPP were determined to be (2.08 ± 4.84) x 10^{-6} and (7.57 ± 0.07) x 10^{-5} mM (Figures 15 and 16), by fitting the kinetic and [inhibitor] data to the strong inhibition Eq. (5)[82]:

$$(5)\quad k_{obs} = k_{cat}(1-(1+K_{inhib}*[S]+[Cat]*K_{inhib}-X))/(2K_{inhib})/[S]$$

where:

$$X = (1+2K_{inhib}*[S]+2*[Cat]*K_{inhib}+K_{inhib}{}^2*[S]^2-2*K_{inhib}{}^2*[Cat][S]+[Cat]^2*K_{inhib}{}^2)^{0.5}$$

where [Cat] is the concentration of the dinuclear Zn(II) complex of **53** or **36** corrected for triflate inhibition (K_i = 7.2 mM for **53**:Zn(II)$_2$:($^-$OCH$_3$) (Chapter 3, Figure 7) and 14.9 mM for **36**:Zn(II)$_2$:($^-$OCH$_3$)[96]), X is the concentration of uridine, and a is the Y-intercept.

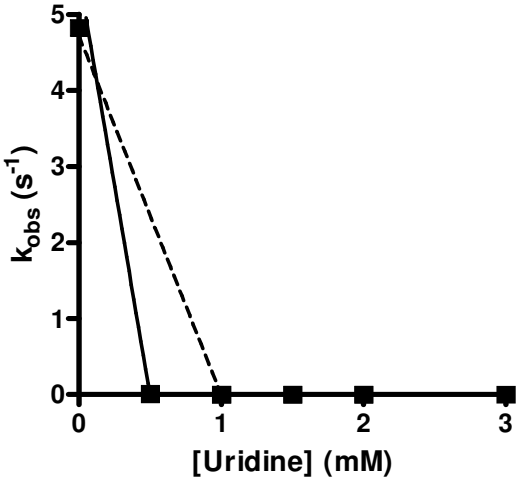

Figure 15. Plot of the observed first order rate constants for the methanolysis of HPNPP (0.05 mM) catalyzed by [**53**:$Zn(II)_2$:($^{-}OCH_3$)]$_{total}$ (1.0 mM) as a function of increasing amounts of [uridine] at 25.0 ± 0.1°C, $^{s}_{s}$pH 9.47 ± 0.17. The dotted line is a fit of the data to the strong inhibition Eq. (5) and assuming a 1:1 inhibition of the catalyst by uridine. The unbroken line is a fit of the data to the strong inhibition Eq. (5) assuming a 1:2 inhibition of two molecules of catalyst for every molecule of uridine giving a uridine inhibition constant, K_{inhib}, of (2.08 ± 4.84) x 10^{-6} mM, r^2 = 0.990.

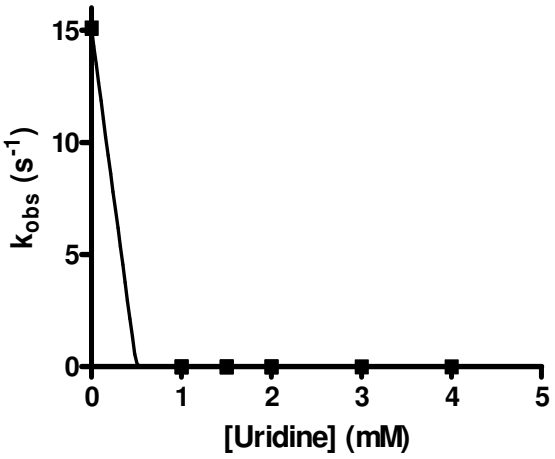

Figure 16. Plot of the observed first order rate constants for the methanolysis of HPNPP (0.05 mM) catalyzed by [**36**:$Zn(II)_2$:($^{-}OCH_3$)]$_{total}$ (1.0 mM) as a function of increasing amounts of [uridine] at 25.0 ± 0.1°C, $^{s}_{s}$pH 9.47 ± 0.17. Fitting of the data to the strong inhibition Eq. (5) and assuming a 1:2 inhibition of two molecules of catalyst for every molecule of uridine gives a uridine inhibition constant, K_{inhib}, of (7.57 ± 0.07) x 10^{-5} mM, r^2 = 1.000.

4.2.2 The stability of 36:Zn(II)$_2$:($^-$OCH$_3$) in methanol

The stability of **36**:Zn(II)$_2$:($^-$OCH$_3$) as a function of time was examined to minimize the depression of observed rate constants due to complex decomposition as a function of time. A fit of the observed catalytic first order rate constant (k_{obs}) for promoting the cleavage of **1**a vs time reveals a decrease in activity that can be fit to a first order decay, giving a kinetic stability constant (k_s) of (3.86 ± 0.07) x 10^{-6} s^{-1} ($t_{1/2}$ of 50 h) (Figure 17). The stability of the dinuclear Zn(II)$_2$ complexes of **36** and **53** in methanol were both corrected for as the time course of their reaction with diribonucleotide substrates impinges on their stability. This is discussed below.

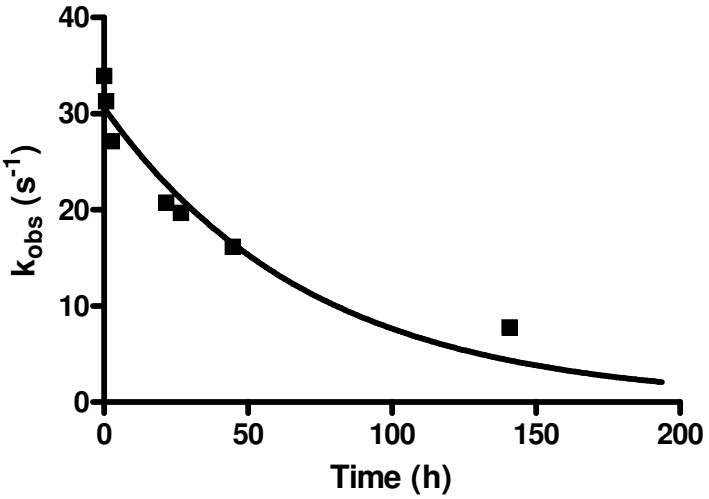

Figure 17. Plot of the observed first order rate constants for the methanolysis of 0.05 mM **1**a catalyzed by 1.0 mM [**36**:Zn(II)$_2$:($^-$OCH$_3$)]$_{total}$ (allotted 45 minutes for formation) as a function of time determined from the rate of appearance of product phenol at 320nm, ^s_spH 9.8 ± 0.1, and 25.0 ± 0.1°C. Fitting of the data to a first-order exponential decay equation ($k_{obs}(t) = k_{obs}(0)e^{-ks*t} + A$, where at A is the plateau and is assumed to be 0) gives a stability constant, k_s, of (3.86 ± 0.07) x 10^{-6} s^{-1} ($t_{1/2}$ = 50 h) for **36**:Zn(II)$_2$:($^-$OCH$_3$), r^2 = 0.928.

4.2.3 Transesterification of 2':3'-cUMP promoted by 36:Zn(II)$_2$:($^-$OCH$_3$) in methanol

In the presence of 1.0 mM **36**:Zn(II)$_2$:($^-$OCH$_3$) the ring opening of 2':3'-cUMP was examined in methanol at ambient temperature. Immediately following the introduction an internal standard (*p*-nitrophenol, 5 mM) and a 1:2:3:4 HPLC marker (0.25 mM) consisting of uridine, 2'-UMP, 3'-UMP, and 2':3'-cUMP, respectively, to the catalyst complex a 15 μL aliquot of the reaction mixture was removed and injected into the HPLC instrument for analysis. The resulting HPLC chromatogram was compared to the retention times previously determined for the marker in the absence of catalyst. Two peaks belonging to 2'-UMP and 3'-UMP were present in the chromatogram, however the peak corresponding to 2':3'-cUMP was absent and it can be concluded that ring opening occurs too quickly to be observed using the methodology employed (Figure 18). The two peaks present in the HPLC chromatogram between 8 and 10 minutes were interpreted to belong to methyl 2'-UMP and methyl 3'-UMP, respectively. It is reasonable to assume that methyl 2'-UMP was eluted before methyl 3'UMP as 2'-UMP eluted before 3'-UMP from the C18 reverse phase column and under the HPLC conditions used. Their production and presence in the reaction mixture was confirmed by ES$^-$/MS. Authentic methyl 2'-UMP and methyl 3'-UMP were not commercially available nor were they synthesized for their use in determining retention times for these analytes under the HPLC conditions employed in this study.

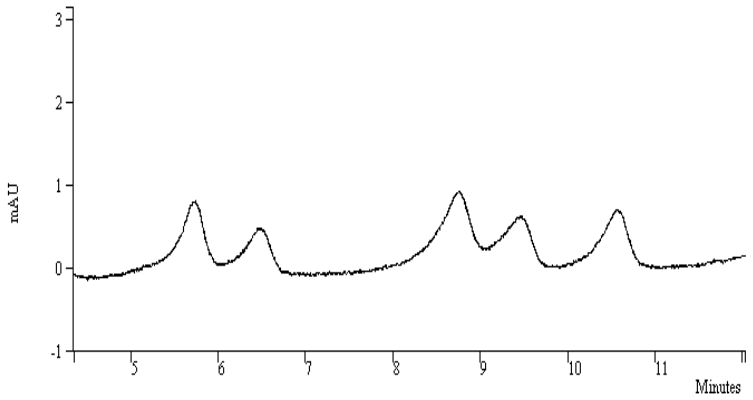

Figure 18. An HPLC chromatogram depicting the elution of a 1:2:3:4 HPLC marker (0.25 mM) consisting of uridine, 2'-UMP, 3'-UMP, and 2':3'-cUMP from a reverse phase analytical column at ambient temperature using a phosphate buffer (pH 2.8, 25 mM):methanol gradient. The transesterification of 2':3'-cUMP catalyzed by **36**:$Zn(II)_2$:($^-OCH_3$) (1.0 mM) resulted in the peaks belonging to methyl 2'-UMP and methyl 3'-UMP and the absence of the peak corresponding to 2':3'-cUMP. The order of elution from left to right is 2'-UMP, 3'-UMP, methyl 2'-UMP, methyl 3'-UMP, and uridine.

4.2.4 Transesterification of UpU promoted by 36:$Zn(II)_2$:($^-OCH_3$) and 53:$Zn(II)_2$:($^-OCH_3$) in methanol

The catalytic efficacies of two dinuclear Zn(II) small molecule catalysts towards the cleavage of UpU were studied in methanol. The substrate reactivity was measured by the HPLC methodology described above and the rate of catalyzed transesterification was determined from the relative areas of the product peaks methyl 2'-UMP, methyl 3'-UMP, and uridine (Figures 19 and 20, also see Appendix II, Figures 7-26S). First order rate constants (k_{obs}) were determined and corrected for diminishing catalyst activity over the course of the reaction by fitting the relative product peak area vs time data to Eq. (6):

$$(6) \qquad [P]_t = R\infty*(1-e^{(-kobs/ks)*[Cat]*(1-X))})$$

where,

$$X = e^{(-ks*t)}$$

and,

$$R\infty = [P]_t/(1 - [S]_t/[S]_0)$$

and $[P]_t$ is the relative product peak area at some time, $R\infty$ is the relative product peak area at $t = \infty$, $[S]_t$ is the relative substrate peak area at some time, $[S]_0$ is the relative substrate peak area at $t = 0$, [Cat] is the concentration of **53**:$Zn(II)_2$:($^-OCH_3$) or **36**:$Zn(II)_2$:($^-OCH_3$), and k_s is the stability constant determined for each catalyst complex. Relative product peak areas were determined from the summation of the area (counts) of methyl 2'-UMP, methyl 3'-UMP, and uridine taken over the area of the internal standard *p*-nitrophenol peak.

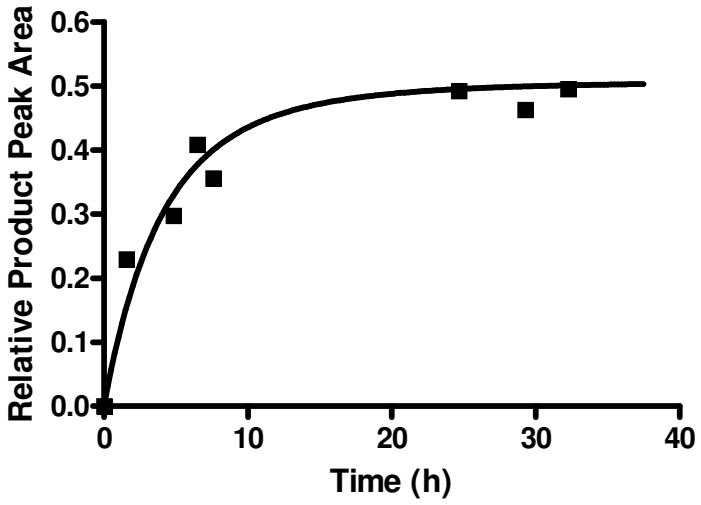

Figure 19. The decomposition of UpU (0.25 mM) catalyzed by [**53**:$Zn(II)_2$:($^-OCH_3$)]$_{free}$ (0.64 mM) in methanol at ambient temperature. Fitting the relative product peak area (see text) vs time data to Eq. (6) gives $k_{obs} = (6.64 \pm 0.77) \times 10^{-5}$ s^{-1}, $y_{max} = 0.510$, and $r^2 = 0.945$.

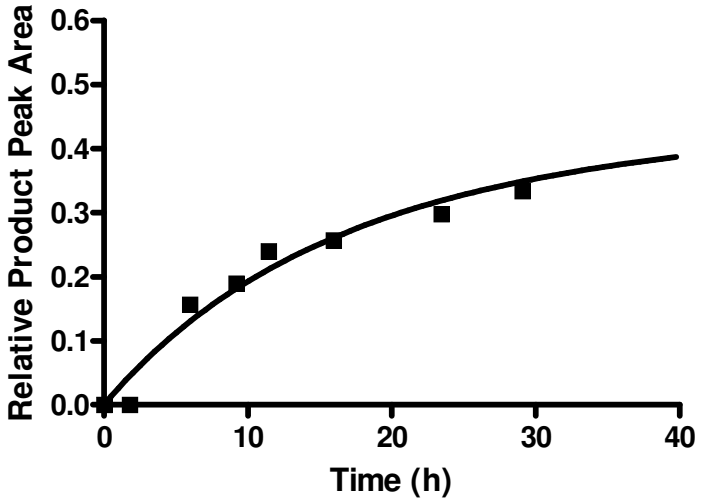

Figure 20. The decomposition of UpU (0.25 mM) catalyzed by [**36**:$Zn(II)_2$:($^{-}OCH_3$)]$_{free}$ (0.79 mM) in methanol at ambient temperature. Fitting the relative product peak area (see text) vs time data to Eq. (6) gives k_{obs} = (1.57 ± 0.10) x 10^{-5} s^{-1}, y_{max} = 0.470, r^2 = 0.962.

The k_{obs} data obtained were plotted as a function of [catalyst]$_{free}$ by accounting for triflate inhibition (K_i = 14.9 mM for **36**:$Zn(II)_2$:($^{-}OCH_3$) and K_i = 7.2 mM for **53**:$Zn(II)_2$:($^{-}OCH_3$), Chapter 3).[53] The data were fit to a linear regression analysis and the second order rate constants obtained for the decomposition of UpU catalyzed by **53**:$Zn(II)_2$:($^{-}OCH_3$) and **36**:$Zn(II)_2$:($^{-}OCH_3$) in methanol. These values are 1.21 ± 0.17 $M^{-1}s^{-1}$ and (7.04 ± 0.99) x10^{-2} $M^{-1}s^{-1}$, respectively (Figures 21 and 22).

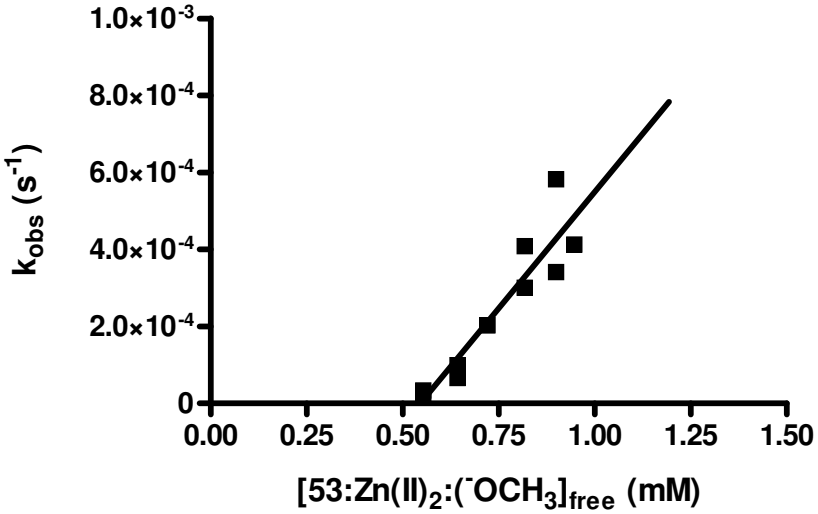

Figure 21. A plot of k_{obs} vs [**53**:$Zn(II)_2$:($^-OCH_3$)]$_{free}$ for the catalyzed methanolysis of UpU (0.25 mM) determined from the rate of appearance of product peaks corresponding to methyl 2'-UMP, methyl 3'-UMP, and uridine at 260 nm, and ambient temperature. The linear regression gives $k_2 = 1.21 \pm 0.17$ $M^{-1}s^{-1}$ with an intercept of X = 0.546 mM, $r^2 = 0.857$.

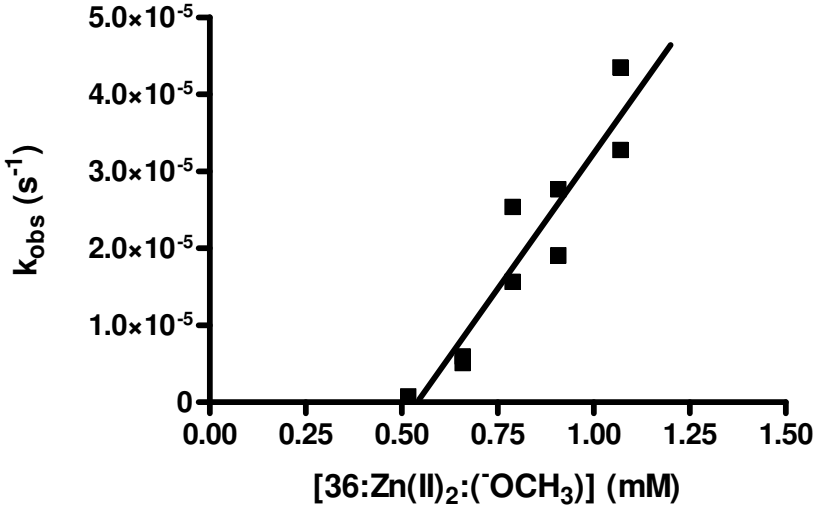

Figure 22. A plot of k_{obs} vs [**36**:$Zn(II)_2$:($^-OCH_3$)]$_{free}$ for the catalyzed methanolysis of UpU (0.25 mM) determined from the rate of appearance of product peaks corresponding to methyl 2'-UMP, methyl 3'-UMP, and uridine at 260 nm, and ambient temperature. The linear regression gives $k_2 = (7.04 \pm 0.99) \times 10^{-2}$ $M^{-1}s^{-1}$ with an intercept of = 0.540 mM, $r^2 = 0.879$.

A constant X-intercept of ~ 0.50 mM was observed for the cleavage of 0.25 mM of UpU over the concentrations of dinuclear Zn(II) complexes of **53** and **36** employed. This can be interpreted to imply a requirement for more than two equivalents of each catalyst to cleave an equivalent of substrate.

4.2.5 Transesterification of ApC promoted by 53:Zn(II)$_2$:($^-$OCH$_3$) in methanol

The **53**:Zn(II)$_2$:($^-$OCH$_3$)-catalyzed decomposition of ApC in methanol was explored at ambient temperature using the HPLC methodology described above. The rate of catalyzed substrate cleavage was determined from the relative area of the product peaks methyl 2'-AMP, methyl 3'-AMP, and cytosine. The selection of this dinucleotide was based upon the substantial inhibition uridine imbued upon **53**:Zn(II)$_2$:($^-$OCH$_3$) and **36**:Zn(II)$_2$:($^-$OCH$_3$) in methanol. Nucleotide bases A and C lack the acidic N3 proton that uridine possesses and that is known to bind to and kill the activity of metallic small molecule complexes.[100] Despite the absence of Zn(II) ion binding to the nucleobase, cleavage of ApC occurred on an extremely slow time scale. The slow reactivity of ApC taken together with the instability of the catalyst complex over time make ApC an undesirable substrate for the study of diribonucleotide decomposition; the **53**:Zn(II)$_2$:($^-$OCH$_3$)-catalyzed cleavage of ApC was not explored further.

4.2.6 Transesterification of UpU and ApC promoted by Zn^{2+}:($^-$OEt) in ethanol

The transesterification of diribonucleotides UpU and ApC catalyzed by Zn^{2+}:($^-$OEt) was examined in ethanol. Eliminating the bulky ligand (**36** and **53**) was suspected to enhance the reactivity of these bulky substrates. In addition, substantial rate accelerations had been reported by our group for the transesterification of HPNPP

catalyzed by Zn^{2+}:($^{-}$OEt).[99] Substrate reactivity was measured by the HPLC methodology described above. The cleavage of UpU was extremely slow and uninteresting; a thorough analysis of reaction rates was not performed. Cleavage of ApC was unobserved in the presence of Zn^{2+} ions in ethanol. However, isomerization of the (3'→5') diribonucleotide to its (2'→5') isomer was, remarkably, observed and the peak corresponding to ApC was observed to split into two peaks as a function of time. This observation was interpreted to be caused by the isomerization of the diribonucleotide. (2'→5')ApC was not commercially available or synthesized to unmistakably identify the peak, however its retention time and the absence of any peaks corresponding products support it being the ApC isomer. More work needs to be executed to confirm its identity. Of the catalytic systems employed for the cleavage of UpU and ApC the Zn^{2+}:($^{-}$OEt) complex in ethanol was the only catalyst to mediate isomerization. A thorough analysis was hindered by time restraints and is the future work of our group.

4.3 Discussion

The catalyzed cleavage of UpU and ApC by the dinuclear Zn(II) complexes of **36** and **53**, and Zn(II) ions in media of reduced polarity was investigated. While the rates of reaction observed can hardly be characterized as impressive even for the most reactive of the systems employed, there are a few noteworthy observations that can be made.

Firstly, the transesterification of UpU promoted by the dinuclear Zn(II) complexes of **36** and **53** produce what we surmise are methyl 2'-UMP and methyl 3'-UMP without the observable formation of the cyclic intermediate 2':3'-cUMP. In fact, the cleavage of authentic 2':3'-cUMP catalyzed by **36**:$Zn(II)_2$:($^{-}OCH_3$) occurred too

quickly to be observed using the HPLC methodology employed in this study. Additionally, the cleavage of (3'→5')UpU was unaccompanied by isomerization as (2'→5')UpU was unobserved. These findings could support a concerted intramolecular attack of the 2'-OH group on the phosphorus centre and departure of the uridine leaving group subsequently followed by a fast ring opening of the 2':3'-cUMP intermediate (Chapter 1, Scheme 1). Alternatively, a two step reaction with fast cleavage of a phosphorane intermediate coupled with the fast opening of 2':3'-cUMP could account for the observations. Further experimentation is required to distinguish between a general base-catalyzed deprotonation of the 2'-OH group and a metal-coordinated intramolecular nucleophile (Chapter 1, Figure 3).

The involvement of a general base to deprotonate the 2'-OH group can be observed by substituting the methanol solvent for CH_3OD or CD_3OD. A solvent deuterium kinetic isotope effect greater than unity would be observed in this case. If the reaction proceeds through a metal-coordinated intramolecular nucleophile then no, or possibly a small inverse, kinetic isotope effect would be observed. CD_3OD is slightly more acidic than CH_3OH and would account for a small inverse effect.

The second order rate constants obtained for the cleavage of UpU were a factor of ~ 20 greater for the dinuclear Zn(II) complex of **53** over that of **36**. The enhanced reactivity of **53**:Zn(II):($^-OCH_3$) may be attributed to the additional flexibility imparted by the extended methylene bridge spacer of **53** with respect to **36** and its ability to better accommodate the bulky diribonucleotide substrate.

The dinuclear Zn(II) complexes of **53** and **36** afforded rate enhancements of ~ 10^{11} and 10^{12}, respectively, for the catalyzed cleavage of HPNPP in methanol over the background methoxide-promoted reaction.[67] While the rate of the methoxide-promoted transesterification of UpU has yet to be determined, a second order rate constant of 0.0011 $M^{-1}s^{-1}$ for the hydroxide-promoted decomposition of UpU has been reported.[62a] The hydroxide-promoted cleavage of phosphate diesters are typically 10-fold greater than those observed for the methoxide-promoted reactions and this discrepancy is a feature of moving to a medium of reduced polarity which more poorly solvates the anionic nucleophile and substrate. Clearly, the reactivity increase expected for the catalyzed decomposition of UpU with respect to the base-promoted reaction was not seen. It has been previously shown that the acidic N3 protons of uridine and thymidine inhibit the catalytic activity of metal-binding complexes in solution.[100] Uridine inhibition constants of (7.12 ± 0.01) x 10^{-4} mM and (1.27 ± 0.20) x 10^{-4} mM were determined respectively for **53**:$Zn(II)_2$:($^-OCH_3$) and **36**:$Zn(II)_2$:($^-OCH_3$). Uridine inhibition helps to reconcile the depressed rates of catalyzed UpU decomposition in methanol with respect to the expected rate for the methoxide-promoted reaction.

Upon inspection of the k_{obs} vs $[catalyst]_{free}$ plots in Figures 21 and 22, a notable X-intercept of ~ 0.50 mM was observed for the cleavage of 0.25 mM of UpU. It is apparent that catalytic activity requires more than two equivalents of each catalyst complex (**53**:$Zn(II)_2$:($^-OCH_3$) or **36**:$Zn(II)_2$:($^-OCH_3$)) per equivalent of substrate. Likely, the uridine moieties of UpU bind the dinuclear Zn(II) complexes with a higher affinity than does the phosphate diester.[100] Additionally, the electrostatic repulsion resulting

from the binding of multiple metal-binding complexes to UpU increasingly diminishes the attraction of the catalyst to the phosphate core and supresses the rate of the catalyzed diribonucleotide cleavage**.**

The **53**:$Zn(II)_2$:($^-OCH_3$)-catalyzed transesterification of ApC was examined to eliminate the effects that uridine inhibition has on the cleavage of UpU. The dinuclear Zn(II) complex of **53** was selected as it displayed greater activity towards the transesterification of UpU over **36**:$Zn(II)_2$:($^-OCH_3$). ApC exhibited even less reactivity towards catalyzed cleavage than what was observed for UpU. A full analysis of the rate of **53**:$Zn(II)_2$:($^-OCH_3$)-catalyzed cleavage of ApC was not undertaken due to its inconsequential reactivity. Considerable attention should be paid to the suppressed reactivity of ApC with respect to that of UpU mediated by the dinuclear Zn(II) catalyst. It is reasonable to speculate that leaving group assistance is afforded by the complex coordinating itself to a 5'-uridine moiety. It is also reasonable to attribute the enhanced reactivity of the uridine containing substrate to a better recruitment and binding of catalyst. Obviously, a tradeoff may exist between leaving group assistance and catalyst recruitment and the inhibition of catalytic activity caused by substrates containing a uridine nucleobase.

It could be contended that the depressed rate of UpU cleavage mediated by dinuclear Zn(II) complexes **53** and **36** in methanol was a symptom not only of uridine inhibition but of the bulk of the substrate and these catalysts. Higher cleavage rates were observed for the complex with the more flexible alkane spacer and thus it was assumed that by eliminating the bulk of the metal-binding complex the rate of catalyzed UpU

decomposition may be enhanced . The Zn^{2+}:($^{-}$OEt)-catalyzed cleavage of UpU and ApC was explored in ethanol. While appreciable rates of catalysis have been observed for the cleavage of HPNPP by Zn^{2+}:($^{-}$OEt) in ethanol,[98] the cleavage of the aforementioned diribonucleotides by Zn^{2+}:($^{-}$OEt) in ethanol was unimpressive.

It has been previously reported that anionic phosphate diesters bind tightly to Zn^{2+} ions in ethanol[60a] and that this effect is imbued by the depressed dielectric constant (~ 23.4) of this solvent.[98] Enhancing the binding of metal ions to the phosphate centre of diribonucleotides was thought to alleviate the inhibition imparted by uridine containing phosphodiesters. The reactivity of UpU in the presence of Zn^{2+} ions in ethanol was investigated and unfortunately the transesterification reaction was exceedingly slower than that observed for the dinuclear Zn(II) complexes of **53** and **36** in methanol. The suppressed reactivity of UpU in the presence of Zn^{2+} ions in ethanol resulted in the dismissal of this catalytic system from further analysis. Additionally, no cleavage products were observed for the exposure of ApC to Zn^{2+} ions in ethanol. Interestingly, upon continued exposure to Zn^{2+}:($^{-}$OEt) the peak corresponding to ApC in the HPLC chromatogram was diminished and a peak which can be interpreted to belong to (2'→5')ApC developed. Thus, while Zn^{2+} ions in ethanol did not mediate the cleavage of ApC the electropositive metal ions in a reduced polarity medium were able to stabilize the dianionic phosphorane intermediate that is required for the isomerization of this substrate. This is the only system explored in this study wherein the isomerization reaction was observed. The isomerization of UpU in water has only been recently

reported[72] and is the only other example of a metal-complex stabilized phosphorane intermediate observed during the exploration of diribonucleotide cleavage.

4.4 Conclusions and future directions

A series of catalysts were explored in media of reduced polarity. The dinuclear Zn(II) complexes of **53** and **36** displayed the greatest activity towards the cleavage of UpU and as a result were most extensively studied. However, the second order rate constants for the cleavage of this substrate were less significant than the rate accelerations afforded by these complexes towards the cleavage of a series of RNA models (Chapter 3).[67] The reduced activity of these Zn(II) containing catalysts was attributed to inhibition due to loss of the acidic N3 proton of the substrate uridine moiety and the bulk of the complex and substrate. In the absence of uridine inhibition, diribonucleotide cleavage mediated by **53**:$Zn(II)_2$:($^-OCH_3$) was not improved and the rate of ApC cleavage was unimpressive. Reducing the bulk of the catalyst complexes and enhancing the binding of the phosphate centre to Zn^{2+} ions by studying the Zn^{2+}:($^-$OEt)-catalyzed cleavage of UpU and ApC in ethanol did not yield impressive rates of reaction. Catalyzed cleavage of the former was slow, however, reaction with the latter resulted in the production of (2'→5')ApC which confirms the existence of a pentacoordinate phosphorane intermediate.

It is apparent that the cursory results reported herein initiate the vast amount of research needed to be performed on the cleavage of ribonucleotides in reduced polarity media catalyzed by Zn^{2+} ions and Zn(II) ion complexing small molecules. Additional efforts are required to examine potential contributions of a 5'-uridine nucleobase to

leaving group assistance in the cleaving of diribonucleotides catalyzed by dinuclear Zn(II) complexes. A better understanding of the involvement of the 5'-uridine moiety can be achieved by investigating the catalyzed cleavage of a series of (3'→5')XpU diribonucleotides, where X can be adenosine, cytosine, or guanine, and the reactivity of these substrates can be compared to (3'→5')XpX and (3'→5')UpX substrates. Moreover, the recruitment of Zn(II)-binding complexes by uridine may provide site selectivity for base specific cleavage of oligoribonucleotides and further probing needs to be done.

Considerable efforts need to be applied also to a thorough ellucidation of the mechanism of the Zn^{2+}:($^{-}$OEt)-catalyzed cleavage of ApC in ethanol to confirm the existence of a pentacoordinate phosphorane intermediate which to date has only recently been observed.[72]

Chapter 5. Isomerization and cleavage of an RNA model by a dinuclear Zn(II) complex 36:$Zn(II)_2$:($^-OCH_3$)

Five-membered ring cyclic phosphate esters are possible intermediates in the hydrolysis of RNA under certain circumstances.[101] As the study of the cleavage of phosphate diesters with poor leaving groups is a challenge, cyclic phosphates serve as good substitutes as the strain associated with the ring makes them more reactive than their alkoxy counterparts.[102] The reactivity of the cyclic phosphate can be explored through the use of RNA models, such as HPNPP, which undergo an intramolecular transesterification to yield the cyclic intermediate (Scheme 14).[1a] HPNPP and 2-hydroxylpropyl methyl phosphate (HMP, **54**) were used to examine the reactivity of the cyclic phosphate (**56**). In this work we show that **36**:$Zn(II)_2$:($^-OCH_3$) catalyzes the ring opening of **56** with spectacular catalysis at ambient temperature and neutral $^{s}_{s}$pH (~9.8).[86a] Additionally, in the presence of **36**:$Zn(II)_2$:($^-OCH_3$) the rate of isomerization of **54/54a** exceeds that of expulsion of the methoxy group, thus confirming the existence of a pentacoordinate phosphorane intermediate, which has only recently been observed in a metal ion catalyzed phosphoryl transfer reaction.[72] This deviates from the opinion held to date regarding an associative concerted mechanism[7] and is further support for a two-step phosphate diester cleavage reaction with the formation of a stable dianionic phosphorane intermediate (**57**).

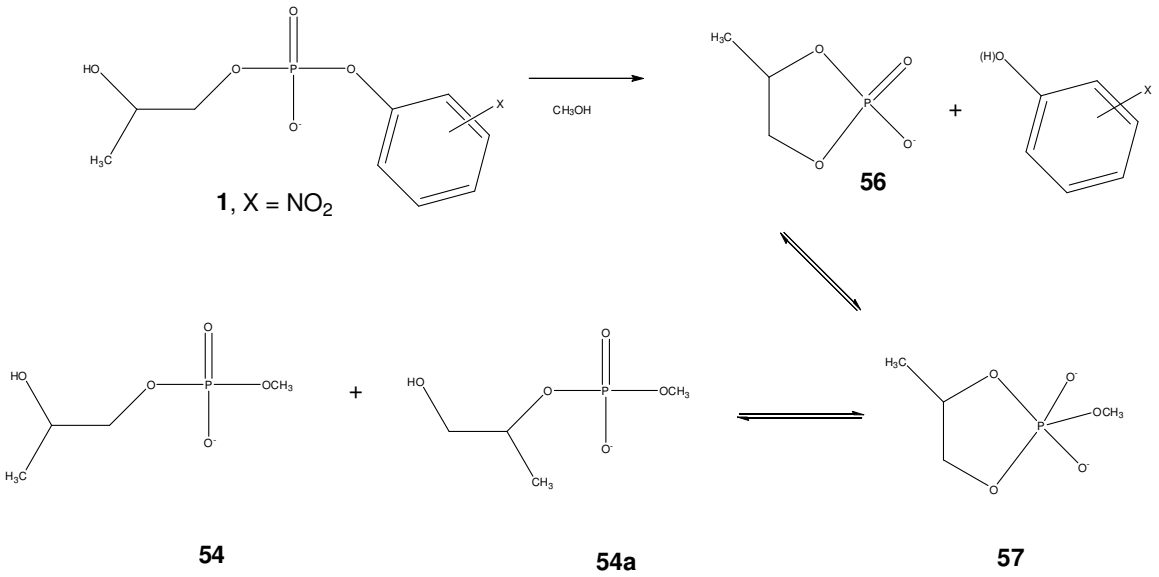

Scheme 14. The cyclization of HPNPP subsequently followed by the opening of cyclic phosphate **56** to yield isomers **54** and **54a**.

5.1 Experimental

5.1.1 Materials

Methanol (99.8% anhydrous), sodium methoxide (0.50 M solution in methanol), zinc(II) trifluoromethanesulfonate (98%), and sodium, lump, in kerosene (99%) were obtained from Aldrich and used without further purification. HCl (1N solution) was provided by Fisher Scientific and used as supplied. Methanol-d4 (D, 99.8%) was used as received from Cambridge Isotope Laboratories, Inc. The sodium salt of HPNPP (**1**a) was prepared by Tony Liu by a modified procedure[67] from that reported previously.[82] The dinuclear Zn(II) ligand (**36**) was prepared by Zhong-Lin Lu as described previously[96] from a procedure that was reported.[54] Z.-L. Lu also prepared sodium methoxide-d3 by adding sodium metal to methanol-d4.

Stock solutions of $Zn(CF_3SO_3)_2$, $NaOCH_3/NaOCD_3$, and **36** were independently

prepared to 50 mM in anhydrous CH_3OH and CD_3OD. A 50 mM stock solution of HCl and LiCl was prepared in anhydrous CH_3OH. A 50 mM stock solution of **54/54a** in a 92:8 ratio was prepared in CD_3OD.

5.1.2 Methods

^1H NMR spectra were determined at 600 MHz using a Bruker Avance-600 NMR spectrometer. High resolution exact MS spectra were obtained in ESI^- mode with N_2 carrier gas and direct syringe injection using an Applied Biosystems/MDS Sciex QSTAR XL QqTOF mass spectrometer. The **36**:$Zn(II)_2$:($^-OCH_3$) and **36**:$Zn(II)_2$:($^-OCD_3$) complexes were prepared in CH_3OH and CD_3OD, respectively, through the sequential 1:1:2 addition of $NaOCH_3$/$NaOCD_3$, **36**, and $Zn(OTf)_2$. The dinuclear Zn(II) complexes were allotted 45 minutes for formation prior to the introduction of substrate.

5.1.2.1 Methoxide-promoted opening of 56 in methanol-d4

The base-promoted cyclization of HPNPP occurs with the expulsion of *p*-nitrophenol which is subsequently followed by the opening of **56** to give isomers **54**(OCD_3) and **54a**(OCD_3). A solution was prepared containing 20.83 mM of HPNPP and 500 mM $NaOCD_3$ in 0.75 mL CD_3OD in an NMR tube and the transesterification of substrate was monitored at 25.0 ± 0.1°C using 600 MHz ^1H NMR.

5.1.2.2 Isomerization and transesterification of 54 promoted by 36:$Zn(II)_2$: ($^-OCH_3$)/($^-OCD_3$) in methanol/methanol-d4

The **36**:$Zn(II)_2$:($^-OCH_3$)-catalyzed cleavage and isomerizaton of **54/54a** was examined experimentally by the following three methods. First, the **36**:$Zn(II)_2$:($^-OCH_3$)-catalyzed cyclization of HPNPP and subsequent opening of **56** to give isomers **54** and

54a was followed by ^{1}H NMR (600 MHz) by preparing five solutions containing 3.13 mM of **36**:Zn(II)$_2$:($^-$OCH$_3$) and 2.81 mM of HPNPP in 1.50 mL of anhydrous CH$_3$OH at ambient temperature, ^s_spH 9.8 ± 0.1. HPNPP was introduced to the solution of **36**:Zn(II)$_2$:($^-$OCH$_3$) and the reaction was then manually quenched by adding four equivalents HCl and LiCl in one second intervals over the course of five seconds. Each solution was reconstituted in 0.75 mL of CD$_3$OD to provide samples for ^{1}H NMR analysis.

In the second experiment, the **36**:Zn(II)$_2$:($^-$OCH$_3$)-catalyzed isomerization of **54** and **54a** was monitored by preparing six solutions each containing 3.13 mM of **36**:Zn(II)$_2$:($^-$OCH$_3$) and 2.81 mM of HPNPP in 1.50 mL of anhydrous CH$_3$OH at ambient temperature, ^s_spH 9.8 ± 0.1. The reactions were quenched by adding four equivalents HCl and LiCl at 5 sec., 1 min., 4 min., 8 min., 12 min. and 16 min after the addition of substrate to catalyst. Solutions were evaporated to dryness and then each solution was prepared for ^{1}H NMR (600 MHz) in CD$_3$OD as described above.

In the last experiment, the rate constant for the **36**:Zn(II)$_2$:($^-$OCD$_3$)-catalyzed interconversion of **54** and **54a** and the rate of OCH$_3$/OCD$_3$ exchange on P were determined by reacting a 2.025 mM sample of independently synthesized **54/54a** (having a ratio of 92/8) with 2.25 mM of **36**:Zn(II)$_2$:($^-$OCD$_3$) in 0.75 mL of CD$_3$OD at 25.0 ± 0.1 ^{o}C and monitoring the reaction by 600 MHz ^{1}H NMR. The complete exchange of OCH$_3$ for OCD$_3$ was confirmed by ESI$^-$/MS. The NMR data for **54/54a** can be found in Appendix III.

5.2 Results

5.2.1 Methoxide-promoted opening of 56 in methanol-d4

The cyclization of HPNPP (20.83 mM) and opening of **56** promoted by 500 mM of $NaOCD_3$ in CD_3OD to give isomers **54**(OCD_3) and **54a**(OCD_3) was monitored by ^1H NMR (600 MHz) at ambient temperature . The signal at δ 6.45 (2H, d, $^3J_{H-H}$ = 12 Hz) belonging to the *ortho* protons of released *p*-nitrophenol(phenoxide) was used as a reference. Impurity peaks associated with $NaOCD_3$ in CD_3OD were found at 1.15 – 1.35 ppm and are apparent in Figure 23. The $CHC\underline{H}_3$ doublets for **56**, **54**(OCD_3), and **54a**(OCD_3) at δ 1.345 (d, $^3J_{H-H}$ = 6 Hz), δ 1.175 (d, $^3J_{H-H}$ = 6 Hz), and δ 1.265 (d, $^3J_{H-H}$ = 6 Hz), respectively, were monitored (Figure 23). To minimize the influence of impurities and the associated error in integrating the peak areas of the signals of interest the upfield half of each doublet was integrated.

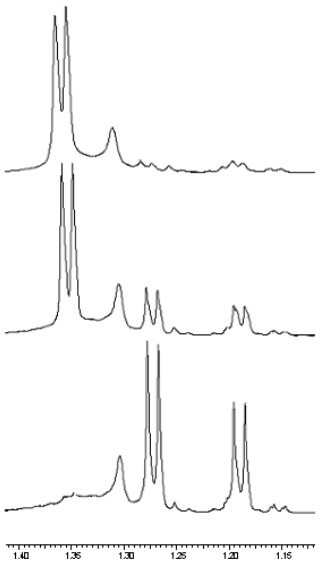

Figure 23. Partial ^1H NMR spectra for the methanolysis of **56** promoted by 500 mM of $NaOCD_3$ at 25.0 ± 0.1 ^oC after: (a) 10 minutes, (b) 5 hours, and (c) 50 hours.

The integrated intensity data as a function of time was plotted for the disappearance of **56** and appearance of **54** and **54a** and fit to Eq. (7):

(7) relative peak area = $A + b*e^{(-k*[Cat])}$

where A is the Y-intercept, k is the rate constant for the disappearance of **56** or appearance of **54** and **54a**, and b is an independent variable which was allowed to "float" to maximize fitting. The rate constant for the formation of the final resulting 79/21 mixture of **54a**(OCD_3)/**54**(OCD_3) was (5.54 ± 0.27) x 10^{-5} s^{-1} and was (6.04 ± 0.64) x 10^{-5} s^{-1} for the disappearance of **56** (Figure 24). The methoxide-promoted opening of **56** in methanol exhibits only an approximate two-fold reduction in the second order rate constant with respect to that determined for the hydroxide-promoted opening (2.35 x 10^{-4} $M^{-1}s^{-1}$).[103]

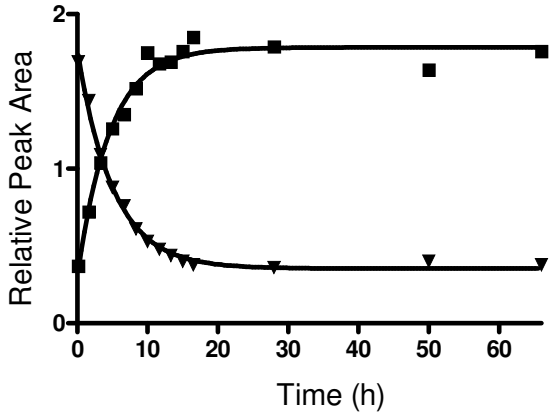

Figure 24. A plot of the relative peak area vs time for the methanolysis of **56** promoted by 500 mM $NaOCD_3$ in CD_3OD determined from: the appearance of peaks at δ 1.175 (d, $^3J_{H-H}$ = 6 Hz) and δ 1.265 (d, $^3J_{H-H}$ = 6Hz) belonging to **54** and **54a**, respectively (■), and; the disappearance of the signal at δ 1.345 (d, $^3J_{H-H}$ = 6 Hz) belonging to **58** (▼) at 25.0 ± 0.1 °C. A signal at δ 6.45 (2H, d, $^3J_{H-H}$ = 12 Hz) belonging to the *ortho* protons of *p*-nitrophenol was used as reference and the peak area of half of the signals corresponding to **54** and **54a** were determined to minimize the influence of impurity. Fitting the integrated intensity data to Eq. (7) gives rate constants of (6.0 ± 0.6) x 10^{-5} s^{-1} (■) and (5.5 ± 0.3) x 10^{-5} s^{-1} (▼).

5.2.2 Opening of 56 promoted by 36:Zn(II)$_2$:($^-$OCH$_3$) in methanol

The rates of cyclization of HPNPP (2.81 mM) and subsequent opening of **56** to give isomers **54** and **54a** catalyzed by 3.13 mM of **36**:Zn(II)$_2$:($^-$OCH$_3$) in methanol were monitored by ^{1}H NMR (600 MHz). The transesterification of HPNPP was monitored by determining the rate of disappearance of the signals at δ 7.435 (d, $^3J_{H-H}$ = 6 Hz) and δ 1.165 (d, $^3J_{H-H}$ = 6 Hz) belonging respectively to the *ortho* protons of HPNPP and the methyl group of HPNPP. The opening of **56** was monitored from the disappearance of the CH<u>CH$_3$</u> doublet at δ 1.355 (d, $^3J_{H-H}$ = 6 Hz) and the appearance of the CH<u>CH$_3$</u> doublets of **54** and **54a** at δ 1.185 (d, $^3J_{H-H}$ = 6 Hz) and δ 1.285 (d, $^3J_{H-H}$ = 6 Hz), respectively (Figure 25). All signals were referenced to the doublet corresponding to the *ortho* protons of released *p*-nitrophenol at δ 6.915 (d, $^3J_{H-H}$ = 6 Hz).

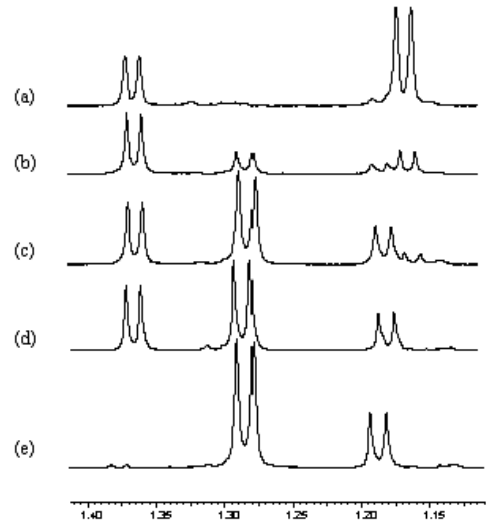

Figure 25. Partial ^{1}H NMR spectra for the opening of **56** catalyzed by 3.13 mM [**36**:Zn(II)$_2$:($^-$OCH$_3$)]$_{total}$ at ambient temperature determined after: (a) 0 seconds, (b) 1 second, (c) 2 seconds, (d) 3 seconds, and (e) 4 seconds. The signal at δ 1.355 (d, $^3J_{H-H}$ = 6 Hz) belongs to **56,** at δ 1.185 (d, $^3J_{H-H}$ = 6 Hz) belongs to **54**, and at δ 1.285 (d, $^3J_{H-H}$ = 6 Hz) belongs to **54a.**

Shown in Figure 26 is a plot of the time course for the integrated intensities of the ^{1}H signals corresponding to HPNPP, **56**, **54**, and **54a**. Using the signal at δ 6.915 (d, $^{3}J_{H\text{-}H} = 6$ Hz) corresponding to the *ortho* protons of released *p*-nitrophenol as a reference, the data were analyzed as follows. From the fitting of the corresponding integrated intensity data to a standard first order exponential equation, the pseudo-first order rate constant for the transesterification of HPNPP was determined to be $1.54 \pm 0.02\ s^{-1}$. This value was held constant to determine the rate constant for the appearance of **56**. The rate constant for the disappearance of **56** was determined from non-linear least squares (NLLSQ) fitting of the integrated intensity date to Eq. (8) and the appearance of **54** and **54a** were determined from an NLLSQ fitting of the integrated intensity data to Eq. (9) where Y is the peak intensity at time, t, C refers to the maximum peak intensity for the given signal, k_1 is the first order rate constant for formation of **56**, and k_2 is the rate constant for the **36**:$Zn(II)_2$:($^{-}OCH_3$)-catalyzed decomposition of **56** and formation of **54** and **54a**, the average of which is $0.9 \pm 0.2\ s^{-1}$.

(8) $Y = ((C*k1)/(k2-k1))*(e^{-k1*t}-e^{-k2*t})$

(9) $Y = C[1+\{(1/((k_1-k_2)*(k_2e^{(-k1*t)}-k_1e^{((k1-k2)*t)}))\}]$

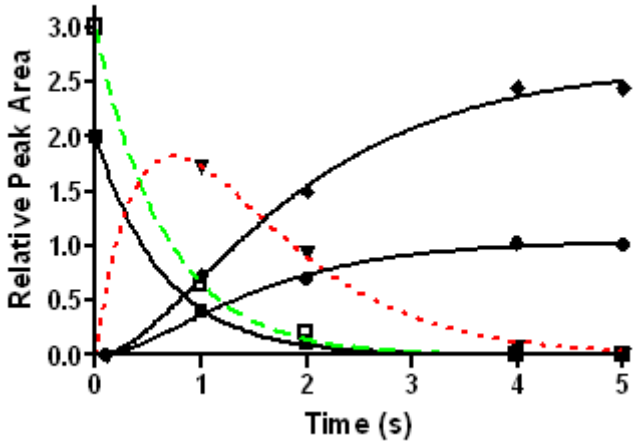

Figure 26. A plot of the relative integrated peak area vs. time for the transesterification of HPNPP (2.81 mM, □ and ■, $O\underline{CH_3}$ and the *ortho* protons at δ 1.165 and δ 7.435, respectively), and the opening of **56** (▼, $CH\underline{CH_3}$, δ 1.355) to give isomers **54** (●,$CH\underline{CH_3}$, δ 1.185) and **54a** (♦, $CH\underline{CH_3}$, δ 1.285) promoted by 3.13 mM of [**36**:$Zn(II)_2$:($^{-}OCH_3$)]$_{total}$ in anhydrous methanol at ambient temperature, $^{s}_{s}$pH 9.8 ± 0.1. The data □ and ■ were fit to first order decay equations ($y(t) = y(0)e^{-k1*t}$), ▼ to Eq. (10), and ● and ♦ to Eq. (11).

The conditional rate constant, k_1, for the decomposition of HPNPP promoted by **36**:$Zn(II)_2$:($^{-}OCH_3$) in methanol is much smaller than that previously seen using stopped-flow spectrophotometry.[67] The discrepancy in the reported values likely arises due the nature of the experiment: poorer mixing associated with the manual introduction of the substrate to the catalyst, the manual quenching of the reactions, and the higher concentration of catalyst and substrate used with a higher concentration of associated counterions to bind to and inhibit the activity of the catalyst complex.

5.2.3 Isomerization of 54 promoted by 36:Zn(II)$_2$:($^-$OCH$_3$) in methanol

The interconversion of **54** and **54a** catalyzed by **36**:Zn(II)$_2$:($^-$OCH$_3$) (3.13 mM) was monitored by ^{1}H NMR (600 MHz) at ambient temperature, ^s_spH 9.8 ± 0.1. The doublet corresponding to the *ortho* protons of released *p*-nitrophenol at δ 6.915 (d, $^3J_{H-H}$ = 6 Hz) was used as reference. Shown in Figure 27 are four partial spectra displaying the CHC<u>H$_3$</u> doublets of **54** and **54a** at δ 1.185 (d, $^3J_{H-H}$ = 6 Hz) and δ 1.285 (d, $^3J_{H-H}$ = 6 Hz), respectively, that clearly show the initially formed 79/21 product mixture of **54a/54** is kinetically controlled and that further exposure to **36**:Zn(II)$_2$:($^-$OCH$_3$) results in a final 35/65 thermodynamic equilibrium mixture of **54a/54**. Fitting the integrated intensity data as a function of time to a standard first order exponential equation gives a rate constant of (4.7 ± 0.5) x 10^{-3} s^{-1} for the catalyzed approach to equilibrium in CH$_3$OH ($t_{1/2}$ = 150 sec.) (Figure 28).

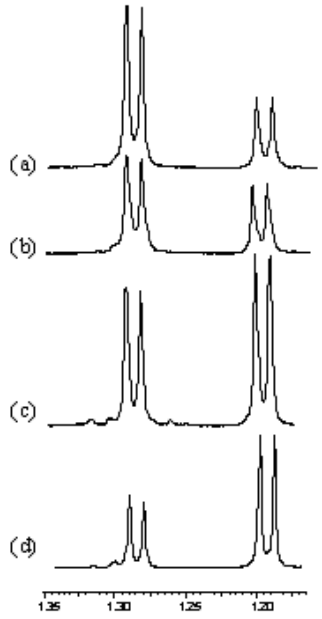

Figure 27. Partial ^{1}H NMR spectra for the methanolysis of **54** (δ 1.185) and **54a** (δ 1.285) catalyzed by 3.13 mM [**36**:Zn(II)$_2$:($^{-}$OCH$_3$)]$_{free}$ at ambient temperature after: (a) 5 seconds, (b) 1 minute, (c) 4 minutes, and (d) 16 minutes.

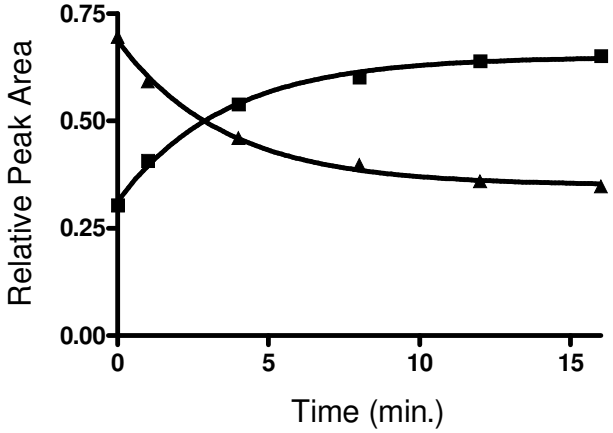

Figure 28. A plot of the relative peak area vs time for the interconversion of **54** and **54a** catalyzed by [**36**:Zn(II)$_2$:($^{-}$OCH$_3$)]$_{total}$ (3.13 mM) in CH$_3$OH determined from the appearance of the signal at δ 1.185 (d, $^{3}J_{H\text{-}H}$ = 6 Hz) belonging to **54** (■) and the disappearance of the signal at δ 1.285 (d, $^{3}J_{H\text{-}H}$ = 6 Hz) belonging to **54a** (▲) at ambient temperature, $^{s}_{s}$pH 9.8 ± 0.1. Peak areas are referenced to the sum of the areas of both peaks. Fitting the data to Eq. (7) gives a rate constant of (4.7 ± 0.5) x 10^{-3} s^{-1} for the catalyzed approach to equilibrium.

5.2.4 Isomerization and transesterification of 54 promoted by 36:Zn(II)$_2$:($^-$OCD$_3$) in methanol-d4

The catalyzed transesterification of **54** was further explored using an independently synthesized 8/92 mixture of **54a/54**. The sample (2.025 mM) was reacted with 2.25 mM **36**:Zn(II)$_2$:($^-$OCD$_3$) in CD_3OD and monitored by ^{1}H NMR (600 MHz) at 25.0 ± 0.1 ^{o}C. The signal at δ 4.60 belonging to $CD_3O\underline{H}$ was used as reference and integrated to a value of 100.00. The rate constant for the isomerization of **54** and **54a** to a final thermodynamic 32/68 mixture of **54a/54** (experimentally the same as in CH_3OH) was determined from the rate of appearance of the signal at δ 1.285 (d, $^3J_{H\text{-}H}$ = 6 Hz) belonging to **54a** and the disappearance of the signal at δ 1.185 (d, $^3J_{H\text{-}H}$ = 6 Hz) belonging to **54**. Fitting the integrated intensity data to a first order exponential expression, the rate constant for the attainment of equilibrium was determined to be (1.21 ± 0.08) x 10^{-3} s^{-1} (Figure 29). Comparing the values in CH_3OH and CD_3OD gives a k_H/k_D of 3.9.

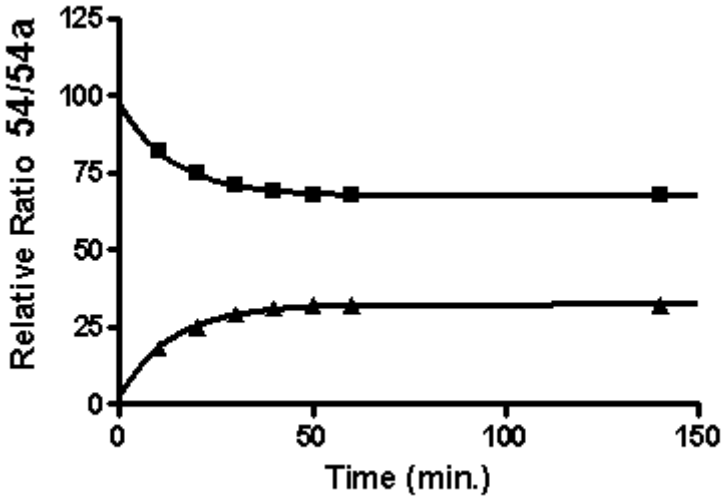

Figure 29. Plot of the time course for isomerization of **54/54a** (2.025 mM) catalyzed by [**36**:$Zn(II)_2$:($^-OCD_3$)]$_{total}$ (2.25 mM) in CD_3OD at 25.0 ± 0.1 ^oC. Relative ratios of **54/54a** were determined from the integrated intensities of the $CHC\underline{H_3}$ doublets of **54** (■) and **54a** (▲) at δ 1.195 and 1.295, respectively. Peak areas are referenced to the sum of the areas of both peaks to determine their relative ratio. Fitting the integrated intensity data to Eq. (7), the rate constant for the attainment of equilibrium was determined to be (1.21 ± 0.08) x 10^{-3} s^{-1}.

This experiment also gave the rate constant for the replacement of OCH_3 by OCD_3 from HMP from the disappearance of the signal at δ 3.685 (d, $^3J_{P-H}$ = 18 Hz) belonging to the OCH_3 group of **54** and **54a** (Figure 30). The integrated intensity data was fit to a first order exponential decay equation and a rate constant of (4.2 ± 0.5) x 10^{-4} s^{-1} was determined for the exchange (Figure 31). The complete exchange of the OCH_3 group for the OCD_3 group was confirmed by ESI$^-$/MS as the m/z = 169 peak of **54/54a** was absent and replaced by a signal at m/z = 172 belonging to **54**(OCD_3)**/54a**(OCD_3).

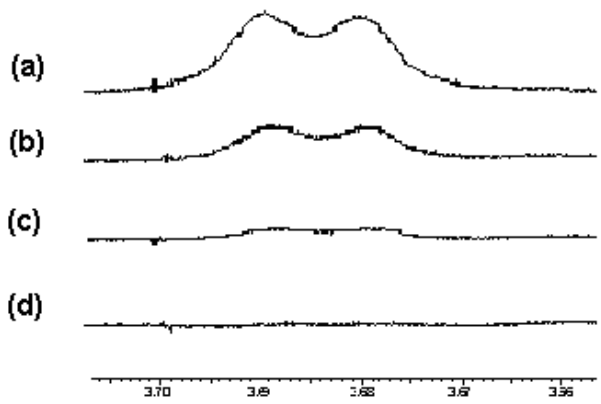

Figure 30. Partial ^{1}H NMR spectra for the methanolysis of **54/54a** (2.025 mM) catalyzed by 2.25 mM of [**36**:Zn(II)$_2$:($^{-}$OCD$_3$)]$_{total}$ at 25.0 ± 0.1 ^{o}C in CD$_3$OD showing the disappearance of the P-OC$\underline{H}_3$ peak at δ 3.685 after: (a) 10 minutes, (b) 40 minutes, (c) 60 minutes, and (d) 140 minutes.

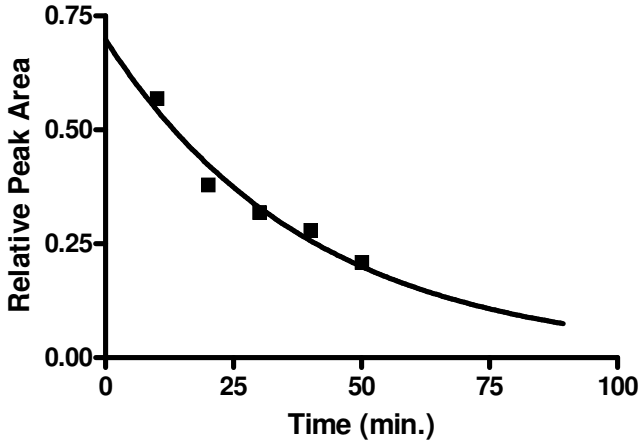

Figure 31. A plot of the relative peak area vs time for the methanolysis of **54** (2.025 mM) catalyzed by 2.25 mM [**36**:Zn(II)$_2$:($^{-}$OCD$_3$)]$_{total}$ determined from the rate of disappearance of the peak at δ 3.685 (d, $^{3}J_{P-H}$ = 18 Hz) corresponding to the methoxy group of **54** and **54a** in CD$_3$OD at 25.0 ± 0.1 ^{o}C. A solvent CD$_3$OH peak at δ 4.66 was used as reference and integrated to a value of 100.00. Fitting of the data to a one-phase exponential decay equation ($y(t) = y(0)e^{-kt} + y(\infty)$) gives a rate constant of (4.2 ± 0.5) x 10^{-4} s^{-1}.

5.3 Discussion

There are three main experimental observations to note. First, the opening of the cyclic phosphate (**56**) is accelerated by the presence of the dinuclear Zn(II) complex of **36**. The rate constant for its decomposition and formation of **54** and **54a** was determined to be 0.9 ± 0.2 s^{-1} in the presence of 3.13 mM **36**:$Zn(II)_2$:($^-OCH_3$) in methanol at ambient temperature. The partitioning of **54** and **54a** constitutes the second observation and requires a more in depth analysis.

In proteated solvent, the initial kinetic mixture of 71/29 of **54a/54** equilibrates to a thermodynamic 35/65 mixture upon further exposure to 3.13 mM **36**:$Zn(II)_2$:($^-OCH_3$) with a rate constant of (4.7 ± 0.5) x 10^{-3} s^{-1}. In deuterated solvent, the same thermodynamic equilibrium is reached and in the presence of 2.25 mM **36**:$Zn(II)_2$:($^-OCH_3$) the isomeric mixture of **54a/54** (2.025 mM) equilibrates from an initial ratio of 8/92 to 32/68 with a rate constant of (1.21 ± 0.08) x 10^{-3} s^{-1}. The rate constants for the approach to equilibrium show a solvent kinetic isotope effect of k_H/k_D = 3.9. This is consistent with a mechanism invoking a general base mediated deprotonation of the 2-OH group followed by the cyclization reaction. A similar mechanism was proposed for the reaction catalyzed by di- and trinuclear Ln(III) complexes in 80% DMSO water.[104] As both isomerization and OCH_3 group exchange require deprotonation of the 2-OH group of HMP the same kinetic isotope effect can be assumed for the **36**:$Zn(II)_2$:($^-OCH_3$)-catalyzed replacement of the OCH_3 group by an OCD_3 group in CD_3OD.

The third observation is the observed rate of exchange of the OCH_3 group of HMP with OCD_3 ((4.2 ± 0.5) x 10^{-4} s^{-1}). Taking into consideration a solvent deuterium

isotope effect of ~3.9, the catalyzed exchange of OCH_3 occurs 3.9-fold slower than the isomerization of **54** and **54a** in either CH_3OH or CD_3OD.

The above observations, when taken together, provide evidence for a two-step cleavage of this RNA model catalyzed by the dinuclear Zn(II) complex of **36** in methanol. This reaction proceeds with formation of a suite of pseudorotating pentacoordinate phosphorane intermediates (**57**) that partition between **56**, **54**, and **54a**, as in Scheme 15. A thorough analysis of the rates of interconversion of **54** and **54a** and partitioning of **57** through ring opening and expulsion of OCH_3 is included in Appendix III.

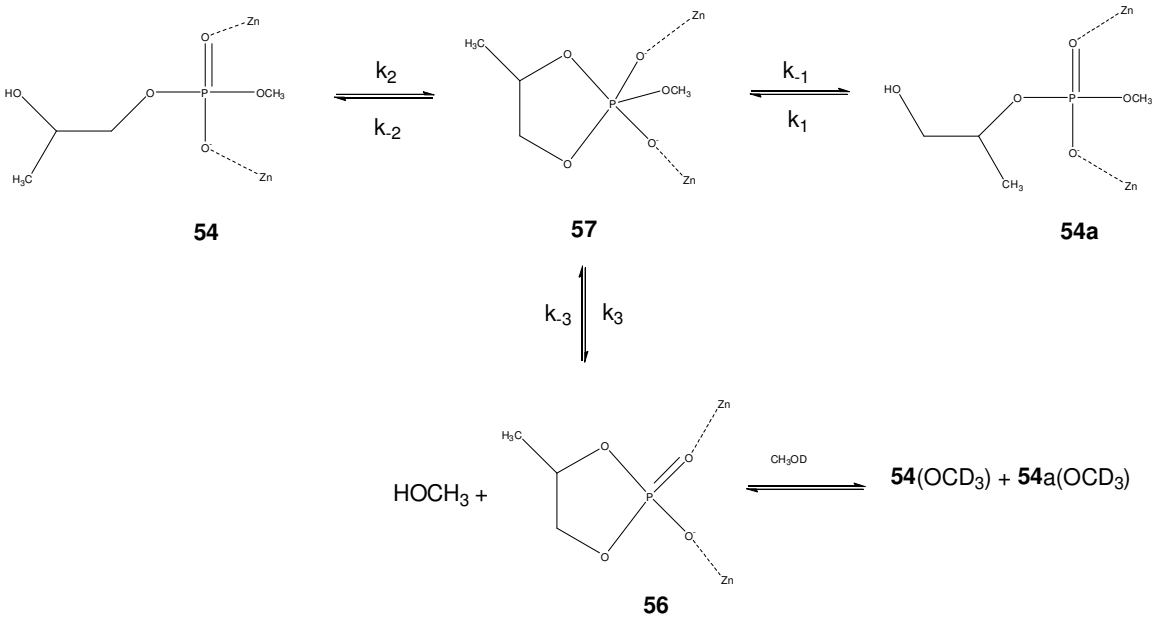

Scheme 15. Interconversion of the various species of interest catalyzed by **36**:$Zn(II)_2$:($^-OCH_3$) in methanol-d4 and the relevant rate constants. Zn(II) charges were omitted for simplicity.

The partitioning of **54a** and **54** from an initial kinetic mixture of 71/29, or 2.5, to the final equilibrium position of 35/65 with a rate constant of 4.7×10^{-3} s^{-1} that is the sum

of the forward and reverse reactions in CH_3OH provides sufficient information for the derivation of the k_1 and k_2 values for the closure of **54a** and **54**, respectively. These values were determined to be 1.06 x 10^{-2} s^{-1} and 2.32 x 10^{-3} s^{-1}, respectively, and their derivation is included in Appendix III. The discrepancy between the values determined for k_1 and k_2 likely arise from the differences in nucleophilicity between primary and secondary alkoxy groups. Factoring in a kinetic isotope effect of 3.9, the rate constant for the formation of **56** from **54** and **54a** in CH_3OH is 1.6 x 10^{-3} s^{-1} (4.2 x 10^{-4} s^{-1} x 3.9). Taken together, the catalyzed breakdown of **57** partitions to a 57:23:20 ratio of **54a**, **54**, and **56**. In other words, phosphorane intermediate **57** partitions into **54a** ~ 57% of the time, **54** ~ 23% of the time, and **56** ~ 20% of the time (Appendix III).

These results strengthen the case for the proposed mechanism previously elucidated for the **36**:$Zn(II)_2$:($^-OCH_3$)-catalyzed cyclization of a series of 2-hydroxylpropyl aryl phosphates (**1**a-g).[67] The Brønsted plot in Figure 32 shows the k_{cat}^{max} values determined for the unimolecular breakdown of substrates **1**a-g and the $^{s}_{s}pK_a$ values of the corresponding phenol. The k_{cat}^{max} values were determined from the rate of formation of phenol products under conditions of saturation binding of substrates **1**a-g to **36**:$Zn(II)_2$:($^-OCH_3$) in methanol. Assuming that the K_M value for **54** binding to **36**:$Zn(II)_2$:($^-OCH_3$) is the same as that determined for the 2-hydroxylpropyl aryl phosphates (~ 9 x 10^{-5} M),[67] a k_{cat}^{max} value can be determined for the cyclization of **54** to form **57** ($k_{cat}^{max} = K_M \times k_2^{max}$). Its inclusion as a datum point in Figure 25 requires that at the concentrations of substrate and catalyst employed incomplete formation of the

Michaelis complex must be accounted for. Only 88% of the phosphate diester is actively bound at the concentrations employed and thus, $k_{cat}^{max} = k_1^{obs}/0.88$, or 2.64 x 10^{-3} s^{-1}.

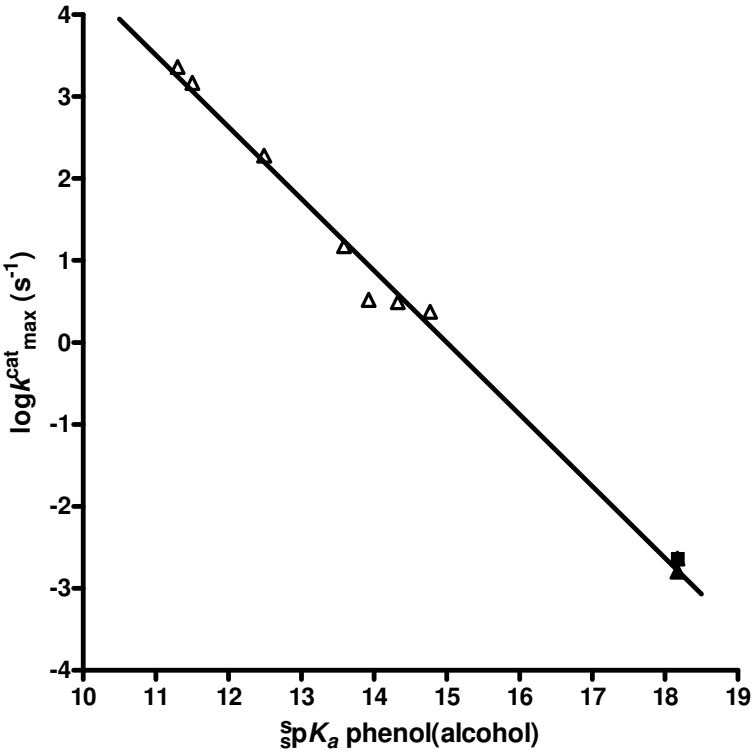

Figure 32. The Brønsted plot for the **36**:$Zn(II)_2$:($^{-}OCH_3$)-catalyzed cyclization of 2-hydroxylpropyl aryl phosphates (**1**a-g, Δ) and **54** (k_1^{max} (■), $^{s}_{s}pK_a$ methanol = 18.17). The datum point (▲) corresponds to the rate k_{cat}^{max} for catalyzed loss of the OCH_3 group from **54** determined in CD_3OD but corrected for the solvent deuterium kinetic isotope effect of ~ 3.9. A β_{lg} of -0.93 ± 0.06 was obtained for the **36**:$Zn(II)_2$:($^{-}OCH_3$)-catalyzed cleavage of **1**a-g.[67] This value changes to the experimentally identical value of -0.87± 0.04 with the inclusion of the data points for the catalyzed closure of **54** and the exchange of OCH_3 for OCD_3 from **54**.

The β_{lg} value determined for the catalyzed decomposition of **1**a-g in Figure 32 changes from -0.93 ± 0.06 to the experimentally identical value of -0.87 ± 0.04 with the inclusion of the data points for the closure of **54** and the exchange of OCH_3 for OCD_3 from **54**.[67] It has been reported for dianionic reaction mechanisms, in which an anionic

nucleophile attacks a monoionic phosphate, that the rate limiting transition state is early and forms products without the generation of a pentacoordinate dianionic phosphorane intermediate.[105] However, the observations reported herein, when taken with the reported β_{lg} for the **36**:$Zn(II)_2$:($^-OCH_3$)-catalyzed cleavage of **1**a-g, support a conserved mechanism that can best be interpreted as involving two-steps proceeding via the formation of a complex-stabilized phosphorane intermediate. For substrates with activated aryloxy leaving groups, formation of the intermediate is rate limiting. Breakdown becomes rate determining for substrates with poor leaving groups such as those of **54** and **54a**.

For substrates **54** and **54a**, the catalyzed isomerization and expulsion of the OCH_3 group is achieved through the formation of a series of pseudo-rotating pentacoordinate phosphorane intermediates, simplistically represented in Scheme 13 by **57**. Until recently,[72] substrate isomerization was observable under only acidic conditions; metal-ion and base-promoted cleavage of of phosphodiesters resulted only in hydrolysis.[106] Exceptions to this have only been observed for phosphates that are capable of cyclization; dianionic phosphorane intermediates have been observed for the base-catalyzed cyclizations of a series of uridine 3'-phosphate esters with leaving groups spanning a pK_a range of 5-17.[80] Additionally, it has been speculated that in the absence of phosphorane protonation its lifetime is too transient to accommodate the pseudorotation required for isomerization.[71, 107] However, a bimetallic complex of **52** has been recently reported to stabilize phosphorane intermediates and the isomerization and hydrolysis of UpU has been observed.[72]

5.4 Conclusions and future directions

For metal-ion complexes that bind phosphates tightly, such as **36**:$Zn(II)_2$:($^-OCH_3$) and the bimetallic complex of **52** reported by Williams *et al.*[72] formation of pentacoordinate phosphorane intermediates is achieved. It is possible that metal-ion complexation to non-bridging phosphoryl oxygen atoms reduces their electron density.[83] According to the Westheimer rules, ligands on the phosphorane must assume an axial position for breakdown during an isomerization or cleavage event.[69, 71] Lewis acidic metal ions assist the ability of the phosphorane intermediate to pseudorotate by violating one of Westheimer's rules and allowing for nonbridging phosphoryl oxygen atoms to occupy equatorial positions.[69] The dinuclear Zn(II) complex reported herein mediates the formation and stabilization of a series of three and possibly four dianionic phosphorane intermediates, termed **57** in Scheme 13, where the rate of isomerization to a thermodynamically favourable ratio of **54** and **54a** exceeds that of exocyclic expulsion of OCH_3 to give cyclic phosphate **56**. With respect to the isomerization and hydrolysis reactions catalyzed in water by the bimetallic complex **52** reported by Williams *et al.*[72] isomerization of **54** and **54a** and cleavage of the exocyclic OCH_3 group occurs 3000- and 100-fold faster, respectively, when catalyzed by **36**:$Zn(II)_2$:($^-OCH_3$) in methanol. This difference is attributable to the medium effect exerted by methanol that synergestically complements the activity of bimetallic catalysts.

While the data presented herein support the formation and existence of a stable pentacoordinate phosphorane intermediate (**57**), a concerted mechanism proceeding with the formation and reopening of the cyclic phosphate **56** cannot be ruled out. To confirm

the existence of **57**, the **36**:$Zn(II)_2$:($^{-}OCH_3$)-catalyzed cleavage of **54** needs to be from the 92/8 mixture originally examined and better resemble the intial kinetic 29/71 mixture of **54/54a** that resulted from the cyclization of HPNPP.

Additionally, the solvent deuterium kinetic isotope effect of ~ 3.9 reported for the isomerization of **54** and **54a** in methanol seems unexplainably large. A more definitive experiment can be undertaken to monitor the catalyzed transesterification of HMP in CD_3OH, where there is no kinetic isotope effect possible, but isomerization of **54** and **54a** and the P-OCH_3 conversion to P-OCD_3 can be observed.

Chapter 6. Cleavage of a highly stable DNA model by a dinuclear Zn(II) complex 36:$Zn(II)_2$:($^-OCH_3$) in methanol

Despite the extensive research done on the decomposition of DNA and RNA models mediated by mono- and dinuclear metal ion small molecule complexes, few of these have been applied to both classes of substrate. Moreover, the complexes studied have relied on the inherent reactivity of activated substrates and few successful contributions have been made to the decomposition of unactivated phosphodiesters.[1b] Herein, the **36**:$Zn(II)_2$:($^-OCH_3$) complex previously used by our group to examine the decomposition of RNA models (**1**a-g) and DNA models (**4**a-h) in methanol was employed to examine the reactivity of the highly stable phosphate diester, dimethyl phosphate (DMP, **2**).

The transesterification of DMP was catalyzed by **36**:$Zn(II)_2$:($^-OCD_3$) in CD_3OD at ambient temperature and followed by high resolution exact mass spectrophotometry. The appearance of a peak at m/z = 128.0 corresponding to **2**(OCD_3) (**2a**) and the disappearance of the peak at m/z = 125.0 corresponding to **2** were both monitored and the rate of OCH_3/OCD_3 exchange was determined as a function of time and percent reaction progress.

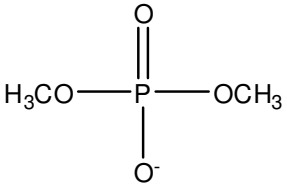

2

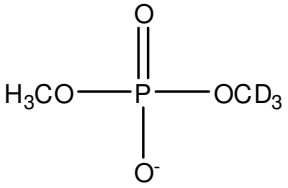

2a

6.1 Experimental

6.1.1 Materials

Dimethyl phosphate (98%) was purchased from Acros Organics and was used as supplied. Methanol (99.8% anhydrous), zinc(II) trifluoromethanesulfonate (98%), and sodium, lump, in kerosene (99%) were obtained from Aldrich and used without further purification. HCl (1N solution) was provided by Fisher Scientific and used as supplied. Methanol-d4 (D, 99.8%) was used as received from Cambridge Isotope Laboratories, Inc. Zhong-Lin Lu synthesized ([12]andN_3)$_2$ (**36**) as described[96] from a previously described methodology[54] and also prepared sodium methoxide-d3 by adding sodium metal to methanol-d4.

Stock solutions of Zn(CF_3SO_3)$_2$,$NaOCD_3$, and **36** were independently prepared to 50 mM in CD_3OD. Monoanionic DMP was prepared as a 50 mM stock solution in CD_3OD with an equimolar amount of $NaOCH_3$ or $NaOCD_3$ added to it. A 50 mM stock solution of HCl and LiCl was prepared in anhydrous methanol.

6.1.2 Methods

The rate of **36**:Zn(II)$_2$:($^-OCD_3$)-catalyzed methanolysis of **2** was followed using an Applied Biosystems/MDS Sciex QSTAR XL QqTOF mass spectrometer. High resolution exact MS spectra were obtained in ESI$^-$ mode with N_2 carrier gas and direct syringe injection. The **36**:Zn(II)$_2$:($^-OCD_3$) complexes were prepared in methanol-d4 to 1 mM in individual vials to a final volume of 1.0 mL by the sequential 1:1:2 addition of $NaOCD_3$, **36**, and Zn(OTf)$_2$. The complex was allotted 45 minutes for formation prior to the introduction of 0.9 equivalents of **2**. The reaction was followed at ambient

temperature. Each reaction was performed in duplicate and quenched by the addition of 4 equivalents of each HCl and LiCl at 0, 7.3, 18.3, and 24.0 hours. The integrity of **36**:$Zn(II)_2$:($^-OCH_3$) in methanol at ambient temperature is compromised by time after formation; it has a half-life of 50 hours. However, the stability of **36**:$Zn(II)_2$:($^-OCH_3$) was determined in the absence of phosphate and it is unknown what the presence of **2** in the reaction mixture would contribute to the integrity of the complex as a function of time. As the percent reaction progress for the catalyzed decomposition of **2** vs time plot is linear over 24 hours (see below), the catalyst can be assumed to be fully formed over the course of the reaction and a correction for complex decomposition is not required.

6.2 Results

6.2.1 Kinetic Measurements

The **36**:$Zn(II)_2$:($^-OCD_3$)-catalyzed transesterification of **2** (m/z = 125.0) was followed by the appearance of a peak at m/z = 128.0 corresponding to **2a**. The rate of exchange of OCH_3 for OCD_3 was determined as a function of time and percent reaction progress (Figure 33). The reaction progress was determined from the ratio of the peak area (counts) of the (M^* + 3) peak to the accumulative peak areas of the M^* and (M^* + 3) peaks.

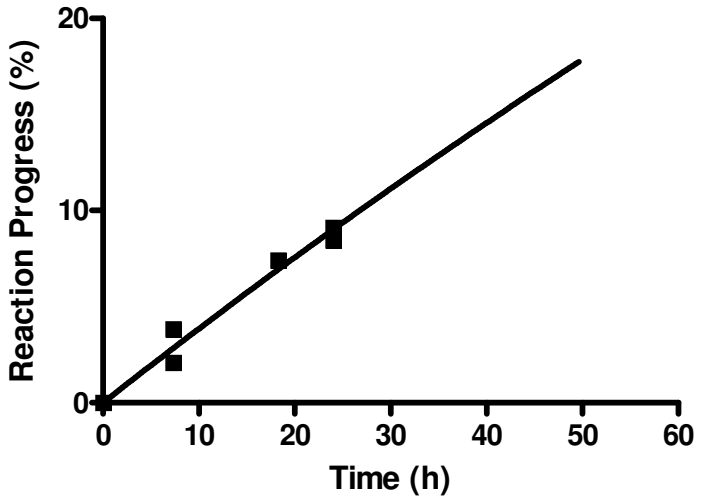

Figure 33. A plot of percent reaction progress vs time for the methanolysis of DMP (**2,** 0.9 mM) catalyzed by 1.0 mM [**36**:$Zn(II)_2$:($^{-}OCD_3$)]$_{total}$ in CD_3OD determined from the appearance of the (M^{+} + 3) peak of **59a** by ESI⁻/MS at ambient temperature. The data is fit to a first order exponential equation ($y(t) = Ae^{-kt} + y_{max}$, where y_{max} is equal to 100%).

The observed rate constant (k_{cat}^{obs}) for formation of **2a** was determined by fitting the data to a pseudo-first order equation, where y_{max} was fit to 100%. An average k_{cat}^{obs} was determined for the duplicate experiments. The $k_{cat}^{ave.}$ was corrected for an incomplete binding of the substrate to the complex and the exchange of OCH_3 for OCD_3 was statistically accounted for as follows.

Using the smallest K_B value (0.13 mM for methyl *p*-chlorophenyl phosphate)[53] determined for the **36**:$Zn(II)_2$:($^{-}OCH_3$)-catalyzed methanolyses of a series of methyl aryl phosphates with poor leaving groups previously determined by our group[53] and the concentrations of catalyst and substrate initially in the reaction mixture, a curve could be emulated from Eq. (2) in Chapter 3 to determine the percent of catalyst that was bound by substrate. The $k_{cat}^{ave.}$ value could then be corrected for incomplete binding. It was found

at the concentration of catalyst and substrate employed 72.7% was complexed as **36**:$Zn(II)_2$:($^-OCD_3$):**2**. The $k_{cat}^{ave.}$ was modified to assume that 100% of **2** was bound to the catalyst as **36**:$Zn(II)_2$:($^-OCH_3$):**2** using Eq. (10).

(10) $k_{cat}^{\mathbf{36}:Zn(II)2:(-OCD3):\mathbf{2}} = k_{cat}^{ave.}*(1/0.727)$

Although the following correction factor is not required if the reaction is concerted, the exchange of OCH_3 for OCD_3 from a putative phosphorane intermediate (**59**) needs to be statistically accounted for by correcting the $k_{cat}^{\mathbf{36}:Zn(II)2:(-OCD3):\mathbf{2}}$ by $^3/_2$. This correction factor takes into consideration the two ways of forming **2a** and the one way in which **2a** can react to restore **2**. The resulting k_{cat}^{max} was determined to be (2.27 ± 0.03) x 10^{-6} s^{-1}, corresponding to a $t_{1/2}$ of 85 hours. This value is comparable to a value of (9 ± 3) x 10^{-6} s^{-1} reported for the transesterification of DMP promoted by a dinuclear Cu(II) complex in CD_3OD at 25 °C.[108] The dinuclear Cu(II) catalyst is peculiar as it is capable of obtaining a rate of reaction for the transesterification of DMP that exceeds both the rate of CH_3O exchange of methyl *p*-nitrophenyl phosphate (**4**c) by 6-fold and the loss of the *p*-nitrophenoxy group of **4**c by 5.5-fold.

6.3 Discussion

The **36**:$Zn(II)_2$:($^-OCH_3$)-catalyzed methanolyses of a series of methyl aryl phosphodiesters (**4**a-h) has been explored by our group,[53] and the observed rate constants (k_{cat}^{max}) for their decomposition have been plotted against the $^s_s pK_a$ of the corresponding leaving group phenol. Included in Figure 34 is a point (□) for 0.9 mM **2** reacting with 1.0 mM **36**:$Zn(II)_2$:($^-OCD_3$) in CD_3OD at ambient temperature.

Interestingly, despite its having a nonactivated leaving group with respect to those of the methyl aryl phosphate series, DMP fits very near the Brønsted line (β_{lg} -0.59)[53] which suggests that the mechanism of cleavage is the same as that for the activated substrates. Consistent with these observations are four possible mechanisms of decomposition: a concerted or two-step reaction and nucleophilic attack by either an external or a metal-coordinated intramolecular methoxide.

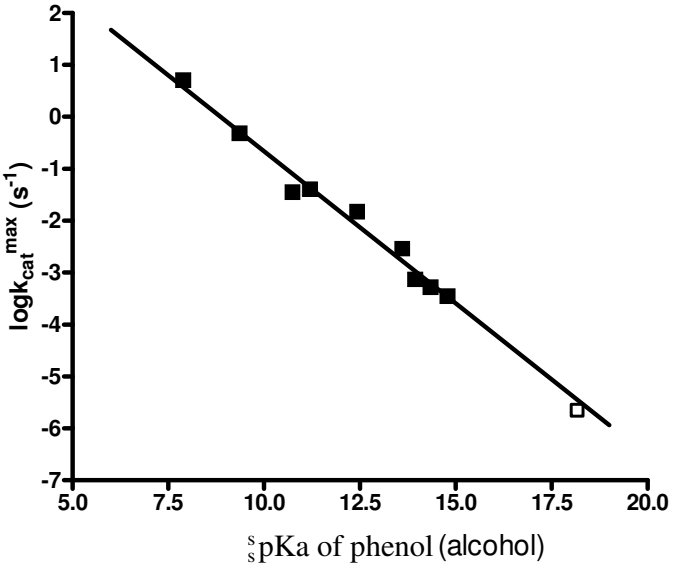

Figure 34. Brønsted plot of log k_{cat}^{max} vs the $^{s}_{s}pK_a$ values for the [**36**:$Zn(II)_2$:($^{-}OCH_3$)]$_{free}$-catalyzed methanolysis of methyl aryl phosphates **4**a-h (■) which fit a linear regression of k_{cat}^{max} = (-0.59 ± 0.03) $^{s}_{s}pK_a$ + (5.2 ± 0.4), r^2 = 0.982.[53] The datum point for DMP (□, k_{cat} = 2.2 x 10^{-6} s^{-1}; $^{s}_{s}pK_a$ = 18.16) rests near the Brønsted line for the phosphates with activated leaving groups. The point for DMP was not used to define the linear regression.

For the series of methyl aryl phosphates, the extent of cleavage of the P-OAr bond in the transition state can be estimated from the β_{lg}.[53] Due to coordination of the phosphate anion to two Zn(II) ions, the aryloxy oxygen of the coordinated methyl aryl

phosphate has a net positive charge of ~0.83.[7, 109] If the mechanism is concerted, the aryloxy oxygen would have a charge of +0.24 in the transition state. The cleavage of the P-OAr bond would have progressed only 32% of the way (Scheme 16).[53] and the transition state would be termed associative.[110] If electrophilic activation of the bridged phosphodiester through charge removal from the coordinated phosphoryl oxygen atoms by the dinuclear Zn(II) complex is strong enough, an associative mechanism could be deflected away from a concerted reaction to a two-step process with rate limiting formation of a pentacoordinate phosphorane intermediate followed by fast breakdown to product.

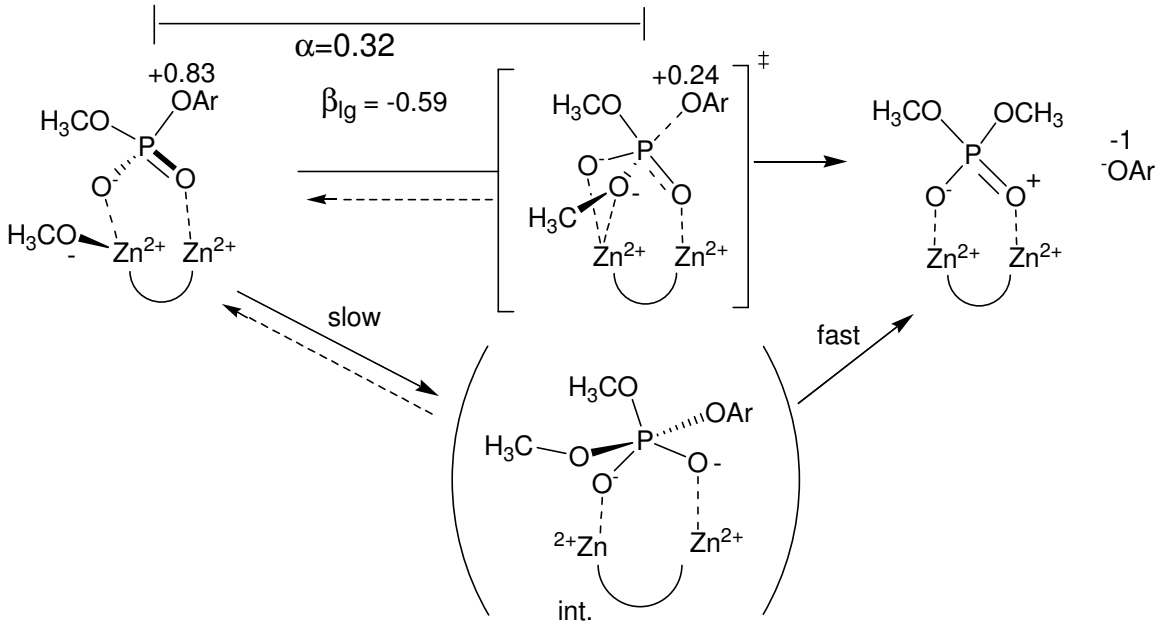

Scheme 16. The Leffler index[91(b), 93(b)] α is given as $\beta_{lg}/\beta_{eq} = -0.59/-1.83 = 0.32$ and represents the extent of P-OAr bond cleavage in the transition state.[53]

Both the concerted and the two-step mechanism are elucidated in Scheme 16 and the reactions are depicted to be mediated by an internal metal-bound methoxide. Support for this metal-coordinated methoxide comes from the X-ray diffraction structure of the

closely related **36**:$Zn(II)_2$:($^-$OH) complex showing a hydroxide anion bridged by the two Zn(II) ions.[53] It is a reasonable assumption that this structure is conserved for the methoxide complex prior to substrate binding. Additionally, bridging of a phosphate diester and hydroxide between two divalent metal ions is seen in the X-ray diffraction structure reported for the **36**:$Cu(II)_2$:($^-$OH):(($C_6H_5CH_2O)_2PO_2^-$) complex.[96] Taken with the bell-shaped pH-rate profile for the **36**:$Zn(II)_2$:($^-OCH_3$)-promoted methanolysis of **4**f that maximizes when the [$^-OCH_3$]/**36**:$Zn(II)_2$] is unity, it can be held that the optimal transition state stoichiometry is comprised of a 1:2:1:1 ratio of ligand, Zn(II) ion, methoxide, and substrate.[53] These observations provide support for a metal-coordinated methoxide in the **36**:$Zn(II)_2$:($^-OCH_3$)-catalyzed decomposition of methyl aryl phosphates **4**a-h and DMP, although an external methoxide cannot be ruled out. A metal-coordinated methoxide has an ${}^{s}_{s}pK_a$ that is lower than that of an uncoordinated metal ion. However, its nucleophilicity is reduced and thus an uncoordinated methoxide may be a better nucleophile. More work needs to be done to distinguish between the involvement of an internal vs an external methoxide.

6.4 Conclusions and future directions

Assuming a 1:2:1:1 transition state stoichiometry of ligand, Zn(II) ion, methoxide, and substrate, the methanolysis of DMP is a symmetrical reaction mediated by the formation of this Michaelis complex. In compliance with the principle of microscopic reversibility, a two-step mechanism involving the attack of an internal methoxide requires that the departure of the leaving group be metal-assisted. Thus, methoxide interchange between the pentacoordinate phosphorane intermediate and the dinuclear Zn(II) complex

must be geometrically feasible and must not limit decomposition. A mechanism in which the rate limiting step moves from formation to breakdown of the phosphorane intermediate can be invisioned for substrates with unactivated leaving groups. As the datum point for DMP lies slightly below the Brønsted line derived for methyl aryl phosphates (**4**a-h), this point can be taken as the onset of an anticipated break in the curve where there is an expected change in the rate limiting step. The validity of this contention needs to be further probed through the decomposition of methyl *O*-alkyl phosphates with nonactivated leaving groups (ie. an ${}^{s}_{s}pK_a$ that is greater than that of methanol).[53]

Chapter 7. Conclusions

The design of a metallic system capable of efficaciously cleaving DNA, RNA, and their models is not trivial. Much work has been done to highlight the factors contributing to efficient catalysis.

The catalyst complex, **53**:$Zn(II)_2$:($^-OCH_3$), reported herein achieves remarkable rates of catalysis for the cyclization of a series of 2-hydroxylpropyl aryl phosphates (**1**a-g) that are noteworthy with respect to those reported for the hydrolysis of this class of substrates by other catalytic systems (Chapter 3). The medium effect introduced by methanol enhances the reactivity of this complex as seen likewise for the more rigid **36**:$Zn(II)_2$:($^-OCH_3$).[67] The dinuclear Zn(II) complex of **53** provides ~10^{11} to 10^{12}-fold rate acceleration while that of **36** offers 10^{12}-fold rate acceleration over the background methoxide-promoted reaction. However, the flexibility in **53**:$Zn(II)_2$ seems to make this a more fragile catalyst as it is sensitive to acidic conditions such that a first ^s_spKa cannot be experimentally determined. Additionally, the flexibility added by the butane spacer of **53** with respect to the propane space of **36** reduces the catalytic activity of this dinuclear Zn(II) complex towards the cleavage a series of 2-hydroxylpropyl aryl phosphates, **1**a-g.

An investigation of the catalytic activity of the dinuclear Zn(II) complexes **53** and **36** in methanol was applied to biologically relevant substrates UpU and ApC (Chapter 4). The dinuclear Zn(II) complexes of **53** and **36** displayed the greatest activity towards cleavage of UpU and as a result were most extensively studied. However, the second order rate constants for the cleavage of this substrate were less significant than the rate

accelerations afforded by these complexes towards the cleavage of a series of RNA models (Chapter 3).[67] The reduced activity of these Zn(II) containing catalysts was attributed to inhibition due to loss of the acidic N3 proton of the substrate uridine moiety and the bulk of the complex and substrate.

The bulk of the catalyst complex was reduced and binding of metal ions to the phosphate centre was enhanced by studying the Zn^{2+}:($^{-}$OEt)-catalyzed cleavage of UpU and ApC in ethanol. Catalyzed cleavage was absent, however, reaction with the latter resulted in the production of (2'→5')ApC confirming the existence of a pentacoordinate phosphorane intermediate. Only recently has the existence of a dianionic phosphorane intermediate been reported during the metal ion-catalyzed cleavage of a diribonucleotide.[72]

The existence of a pentacoordinate phosphorane intermediate stabilized by **36**:$Zn(II)_2$:($^{-}OCH_3$) in methanol was investigated (Chapter 5). The dinuclear Zn(II) complex of **36** mediated the formation and stabilization of a series of three and possibly four dianionic phosphorane intermediates (**57**) and the rate of isomerization of **54** and **54a** exceeded that of exocyclic expulsion of OCH_3 to give the cyclic phosphate **56**. The formation of a stable pentacoordinate phosphorane intermediate provides additional support for a two-step mechanism for a dinuclear Zn(II) complex-catalyzed transesterification of the RNA model, 2-hydroxylpropyl methyl phosphate (**54/54a**).

In a final experiment, the transesterification of the highly stable DNA model, DMP (**2**), was monitored in the presence of **36**:$Zn(II)_2$:($^{-}OCD_3$) in CD_3OD. Assuming a 1:2:1:1 transition state stoichiometry of methoxide, Zn(II) ion, ligand, and substrate the

methanolysis of DMP is a symmetrical reaction mediated by the formation of this Michaelis complex. In compliance with the principle of microscopic reversibility, a two-step mechanism involving the attack of an internal methoxide requires that the departure of the leaving group be metal-assisted. Thus, methoxide interchange between the pentacoordinate phosphorane intermediate and the dinuclear Zn(II) complex must be geometrically feasible and must not limit decomposition. A mechanism in which the rate limiting step moves from formation to breakdown of the phosphorane intermediate can be invisioned for substrates with unactivated leaving groups. As the datum point for DMP lies slightly below the Brønsted line derived for methyl aryl phosphates (**4**a-h), this point can be taken as the onset of an anticipated break in the curve where there is an expected change in the rate limiting step.

References

[1] (a) Mancin, F.; Tecillia, P. *New J. Chem*. **2007**, *31*, 800. (b) Weston, J. *Chem. Rev.* **2005**, *105*, 2151. (c) Molenveld, P.; Engbertsen, J. F. J. ; Reinhoudt, D. N. *Chem. Soc. Rev.* **2000**, *29*, 75. (d) Williams, N. H.; Takasaki, B.; Wall, M.; Chin, J. *Acc. Chem. Res*. **1999**, *32*, 485. (e) Mancin, F.; Scrimin, P. ; Tecilla, P.; Tonellato, U. *Chem. Commun*. **2005**, 2540. (f) Morrow, J. R.; Iranzo, O. *Curr. Opin. Chem. Biol*. **2004**, *8*, 192.

[2] Dalby, K. N.; Kirby, J.; Hollfelder, F. *J. Chem. Soc. Perkin Trans 2* **1993**, *7*, 1269.

[3] (a) Williams, N. H.; Wyman, P. *Chem. Commun*. **2001**, 1268. (b) Haake, P. C.; Westheimer, F. H. *J. Am. Chem. Soc.* **1961**, *83*, 1102. (c) Guthrie, J. P. *J. Am. Chem. Soc*. **1977**, *99*, 3991. (d) Bunton, C. A.; Mhala, M. M.; Oldham, K. G.; Vernon, C. A. *J. Chem. Soc.* **1960**, 3293.

[4] Lad, C.; Williams, N. H.; Wolfenden, R. *Proc. Natl. Acad. Sci. U.S.A.* **2003**, *100*, 5607.

[5] Torriani-Gorini, A.; Yagil, E.; Silver, S. *Phosphate in Microorganisms: Cellular and Molecular Biology,* ASM Press, Washington, **1994.**

[6] Wilcox, D. E. *Chem. Rev.* **1996**, *96*, 2435.

[7] Williams, N. H.; Cheung, W.; Chin, J. *J. Am. Chem. Soc.* **1998**, *120*, 8079.

[8] Rawlings, J.; Cleland, W.; Hengge, A. C., *J. Am. Chem. Soc.* **2006**, *128*, 17120.

[9] (a) Wolfenden, R. *Chem. Rev.* **2006**, *106*, 3379. (b) Wolfenden, R.; Snider, M. *J. Acc. Chem. Res.* **2001**, *34*, 938. (c) Schroeder, G. K.; Lad, C.; Wyman, P.; Williams, N. H.; Wolfenden, R. *Proc. Natl. Acad. Sci. U.S.A.* **2006**, *103*, 4052.

[10] Zalatan, J. G.; Herschlag, D. *J. Am. Chem. Soc.* **2006**, *128*, 1293.

[11] O'Brien, P. J.; Herschlag, D. *Biochemistry* **2001**, *40*, 5691.

[12] Holtz, K. M.; Kantrowitz, E. R. *FEBS Letters* **1999**, *462*, 7.

[13] Kim, E. E.; Wyckoff, H. W. *J. Mol. Biol*. **1991**, *218,* 449.

[14] (a) Gettins, P.; Coleman, J. E. *J. Biol. Chem*. **1984**, *250*, 4991. (b) Hull, W. E.; Halford, S. E.; Gutfreund, H.; Sykes, B. D. *Biochemistry* **1976**, *15* 1547. (c) Bock, J. L.; Cohn, M. *J. Biol. Chem*. **1978**, *253*, 4082.

[15] Jones, S. R.; Kindman, L. A.; Knowles, J. R. *Nature* **1978**, *275*, 564.

[16] Sträter, N.; Lipscomb, W. N.; Klabunde, T.; Krebs, B. *Angew. Chem. Int. Ed. Engl.* **1996**, *35*, 2024.

[17] Lipscomb, W. N.; Sträter, N. *Chem. Rev.* **1996**, *96*, 2375.

[18] (a) Little, C.; Otnaess A. *Biochim. Biophys. Acta* **1975**, *391*, 326. (b) Little, C. *Acta Chem. Scand. B* **1981**, *35*, 39.

[19] Hough, E.; Hansen, L. K.; Birkness, B.; Jynge, K.; Hansen, S.; Hordvik, A.; Little, C.; Dodson, E.; Derwenda, Z. *Nature* **1989**, *338*, 355.

[20] Yatsimirsky, A. K. *Coord. Chem. Rev.* **2005**, *249*, 1997.

[21] (a) Yang, M.-Y.; Morrow, J. R.; Richard, J. P. *Bioorg. Chem.* **2007**, *35*, 366. (b) Iranzo, O.; Kovalevsky, A. Y.; Morrow, J. R.; Richard, J. P. *J. Am. Chem. Soc.* **2003**, *125*, 1988.

[22] Lindahl, T. *Nature*, **1993**, *362*, 709.

[23] Radzicka A.; Wolfenden, R. *Science* **1995**, *267*, 90.

[24] Kumamoto, J.; Cox, Jr., J. R.; Westheimer, F. H. *J. Am. Chem. Soc*. **1956**, *78*, 4858.

[25] Schneider, H.-J.; Yatsimirsky, A. K. "Lanthanide-catalysed hydrolysis of phosphate esters and nucleic acis." In *The Lanthanides and Their Interrelations with Biosystems.* Edited by Sigel H. New York: Marcel Dekker, Inc.; **2003**. Metal ions in biological systems, vol 40.

[26] Wang, Q.; Lönnberg, H. *J. Am. Chem. Soc.* **2006**, *128*, 10716.

[27] Lopez, C. S.; Faza, O. N.; de Lera, A. R.; York, D. M. *Chem. Eur. J.* **2005**, *11*, 2081.

[28] Cowan, J. A. *Curr. Opin. Chem. Biol.* **2001**, *5*, 634.

[29] Hegg, E. L.; Burstyn, J. N. *Coord. Chem. Rev.* **1998**, *173*, 133.

[30] Hendry, P.; Sargeson, A. M. *Prog. Inorg. Chem.* **1990**, *38*, 201.

[31] Branum, M.; Que, L. J. *Biol. Inorg. Chem.* **1999**, *4*, 593.

[32] Mikkola, S.; Kaukinen, U.; Lönnberg, H. *Cell Biochem. Biophys.* **2001**, *34*, 95.

[33] Komiyama, M. "Sequence-selective scission of DNA and RNA by lanthanide ions and their complexes." In *The Lanthanides and Their Interrelations with Biosystems."* Edited by Sigel H. New York: Marcel Dekker, Inc.; **2003**: 462-475. Metal ions in biological systems, vol. 40.

[34] calculated[1a] from Chin, J.; Banaszczyk, M.; Jubian, V.; Zou, X. *J. Am. Chem. Soc.* **1989**, *111*, 186.

[35] de Rosch, M. A.; Trögler, W. C. *Inorg. Chem. Soc.* **1990**, *29*, 2409.

[36] Koike, T.; Kimura, E. *J. Am. Chem. Soc.* **1991**, *113*, 8935.

[37] Bonfá, L.; Gatos, M.; Mancin, F.; Tecilla, P.; Tonellato, U. *Inorg. Chem.* **2003**, *42*, 3943.

[38] Ichikawa, K.; Tarnai, M.; Uddin, M. K.; Nakata, K.; Sato, S. J. *Inorg. Biochem.* **2002**,

91, 437.

[39] (a) Gani, D.; Wilkie, J. *Chem. Soc. Rev*. **1995**, *24*, 55. (b) Lahm, A.; Volbeda, S.; Suck, D. *J. Mol. Biol*. **1990**, *252*, 88. (c) Beese, L. S.; Steitz, T. A. *EMBO J*. **1991**, *10*, 25.

[40] Williams, N. H.; Chin, *J. Chem. Commun*. **1996**, 131.

[41] (a) Wall, M.; Hynes, R. C.; Chin, J. *Angew. Chem., Int. Ed. Engl*. **1993**, *32*, 1633. (b) Gajda, T.; Krämer, R.; Jancso, A. *Eur. J. Inorg. Chem*. **2000**, 1635. (c) Albedyhl, S.; Schnieders, D.; Jancso, A.; Gajda, T.; Krebs, B. *Eur. J. Inorg. Chem*. **2002**, 1400. (d) Gajda, T.; Jancso, A.; Mikkola, S.; Lönnberg, H.; Sirges, H. *J. Chem. Soc., Dalton Trans*. **2002**, 1757.

[42] Iranzo, O.; Elmer, T.; Richard, J. P.; Morrow, J. R. *Inorg, Chem*. **2003**, *42*, 7737.

[43] Chapman, Jr., W. H.; Breslow, R. *J. Am. Chem. Soc.* **1995**, *117*, 5462.

[44] Bazzicalupi, C.; Bencini, A.; Bianchi, A.; Fusi, V.; Giorgi, C., Paoletti, P.; Valtancoli, B.; Zanchi, D. *Inorg. Chem*. **1997**, *36*, 2784.

[45] Kaminskaia, N. V.; He, C.; Lippard, S. *J. Inorg. Chem*. **2000**, *39*, 3365.

[46] (a) Bauer-Siebenlist, B.; Meyer, F.; Farkas, E.; Vidovic, D.; Cuesta-Seijo, J. A.; Herbst-Irmer, R.; Pritzkow, H. *Inorg. Chem.* **2004**, *43*, 4189. (b) Bauer-Siebenlist, B.; Meyer, F.,; Farkas, E.; Vidovic, D.; Dechert, S. *Chem.-Eur. J.* **2005**, *11*, 4349. (c) Meyer, F. *Eur. J. Inorg. Chem.* **2006**, 3789.

[47] Vichard, C.; Kaden, T. A. *Inorg. Chim. Acta* **2002**, *337*, 173.

[48] Arca, M.; Bencini, A.; Berni, E.; Caltagirona, C.; Devillanova, F. A.; Isaia, F.; Garau,

A.; Giorgi, C.; Lippolis, V.; Perra, A.; Tei, L.; Baltancoli, B. *Inorg. Chem.* **2003**, *42*, 6929.

[49] Kimura, E.; Kodama, Y.; Koike, T.; Shiro, M. *J. Am. Chem. Soc.* **1995**, *117*, 8304.

[50] Bazzicalupi, C.; Bencini, A.; Berni, E.; Vianchi, A.; Fedi, V.; Fusi, V.; Giorgi, C.; Paoletti, P.; Valtancoli, B. *Inorg. Chem.* 1999, 38, 4115.

[51] Chen, J.; Wang, X.; Zhu, Y.; Lin, J.; Yang, X.; Li, Y.; Lu, Y.; Guo, Z. *Inorg. Chem.* **2005**, *44*, 3422.

[52] (a) Livieri, M.; Mancin, F.; Tonellato, U.; Chin, J. *Chem. Commun.* **2004**, 2862; (b) Livieri, M.; Mancin, F.; Saielli, G.; Chin, J.; Tonellato, U. *Chem. Eur. J.* **2007**, *13*, 2246.

[53] Neverov, A. A.; Liu, C. T.; Bunn, S. E.; Edwards, D.; White, C. J.; Melnychuk, S. A.; Brown, R. S. *J. Am. Chem. Soc*. **2008**, *130*, 6639.

[54] Kim, J.; Lim, H. *Bull. Korean Chem. Soc*. **1999**, *20*, 491. The second order rate constant for the **35**:$Zn(II)_2$ catalyzed cleavage of bis-(2,4-dinitrophenyl)phosphate in water was reported to be 7 x 10^{-3} $M^{-1}s^{-1}$ at pH 7, which was not significantly greater than that seen with the mononuclear Zn(II) complex of 1,5,9-triazacyclododecane. In methanol at $^{s}_{s}$pH 9.8 the cleavage of the less reactive substrate bis-(*p*-nitrophenyl) phosphate has a second-order rate constant of 20 $M^{-1}s^{-1}$. Brown, R. S.; Lu, Z.-L. Unpublished results.

[55] Butzow, J. J.; Eichorn, G. L. *Biopolymers* **1965**, *3*, 95.

[56] Breslow, R.; Huang, D.-L.; Anslyn, E. *Proc. Natl. Acad. Sci. U.S.A.* **1989**, *86*, 1746.

[57] Breslow, R.; Berger, D.; Huang, D.-L. *J. Am. Chem. Soc.* **1990**, *112*, 3686.

[58] He, C.; Lippard, S. J. *J. Am. Chem. Soc.* **2000**, *122*, 184.

[59] (a) Yashiro, M.; Ishikubo, A.; Komiyama, M. *Chem. Commun*. **1997**, 83. (b) Yashiro, M.; Ishikubo, A.; Komiyama, M. *J. Chem. Soc., Chem. Commun.* **1995**, 1793.

[60] (a) Molenveld, P.; Engbersen, J. F. J.; Reinhoudt, D. N. *Chem. Soc. Rev.* **2000**, *29*, 75. (b) Molenveld, P.; Stikvoort, W. M. G.; Kooijman, H.; Spek, A. L.; Engbersen, J. F. J.; Reinhoudt, D. N. *J. Org. Chem.* **1999**, *64*, 3896. (c) Molenveld, P.; Engbersen, J. F. J.; Reinhoudt, D. N. *Angew. Chem., Int. Ed.* **1999**, *38*, 3189. (d) Molenveld, P.; Engbersen, J. F. J.; Reinhoudt, N. *Eur. J. Org. Chem.* **1999**, 3269. (e) Molenveld, P.; Kapsabelis, S.; Engbersen, J. F. J.; Reinhoudt, D. N. *J. Am. Chem. Soc*. **1995**, *119*, 2948.

[61] Cacciapaglia, R.; Casnati, A.; Mandolini, L; Reinhoudt, D. N.; Salvio, R.; Sartori, A.; Ungaro, R. *J. Am Chem. Soc*. **2006**, *128*, 12322.

[62] (a) O'Donoghue, A.; Pyun, S. Y.; Yang, M.-Y.; Morrow, J. R.; Richard, J. P. *J. Am. Chem. Soc.* **2006**, *128*, 1615. (b) Iranzo, O.; Richard, J. P.; Morrow, J. R. *Inorg. Chem.* **2004**, *43*, 1743. (c) Yang, M.-Y.; Richard, J. P.; Morrow, J. R. *Chem. Commun.* **2003**, 2832.

[63] Sissi, C.; Rossi, P.; Felluga, F.; Formaggio, F.; Palumbo, M.; Tecilla, P.; Toniolo, C.; Scrimin, P. *J. Am. Chem. Soc.* **2001**, *123*, 3169.

[64] Yamada, K.; Takahashi, Y.; Yamamura, H.; Araki, S.; Saito, K.; Kawai, M. *Chem. Commun*. **2000**, 1315.

[65] (a) Scarso, A.; Zaupa, G.; Bodar Houillon, F.; Prins, L. J.; Scrimin, P. *J. Org. Chem.,*

2007, *72*, 376; (b) Scarso, A.; Scheffer, U.; Göbel, M.; Broxterman, Q. B.; Kaptein, B.; Formaggio, F.; Toniolo, C.; Scrimin, P. *Proc. Natl. Acad. Sci. U.S.A.*, **2002**, *99*, 5144.

[66] Takebayashi, S.; Ikeda, M.; Takeuchi, M.; Shinkai, S. *Chem. Commun.*, **2004**, 420.

[67] Bunn, S.; Liu, C. T.; Lu, Z.-L.; Neverov, A. A.; Brown, R. S. *J. Am. Chem. Soc.* **2007**, *129*,16238.

[68] Covitz, F.; Westheimer, F. H. *ibid.*, **1963**, *85*, 1773.

[69] Westheimer, F. H. *Acc. Chem. Res*. **1968**, *1*, 70.

[70] Buchwald, S. L.; Pliura, D. H.; Knowles, J. R. *J. Am. Chem. Soc*. **1984**, *106*, 4916.

[71] Berry, R. S. *ibid.*, **1960**, 32, 933.

[72] Linjalahti, H.; Feng, G.; Mareque-Rivas, J. C.; Mikkola, S.; Williams, N. H. *J. Am. Chem. Soc*. **2008**, *130*, 4232.

[73] Kosonen, M.; Youseti-Salakdeh, E.; Strömberg, R.; Lönnberg H. *J. Chem. Soc. Perkin Trans. 2* **1997**, 2661.

[74] Perreault, D. M.; Anslyn, E. V. *Angew. Chem. Int. Ed. Eng*. **1997**, *36*, 432.

[75] Vichard, C.; Kaden, T. A. *Inorg. Chim. Acta* **2004**, *357*, 2285.

[76] Taira, K.; Uchimaru, T.; Storer, J. W; Yliniemelä, A.; Uebayasi, M; and Tanabe, K. *J. Org. Chem.* **1993**, *58*, 3009.

[77] Yliniemalä, A.; Uchimaru, T.; Tanabe, K.; Taira, K. *J. Am. Chem. Soc.*, **1993**, *115*, 3032.

[78] Torriani-Gorini, A.; Yagil, E.; Silver, S. "Phosphate in Microorganisms: Cellular and Molecular Biology" *ASM Press*, Washington, **1994.**

[79] Richard, J. P.; Amyes, T. L. *Bioorg. Chem.* **2004**, *32*, 354.

[80] Lönnberg, H.; Strömberg, R.; Williams, A. *Org. Biomol. Chem.* **2004**, *2*, 2165.

[81] Yang, M.-Y.; Iranzo, O.; Richard, J. P.; Morrow, J. R. *J. Am. Chem. Soc.* **2005**, *127*, 1064.

[82] Tsang, J. S.; Neverov, A. A.; Brown, R. S. *J. Am. Chem. Soc.* **2003**, *125*, 1559.

[83] Brown, D. M.; Usher, D. A. *J. Chem. Soc*. **1965**, 6558.

[84] Alder, R. W.; Mowlam, R. W.; Vachon, D. J.; Weisman, G. R. *J. Chem. Soc. Chem. Commun*. **1992**, 507.

[85] Padovani, M.; Williams, N. H.; Wyman, P. *J. Phys. Org. Chem*. **2004**, *17*, 472.

[86] (a) Gibson, G.; Neverov, A. A.; Brown, R. S. *Can. J. Chem*. **2003**, *81*, 495. (b) Gibson, G. T. T.; Mohamed, M. F.; Neverov, A. A.; and Brown, R. S. *Inorg, Chem*. **2006**, *45*, 7891.

[87] Bosch, E.; Rived, F.; Rosés, M.; Sales, J. *J. Chem. Soc., Perkin Trans*. **1999**, *2*, 1953.

[88] Liu, T.; Neverov, A. A.; Tsang, J. S. W.; Brown, R. S. *Org. Biomol. Chem*. **2005**, *3*, 1525.

[89] Eq. (2) was obtained from the equations for equilibrium binding for conservation of mass by using the commercially available MAPLE software, *MAPLE V*, Release 5, Waterloo Maple Inc.: Waterloo, Ontario, Canada.

[90] (a) Brown, R. S.; Neverov, A. A.; Tsang, J. S. W.; Gibson, G. T. T.; Montoya-Pelàez, P. J. *Can. J. Chem*. **2004**, *82*, 1791. (b) Brown, R. S.; Neverov, A. A. *J. Chem. Soc. Perkin 2*. **2002**, 1039.

[91] Davis, A. M.; Hall, A. D.; Williams, A. *J. Am. Chem. Soc*. **1998**, *110*, 5105.

[92] (a) Bourne, N.; Williams, A. *J. Am. Chem. Soc*. **1984**, *106*, 7591. (b) Bourne, N.; Chrystiuk, E.; Davis, A. M.; Williams, A. *Org. Biomol. Chem*. **2004**, *2*, 2165.

[93] (a) Williams, A. *Acc. Chem. Res.* **1984**, *17*, 425. (b) Williams, A. *Chem. Soc. Rev.* **1986**, *15*, 125.

[94] Farquhar, E. R.; Richard, J. P.; Morrow, J. R. *Inorg. Chem*. **2007**, *46*, 7169.

[95] Mathews, R. A.; Rossiter, C. S.; Morrow, J. R.; Richard, J. R. *Dalton Trans*. **2007**, 3804.

[96] Neverov, A. A.; Lu, Z.-L.; Maxwell, C. I.; Mohamed, M. F.; White, C. J.; Tsang. J. S. W.; Brown, R. S. *J. Am. Chem. Soc.* **2006**, *128*, 16398.

[97] Lu, Z.-L.; Liu, T. C.; Neverov, A. A.; Brown, R. S. *J. Am .Chem. Soc.* **2007**, *129*, 11642.

[98] Raines, R. T. *Chem. Rev*. **1998**, *98*, 1045.

[99] Liu, T. C.; Neverov, A. A.; Brown, R. S. *Inorg. Chem.* **2007**, *46*, 1778.

[100] Rossiter, C. S.; Mathews, R. A.; and Morrow, J. R. *Inorg. Chem.* **2005**, *44*, 9397.

[101] Markham, R.; Smith, J. D. *Biochem. J.* **1952**, *52*, 552.

[102] Wall, M.; Linkletter, B.; Williams, D.; Lebuis, A. -M.; Hynes, R. C.; Chin, J. *J. Am. Chem. Soc.* **1999**, *121*, 4710.

[103] Westheimer, F. H. *J. Am. Chem. Soc.* **1956**, *78*, 4858.

[104] Sánchez-Lombardo, I.; Yatsimirsky, A. K. *Inorg. Chem.* **2008**, *47*, 2514.

[105] Lopez, X.; Dejaegere, A.; Leclerc, F.; York, D. M.; Karplus, M. J. *Phys. Chem. B* **2006**, 11525.

[106] Beckmann, C.; Kirby, A. J.; Kuusela, S.; Tickle, D. C. *J. Chem. Soc.,*

Perkin Trans. 2 **1997**, 573.

[107] Thatcher, G. R. J.; Kluger, R. *Adv. Phys. Org. Chem*. **1989**, *25*, 99.

[108] Jagoda, M.; Warzeska,S.; Pritzkow, H.; Wadepohl, H.; Imhof, P.; Smith, J. C.; Krämer, R. *J. Am. Chem. Soc.* **2006**, *127*,15061.

[109] (a) Humphry, T.; Forconi, M.; Williams, N. H.; Hengge, A. C. *J. Am .Chem. Soc.* **2002**, *124*, 14860. (b) Humphry, T.; Forconi, M.; Williams, N. H.; Hengge. A, C. *J. Am. Chem. Soc.* **2004**, *126,* 11864.

[110] Maegley, K.; Admiral, S. J.; Herschlag, D. *Proc. Natl. Acad. Sci. U.S.A.* **1996**, *93*, 8160.

Appendix I. Supplementary material to Chapter 3

Supplementary kinetic data and figures

Table 1S. The second order rate constants for the methoxide-promoted cyclization of 2-hydroxylpropyl aryl phosphates **1**a-g in methanol at 25.0 ± 0.1 ^{o}C.

Substrate	Phenol $^{s}_{s}pK_a$	k_2^{-OMe} ($M^{-1}s^{-1}$)
1a	11.30	(2.6 ± 0.2) x 10^{-3a}
1b	11.50	(5.3 ± 0.2) x 10^{-4b}
1c	12.49	(6.7 ± 0.2) x 10^{-4b}
1d	13.59	(5.2 ± 0.2) x 10^{-5b}
1e	13.93	(1.68 ± 0.06) x 10^{-5b}
1f	14.33	(1.21 ± 0.03) x 10^{-5b}
1g	14.77	(5.9 ± 0.2) x 10^{-6b}

a. Rate constants from ref 82.
b. Rate constants from ref 67.

Table 2S. The observed first order rate constants for the methanolysis of 0.05 mM **1**a catalyzed by 1.0 mM [**53**:$Zn(II)_2$:($^{-}OCH_3$)]$_{total}$ as a function of time determined from the rate of appearance of product phenol at 320 nm, $^{s}_{s}$pH 9.47 ± 0.17, and 25.0 ± 0.1°C.

Time (h)	k_{obs} (s^{-1})
0.5	11.38
0.6	11.51
1.3	11.23
1.9	10.70
2.5	10.26
3.9	9.29
5.2	8.81
5.8	8.50
6.6	7.26
7.4	6.26
25.0	3.99
28.9	3.46
29.9	2.90
31.1	2.67
48.6	2.03
54.9	1.40
72.6	1.22

Table 3S. The observed first order rate constants for the methanolysis of **55** (0.05 mM) catalyzed by [**53**:$Zn(II)_2$:($^{-}OCH_3$)]$_{total}$ (0.50 mM) as a function of increasing amounts of [NH_4^+($^{-}$OTf)] determined from the rate of appearance of product phenol at 320 nm at $^{s}_{s}$pH 9.47 ± 0.17, 25.0 ± 0.1°C.

[NH_4^+($^{-}$OTf)] (mM)	k_{obs} (s^{-1})
2.0	0.011
2.0	0.011
2.5	0.011
2.5	0.009
3.0	0.009
3.0	0.010
3.5	0.009
3.5	0.009
4.0	0.008
4.0	0.008
5.0	0.008
5.0	0.008
6.0	0.007
6.0	0.007
7.0	0.007
7.0	0.007
8.0	0.007
8.0	0.007

Table 4S. The k_{obs} vs [**53**:$Zn(II)_2$:($^{-}OCH_3$)]$_{free}$ data for the catalyzed methanolysis of **1**a (5×10^{-5} M) determined from the rate of appearance of product phenol at 320 nm, $^{s}_{s}$pH 9.47 ± 0.17, and 25.0 ± 0.1°C.

[**53**:$Zn(II)_2$:($^{-}OCH_3$)]$_{free}$ (mM)	k_{obs} (s^{-1})
0.18	0.89
0.18	1.16
0.33	2.96
0.33	3.44
0.45	5.45
0.45	5.51
0.55	7.41
0.55	7.44
0.64	9.09
0.64	9.18
0.72	10.60
0.72	10.48

Table 5S. The k_{obs} vs [**53**:$Zn(II)_2$:($^-OCH_3$)]$_{free}$ data for the catalyzed methanolysis of **1**b (5 x 10^{-5} M) determined from the rate of appearance of product phenol at 323 nm, ^s_spH 9.47 ± 0.17, and 25.0 ± 0.1°C.

[**53**:$Zn(II)_2$:($^-OCH_3$)]$_{free}$ (mM)	k_{obs} (s^{-1})
0.33	1.63
0.33	1.68
0.45	3.17
0.45	3.34
0.55	4.75
0.55	4.97
0.64	5.31
0.64	5.61
0.72	7.60
0.72	7.30
0.85	9.55
0.85	9.71

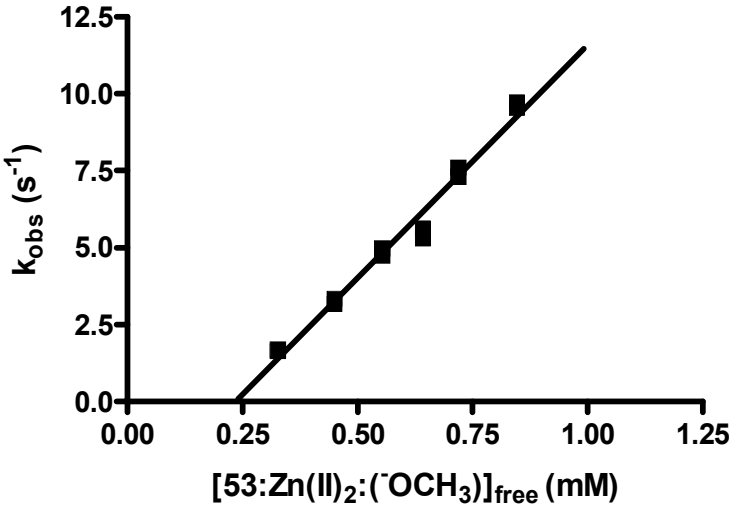

Figure 1S. A plot of k_{obs} vs [**53**:$Zn(II)_2$:($^-OCH_3$)]$_{free}$ for the catalyzed methanolysis of **1**b (5 x 10^{-5} M) determined from the rate of appearance of product phenol at 323 nm, ^s_spH 9.47 ± 0.17, and 25.0 ± 0.1°C. The linear regression of the data in Table 5S gives k_2 = (1.51 ± 0.07) x 10^4 $M^{-1}s^{-1}$ with an intercept of X = 0.23 ± 0.040 mM, r^2 = 0.981.

Table 6S. The k_{obs} vs [**53**:$Zn(II)_2$:($^-OCH_3$)]$_{free}$ data for the catalyzed methanolysis of **1**c (5×10^{-5} M) determined from the rate of appearance of product phenol at 340 nm, ^s_spH 9.47 ± 0.17, and 25.0 ± 0.1°C.

[**53**:$Zn(II)_2$:($^-OCH_3$)]$_{free}$ (mM)	k_{obs} (s^{-1})
0.18	0.28
0.18	0.46
0.33	1.89
0.33	2.39
0.55	3.60
0.55	4.75
0.64	5.91
0.64	6.68
0.72	7.25
0.72	8.10
0.85	9.88
0.85	9.41

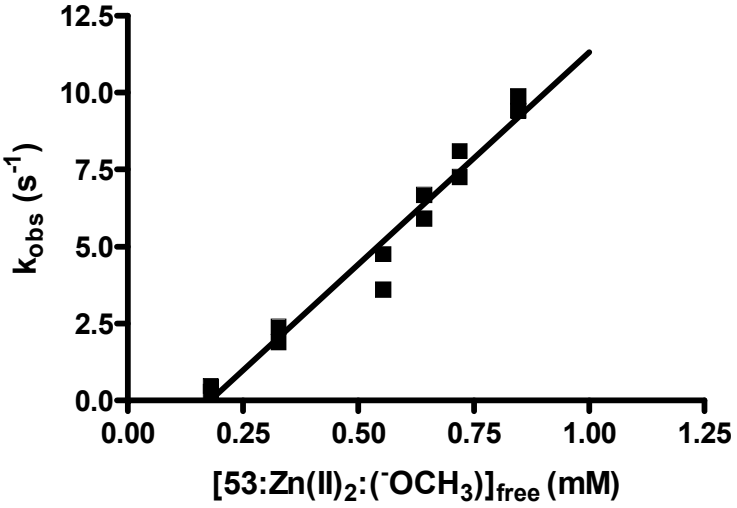

Figure 2S. A plot of k_{obs} vs [**53**:$Zn(II)_2$:($^-OCH_3$)]$_{free}$ for the catalyzed methanolysis of **1**c (5×10^{-5} M) determined from the rate of appearance of product phenol at 340 nm, ^s_spH 9.47 ± 0.17, and 25.0 ± 0.1°C. The linear regression of the data in Table 6S gives k_2 = (1.38 ± 0.08) x 10^4 $M^{-1}s^{-1}$ with an intercept of X = 0.18 ± 0.06 mM, r^2 = 0.965.

Table 7S. The k_{obs} vs [**53**:$Zn(II)_2$:($^{-}OCH_3$)]$_{free}$ data for the catalyzed methanolysis of **1**d (5×10^{-5} M) determined from the rate of appearance of product phenol at 287 nm, $^{s}_{s}$pH 9.47 ± 0.17, and 25.0 ± 0.1°C.

[**53**:$Zn(II)_2$:($^{-}OCH_3$)]$_{free}$ (mM)	k_{obs} (s^{-1})
0.18	0.28
0.18	0.27
0.33	0.76
0.33	0.81
0.55	1.12
0.55	1.16
0.64	1.38
0.64	1.46
0.72	1.68
0.72	1.61
0.85	1.83
0.85	1.77

Table 8S. The k_{obs} vs [**53**:$Zn(II)_2$:($^-OCH_3$)]$_{free}$ data for the catalyzed methanolysis of **1**e (5×10^{-5} M) determined from the rate of appearance of product phenol at 281 nm, ^s_spH 9.47 ± 0.17, and 25.0 ± 0.1°C.

[**53**:$Zn(II)_2$:($^-OCH_3$)]$_{free}$ (mM)	k_{obs} (s^{-1})
0.33	0.16
0.33	0.21
0.45	0.33
0.45	0.31
0.55	0.37
0.55	0.43
0.64	0.42
0.64	0.44
0.72	0.48
0.72	0.49
0.85	0.54
0.85	0.55

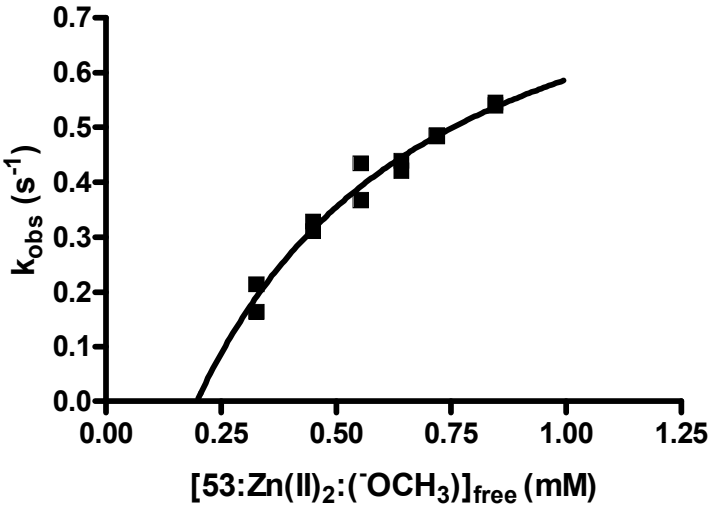

Figure 3S. A plot of k_{obs} vs [**53**:$Zn(II)_2$:($^-OCH_3$)]$_{free}$ for the catalyzed methanolysis of **1**e (5×10^{-5} M) determined from the rate of appearance of product phenol at 281 nm, ^s_spH 9.47 ± 0.17, and 25.0 ± 0.1°C. Fitting of the data in Table 8S to the expression given in Eq. (2) gives $k_{cat}^{max} = (9.50 \pm 1.93) \times 10^{-1}$ s^{-1}, $K_M = (4.78 \pm 3.14) \times 10^{-4}$ M, and an intercept X = 0.20 ± 0.04 mM, $r^2 = 0.972$.

Table 9S. The k_{obs} vs [**53**:$Zn(II)_2$:($^-OCH_3$)]$_{free}$ data for the catalyzed methanolysis of **1**f (5 x 10^{-5} M) determined from the rate of appearance of product phenol at 280 nm, ^s_spH 9.47 ± 0.17, and 25.0 ± 0.1°C.

[**53**:$Zn(II)_2$:($^-OCH_3$)]$_{free}$ (mM)	k_{obs} (s^{-1})
0.33	0.25
0.33	0.27
0.45	0.36
0.45	0.37
0.55	0.47
0.55	0.46
0.64	0.46
0.64	0.45
0.72	0.49
0.72	0.52
0.85	0.54
0.85	0.54

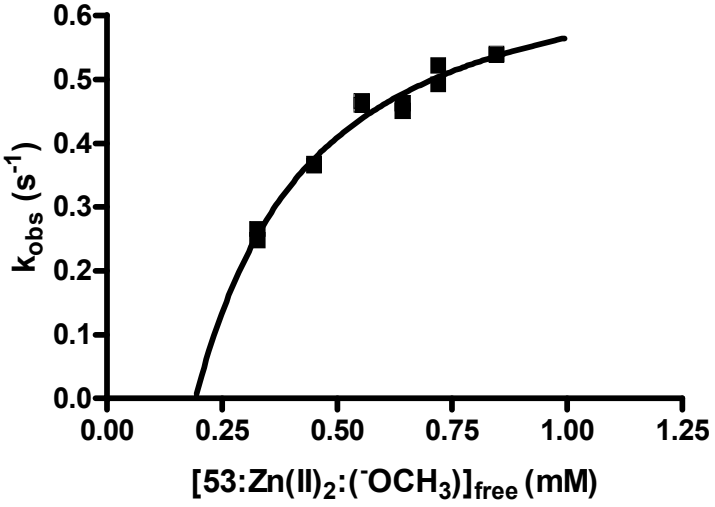

Figure 4S. A plot of k_{obs} vs [**53**:$Zn(II)_2$:($^-OCH_3$)]$_{free}$ for the catalyzed methanolysis of **1**f (5 x 10^{-5} M) determined from the rate of appearance of product phenol at 280 nm, ^s_spH 9.47 ± 0.17, and 25.0 ± 0.1°C. Fitting of the data in Table 9S to the expression given in Eq. (2) gives k_{cat}^{max} = (7.20 ± 0.72) x 10^{-1} s^{-1}, K_M = (1.81 ± 0.41) x 10^{-4} M, and an intercept X = 0.16 ± 0.03 mM, r^2 = 0.973.

Table 10S. The k_{obs} vs [**53**:$Zn(II)_2$:($^{-}OCH_3$)]$_{free}$ data for the catalyzed methanolysis of **1**g (5×10^{-5} M) determined from the rate of appearance of product phenol at 295 nm, $^{s}_{s}$pH 9.47 ± 0.17, and 25.0 ± 0.1°C.

[**53**:$Zn(II)_2$:($^{-}OCH_3$)]$_{free}$ (mM)	k_{obs} (s^{-1})
0.33	0.14
0.33	0.14
0.45	0.22
0.45	0.24
0.55	0.29
0.55	0.30
0.64	0.32
0.64	0.34
0.72	0.35
0.72	0.35
0.85	0.36
0.85	0.36

Table 11S. The observed first-order rate constants for the methanolysis of **1**a (0.05 mM) by [**53**:$Zn(II)_2$:($^-OCH_3$)]$_{total}$ (0.5 mM) in the presence of increasing amounts of MPP, **4**f, at ^s_spH 9.47 ± 0.17, 25.0 ± 0.1°C.

[MPP] (mM)	k_{obs} (s^{-1})
0	5.79
0	5.42
0.05[a]	*3.45*[a]
0.05[a]	*3.72*[a]
0.10	3.94
0.10	3.72
0.20	2.90
0.20	3.01
0.30	1.76
0.30	1.84
0.40	1.49
0.40	1.37
0.50	1.12
0.50	1.05

a. Values in italics were excluded from the determination of the inhibition constant, K_i.

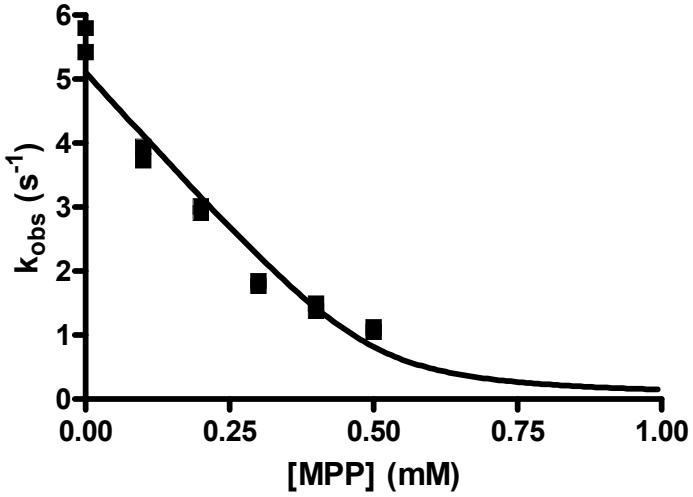

Figure 5S. Plot of the observed first-order rate constants for the methanolysis of **1**a (0.05 mM) by [**53**:$Zn(II)_2$:($^-OCH_3$)]$_{total}$ (0.5 mM) in the presence of increasing amounts of MPP, **4**f, at ^s_spH 9.47 ± 0.17, 25.0 ± 0.1°C. Fitting of the data in Table 11S to a strong inhibition Eq. (5) gives an inhibition constant, K_i, of 0.015 ± 0.002 mM for **53**:$Zn(II)_2$:($^-OCH_3$), K_i $r^2 = 0.953$.

Table 12S. The observed first-order rate constants for the methanolysis of **1**a (0.05 mM) by [**53**:$Zn(II)_2$:($^-OCH_3$)]$_{total}$ (0.5 mM) in the presence of increasing amounts of MPMPP, **4**g, at ^s_spH 9.47 ± 0.17, 25.0 ± 0.1°C.

[MPMPP] (mM)	k_{obs} (s^{-1})
0	5.95
0	4.59
0.05	4.01
0.05	4.68
0.10	4.60
0.10	3.76
0.20	3.51
0.20	3.55
0.30	2.70
0.30	2.66
0.40	1.96
0.40	1.94
0.50	1.46
0.50	1.23

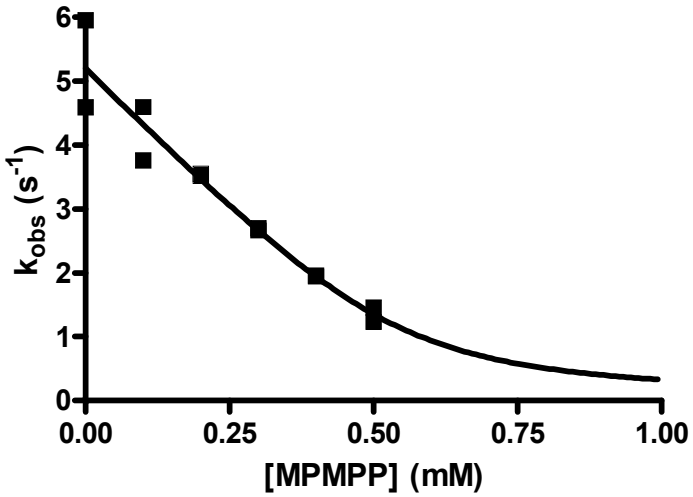

Figure 6S. Plot of the observed first-order rate constants for the methanolysis of **1**a (0.05 mM) by [**53**:$Zn(II)_2$:($^-OCH_3$)]$_{total}$ (0.5 mM) in the presence of increasing amounts of MPMPP, **4**g, at ^s_spH 9.47 ± 0.17, 25.0 ± 0.1°C. Fitting of the data in Table 12S to a strong inhibition Eq. (5) gives an inhibition constant, K_i, of 0.036 ± 0.013 mM for **53**:$Zn(II)_2$:($^-OCH_3$), $r^2 = 0.940$.

Table 13S. The observed first order rate constants for the methanolysis of **1**e (■) (0.05 mM) catalyzed by [**53**:$Zn(II)_2$:($^-OCH_3$)]$_{total}$ (0.50 mM) as a function of the [CH_3O^-]/ [**53**:$Zn(II)_2$] ratio at 25.0 ± 0.1°C.

[CH_3O^-]/[**53**:$Zn(II)_2$]	k_{obs} (s-1)
0.70	0.020
0.93	0.32
0.93	0.33
1.16	0.34
1.16	0.34
1.40	0.25
1.40	0.22
1.63	0.17
1.63	0.18
1.86	0.13
1.86	0.15
2.10	0.05
2.10	0.04
2.33	0.04
2.33	0.02

Appendix II. Supplementary material to Chapter 4

Supplementary kinetic data and figures

Table 14S. The observed first order rate constants for the methanolysis of 0.05 mM **1**a catalyzed by 1.0 mM [**36**:$Zn(II)_2$:($^-OCH_3$)]$_{total}$ as a function of time determined from the rate of appearance of product phenol at 320nm, ^s_spH 9.8 ± 0.1, and 25.0 ± 0.1°C.

Time (h)	k_{obs} (s^{-1})
0	33.98
0.7	31.35
2.7	27.19
21.7	20.78
26.7	19.70
44.7	16.20
140.9	7.83

Table 15S. The observed first order rate constants for the methanolysis of HPNPP (**1**a, 0.05 mM) catalyzed by [**53**:$Zn(II)_2$:($^-OCH_3$)]$_{total}$ (1.0 mM) as a function of increasing amounts of [uridine] determined from the rate of appearance of product phenol at 320nm, 25.0 ± 0.1°C, ^s_spH 9.47 ± 0.17.

[Uridine] (mM)	k_{obs} (s^{-1})
0	4.82
0	5.85
0	5.85
0.5	0.01
0.5	0.01
1.0	0.0002
1.0	0.0002
1.5	0.0001
1.5	0.0001
2.0	0
2.0	0
3.0	0
4.0	0
4.0	0

Table 16S. The observed first order rate constants for the methanolysis of HPNPP (**1**a, 0.05 mM) catalyzed by [**36**:$Zn(II)_2$:($^-OCH_3$)]$_{total}$ (1.0 mM) as a function of increasing amounts of [uridine] determined from the rate of appearance of product phenol at 320nm, 25.0 ± 0.1°C, ^s_spH 9.8 ± 0.1.

[Uridine] (mM)	k_{obs} (s^{-1})
0	15.12
1.0	0.003
1.0	0.003
1.5	0.0008
1.5	0.0008
2.0	0.0004
2.0	0.0004
3.0	0.0002
4.0	0.0001

Table 17S. The decomposition of UpU (0.25 mM) catalyzed by [**53**:$Zn(II)_2$:$(^{-}OCH_3)]_{free}$ (0.55 mM) in methanol at ambient temperature, $^{s}_{s}$pH 9.47 ± 0.17.

Time (h)	Relative Product Peak Area
0	0
1.6	0.10
3.8	0.17
6.0	0.18
7.5	0.20
9.0	0.21

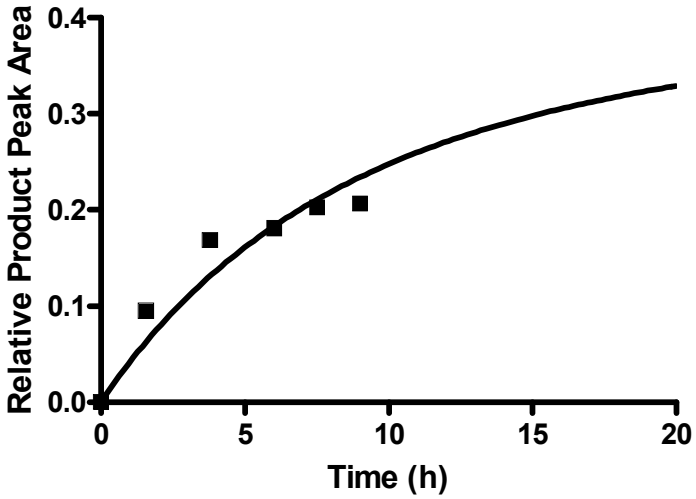

Figure 7S. The decomposition of UpU (0.25 mM) catalyzed by [**53**:$Zn(II)_2$:$(^{-}OCH_3)]_{free}$ (0.55 mM) in methanol at ambient temperature, $^{s}_{s}$pH 9.47 ± 0.17. Fitting the relative product peak area (see text) vs time data in Table 17S to Eq. (6) gives k_{obs}=(3.40 ± 0.30) x 10^{-5} s^{-1}, y_{max} = 0.4543, and r^2 = 0.900.

Table 18S. The decomposition of UpU (0.25 mM) catalyzed by [**53**:$Zn(II)_2$:($^{-}OCH_3$)]$_{free}$ (0.55 mM) in methanol at ambient temperature, $^{s}_{s}$pH 9.47 ± 0.17.

Time (h)	Relative Product Peak Area
0	0
2.2	0.08
3.7	0.10
4.5	0.13
6.0	0.17
7.4	0.20
8.9	0.19

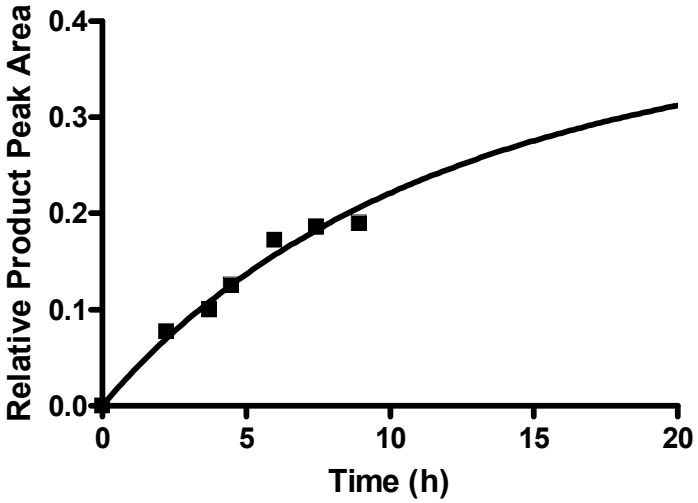

Figure 8S. The decomposition of UpU (0.25 mM) catalyzed by **53**:$Zn(II)_2$:($^{-}OCH_3$) (0.55 mM) in methanol at ambient temperature, $^{s}_{s}$pH 9.47 ± 0.17. Fitting the relative product peak area (see text) vs time data in Table 18S to Eq. (6) gives k_{obs} = (2.23 ± 0.08) x 10^{-5} s^{-1}, y_{max} = 0.547, and r^2 = 0.978.

Table 19S. The decomposition of UpU (0.25 mM) catalyzed by [**53**:$Zn(II)_2$:$(^{-}OCH_3)]_{free}$ (0.64 mM) in methanol at ambient temperature, $^{s}_{s}$pH 9.47 ± 0.17.

Time (h)	Relative Product Peak Area
0	0
1.2	0.20
2.8	0.33
7.6	0.35
10.6	*0.54*
24.9	0.41
32.3	0.45

Values in italics were excluded from the determination of the first order rate constant.

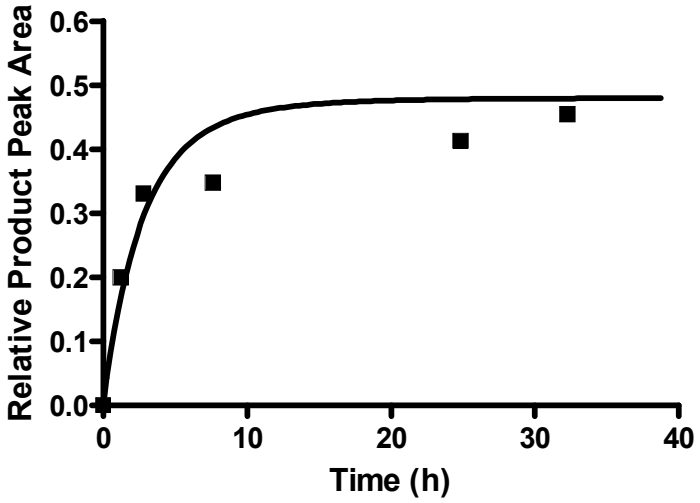

Figure 9S. The decomposition of UpU (0.25 mM) catalyzed by [**53**:$Zn(II)_2$:$(^{-}OCH_3)]_{free}$ (0.64 mM) in methanol at ambient temperature, $^{s}_{s}$pH 9.47 ± 0.17. Fitting the relative product peak area (see text) vs time data in Table 19S to Eq. (6) gives k_{obs}=(1.00 ± 0.22) x 10^{-4} s^{-1}, y_{max} = 0.480, and r^2 = 0.896.

Table 20S. The decomposition of UpU (0.25 mM) catalyzed by [**53**:$Zn(II)_2$:($^{-}OCH_3$)]$_{free}$ (0.64 mM) in methanol at ambient temperature, $^{s}_{s}$pH 9.47 ± 0.17.

Time (h)	Relative Product Peak Area
0	0
1.6	0.23
4.8	0.30
6.5	0.41
7.6	0.36
24.7	0.49
29.3	0.46
32.3	0.50

Table 21S. The decomposition of UpU (0.25 mM) catalyzed by [**53**:$Zn(II)_2$:$(^{-}OCH_3)]_{free}$ (0.72 mM) in methanol at ambient temperature, $^{s}_{s}$pH 9.47 ± 0.17.

Time (h)	Relative Product Peak Area
0	0
0.8	0.25
1.5	0.35
4.0	*0.47*
6.3	*0.47*
9.4	0.36
25.1	0.39

Values in italics were excluded from the determination of the first order rate constant.

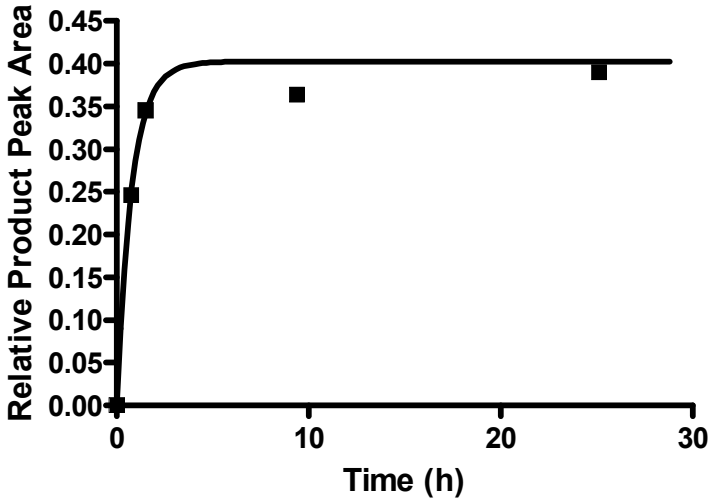

Figure 10S. The decomposition of UpU (0.25 mM) catalyzed by [**53**:$Zn(II)_2$:$(^{-}OCH_3)]_{free}$ (0.72 mM) in methanol at ambient temperature, $^{s}_{s}$pH 9.47 ± 0.17. Fitting the relative product peak area (see text) vs time data in Table 21S to Eq. (6) gives k_{obs}=(3.01 ± 0.33) x 10^{-4} s^{-1}, y_{max} = 0.403, and r^2 = 0.983.

Table 22S. The decomposition of UpU (0.25 mM) catalyzed by [**53**:$Zn(II)_2$:$(^{-}OCH_3)]_{free}$ (0.72 mM) in methanol at ambient temperature, $^{s}_{s}$pH 9.47 ± 0.17.

Time (h)	Relative Product Peak Area
0	0
0.8	0.29
1.5	0.35
2.6	0.35
3.4	0.39
4.1	0.39
20.6	0.38

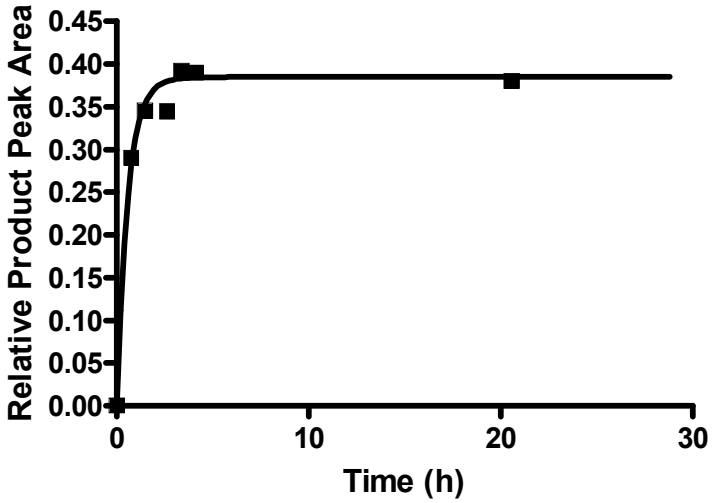

Figure 11S. The decomposition of UpU (0.25 mM) catalyzed by [**53**:$Zn(II)_2$:$(^{-}OCH_3)]_{free}$ (0.72 mM) in methanol at ambient temperature, $^{s}_{s}$pH 9.47 ± 0.17. Fitting the relative product peak area (see text) vs time data in Table 22S to Eq. (6) gives k_{obs}=(4.09 ± 0.42) x 10^{-4} s^{-1}, y_{max} = 0.3848, and r^2 = 0.987.

Table 23S. The decomposition of UpU (0.25 mM) catalyzed by [**53**:$Zn(II)_2$:$(^{-}OCH_3)]_{free}$ (0.82 mM) in methanol at ambient temperature, $^{s}_{s}$pH 9.47 ± 0.17.

Time (h)	Relative Product Peak Area
0	0
0.7	*0.46*
1.2	0.37
1.5	0.44
4.6	0.52

Values in italics were excluded from the determination of the first order rate constant.

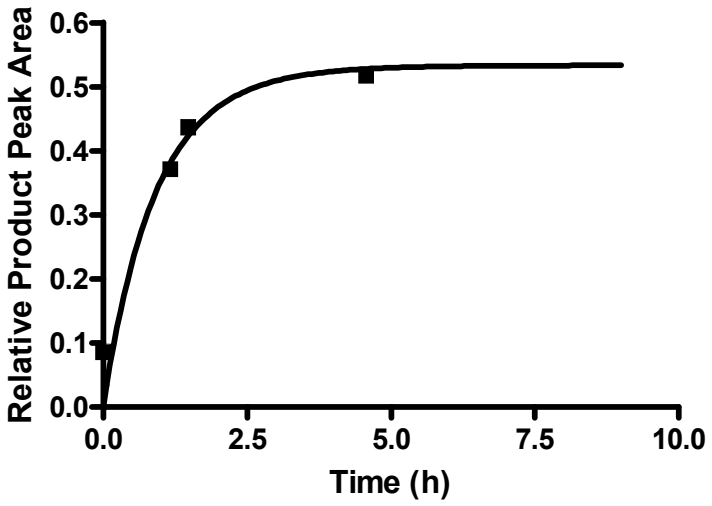

Figure 12S. The decomposition of UpU (0.25 mM) catalyzed by [**53**:$Zn(II)_2$:$(^{-}OCH_3)]_{free}$ (0.82 mM) in methanol at ambient temperature, $^{s}_{s}$pH 9.47 ± 0.17. Fitting the relative product peak area (see text) vs time data in Table 23S to Eq. (6) gives k_{obs}=(2.04 ± 0.40) x 10^{-4} s^{-1}, y_{max} = 0.533, and r^2 = 0.927.

Table 24S. The decomposition of UpU (0.25 mM) catalyzed by [**53**:Zn(II)$_2$:($^-$OCH$_3$)]$_{free}$ (0.82 mM) in methanol at ambient temperature, ^s_spH 9.47 ± 0.17.

Time (h)	Relative Product Peak Area
0	0
0.4	0.27
0.8	0.32
1.1	0.34
1.5	0.40
2.2	0.48

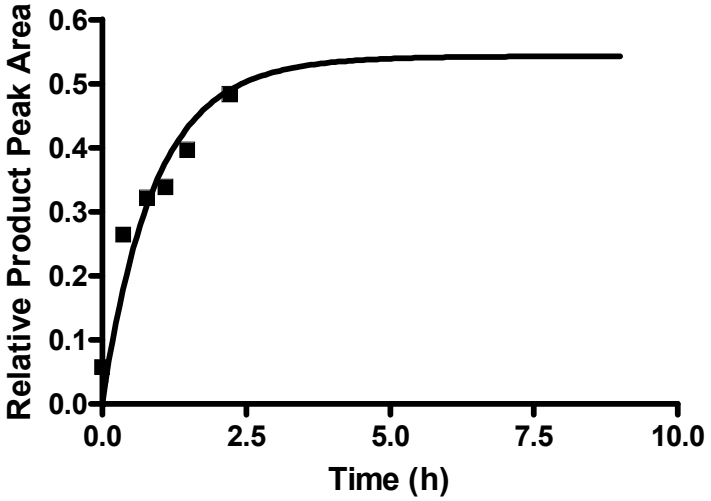

Figure 13S. The decomposition of UpU (0.25 mM) catalyzed by [**53**:Zn(II)$_2$:($^-$OCH$_3$)]$_{free}$ (0.82 mM) in methanol at ambient temperature, ^s_spH 9.47 ± 0.17. Fitting the relative product peak area (see text) vs time data in Table 24S to Eq. (6) gives k_{obs}=(2.04 ± 0.28) x 10^{-4} s^{-1}, y_{max} = 0.543, and r^2 = 0.872.

Table 25S. The decomposition of UpU (0.25 mM) catalyzed by [**53**:$Zn(II)_2$:$(^{-}OCH_3)]_{free}$ (0.90 mM) in methanol at ambient temperature, $^{s}_{s}$pH 9.47 ± 0.17.

Time (h)	Relative Product Peak Area
0	0.03
0.4	0.36
0.8	0.50
1.2	0.45
1.5	*0.39*
1.9	0.56

Values in italics were excluded from the determination of the first order rate constant.

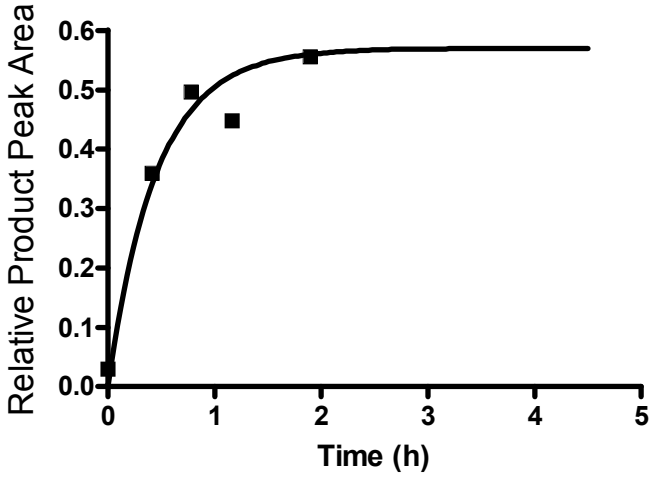

Figure 14S. The decomposition of UpU (0.25 mM) catalyzed by [**53**:$Zn(II)_2$:$(^{-}OCH_3)]_{free}$ (0.90 mM) in methanol at ambient temperature, $^{s}_{s}$pH 9.47 ± 0.17. Fitting the relative product peak area (see text) vs time data in Table 25S to Eq. (6) gives k_{obs}=(3.42 ± 0.51) x 10^{-4} s^{-1}, y_{max} = 0.570, and r^2 = 0.954.

Table 26S. The decomposition of UpU (0.25 mM) catalyzed by [**53**:$Zn(II)_2$:$(^{-}OCH_3)]_{free}$ (0.90 mM) in methanol at ambient temperature, $^{s}_{s}$pH 9.47 ± 0.17.

Time (h)	Relative Product Peak Area
0	0.02
0.4	0.45
0.7	0.59
1.2	0.55

Table 27S. The decomposition of UpU (0.25 mM) catalyzed by [**53**:$Zn(II)_2$:$(^{-}OCH_3)]_{free}$ (0.95 mM) in methanol at ambient temperature, $^{s}_{s}$pH 9.47 ± 0.17.

Time (h)	Relative Product Peak Area
0	0.06
0.4	0.36
0.8	0.47
1.2	*0.42*
3.1	0.47
23.0	0.52

Values in italics were excluded from the determination of the first order rate constant.

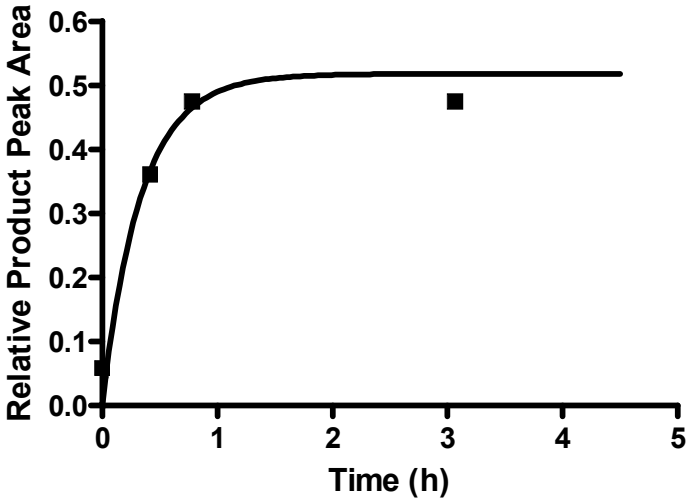

Figure 15S. The decomposition of UpU (0.25 mM) catalyzed by [**53**:$Zn(II)_2$:$(^{-}OCH_3)]_{free}$ (0.95 mM) in methanol at ambient temperature, $^{s}_{s}$pH 9.47 ± 0.17. Fitting the relative product peak area (see text) vs time data in Table 27S to Eq. (6) gives k_{obs}=(4.13 ± 0.68) x 10^{-3} s^{-1}, y_{max} = 0.518, and r^2 = 0.962.

Table 28S. The decomposition of UpU (0.25 mM) catalyzed by [**53**:$Zn(II)_2$:$(^{-}OCH_3)]_{free}$ (0.95 mM) in methanol at ambient temperature, $^{s}_{s}$pH 9.47 ± 0.17.

Time (h)	Relative Product Peak Area
0.1	0.16
0.4	0.40
0.7	0.41
1.1	*0.43*
1.9	0.46
19.9	0.44

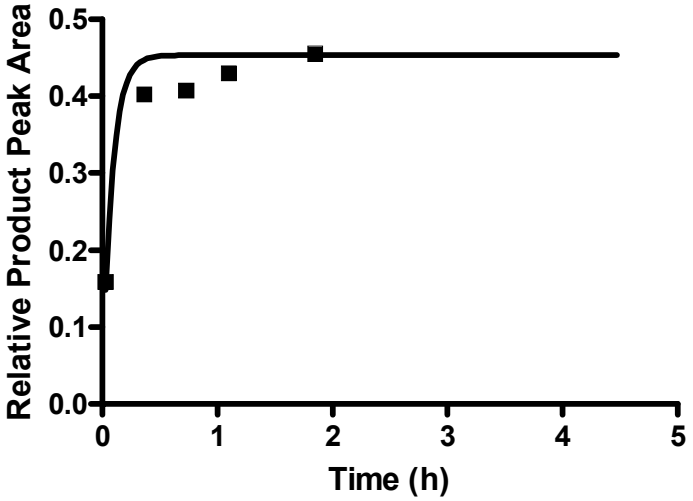

Figure 16S. The decomposition of UpU (0.25 mM) catalyzed by [**53**:$Zn(II)_2$:$(^{-}OCH_3)]_{free}$ (0.95 mM) in methanol at ambient temperature, $^{s}_{s}$pH 9.47 ± 0.17. Fitting the relative product peak area (see text) vs time data in Table 28S to Eq. (6) gives k_{obs}=(1.66 ± 0.42) x 10^{-3} s^{-1}, y_{max} = 0.454, and r^2 = 0.919.

Table 29S. The decomposition of UpU (0.25 mM) catalyzed by [**36**:$Zn(II)_2$:$(^{-}OCH_3)]_{free}$ (0.44 mM) in methanol at ambient temperature, $^{s}_{s}$pH 9.8 ± 0.1.

Time (h)	Relative Product Peak Area
0	0
21.6	0.004
27.8	0.02
31.5	0.02
53.9	0.04
72.8	0.06

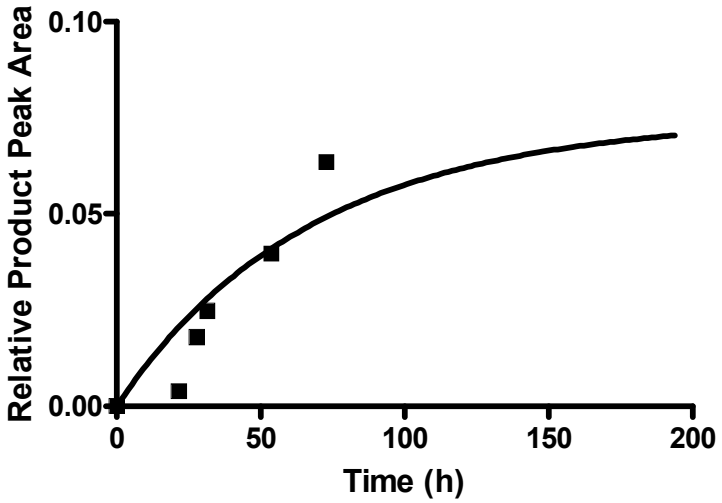

Figure 17S. The decomposition of UpU (0.25 mM) catalyzed by [**36**:$Zn(II)_2$:$(^{-}OCH_3)]_{free}$ (0.44 mM) in methanol at ambient temperature, $^{s}_{s}$pH 9.8 ± 0.1. Fitting the relative product peak area (see text) vs time data in Table 29S to Eq. (6) gives k_{obs}=(1.26 ± 0.18) x 10^{-6} s^{-1}, y_{max} = 0.4995, and r^2 = 0.804.

Table 30S. The decomposition of UpU (0.25 mM) catalyzed by [**36**:$Zn(II)_2$:($^{-}OCH_3$)]$_{free}$ (0.52 mM) in methanol at ambient temperature, $^{s}_{s}$pH 9.8 ± 0.1.

Time (h)	Relative Product Peak Area
0	0
21.4	0.003
31.5	0.006
52.1	0.02
79.5	0.03

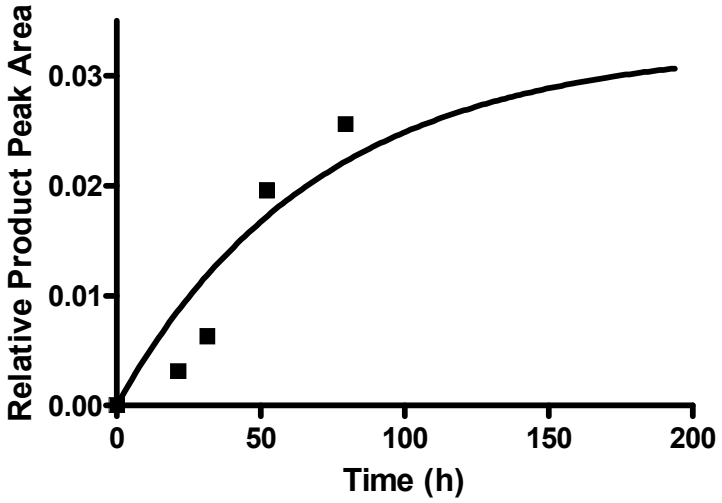

Figure 18S. The decomposition of UpU (0.25 mM) catalyzed by [**36**:$Zn(II)_2$:($^{-}OCH_3$)]$_{free}$ (0.52 mM) in methanol at ambient temperature, $^{s}_{s}$pH 9.8 ± 0.1. Fitting the relative product peak area (see text) vs time data in Table 30S to Eq. (6) gives k_{obs}=(4.38 ± 0.63) x 10^{-7} s^{-1}, y_{max} = 0.500, and r^2 = 0.838.

Table 31S. The decomposition of UpU (0.25 mM) catalyzed by [**36**:$Zn(II)_2$:$(^{-}OCH_3)]_{free}$ (0.52 mM) in methanol at ambient temperature, $^{s}_{s}$pH 9.8 ± 0.1.

Time (h)	Relative Product Peak Area
0	0
31.4	0.02
52.5	0.03
72.7	0.04

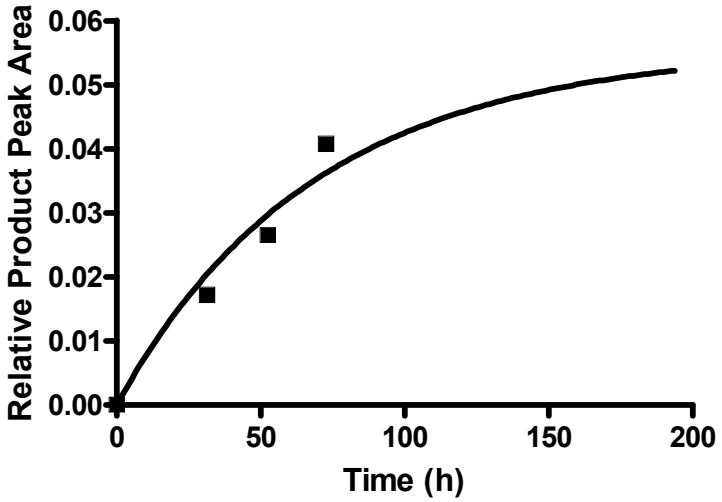

Figure 19S. The decomposition of UpU (0.25 mM) catalyzed by [**36**:$Zn(II)_2$:$(^{-}OCH_3)]_{free}$ (0.52 mM) in methanol at ambient temperature, $^{s}_{s}$pH 9.8 ± 0.1. Fitting the relative product peak area (see text) vs time data in Table 31S to Eq. (6) gives k_{obs}=(7.62 ± 0.57) x 10^{-6} s^{-1}, y_{max} = 0.4995, and r^2 = 0.953.

Table 32S. The decomposition of UpU (0.25 mM) catalyzed by [**36**:$Zn(II)_2$:$(^{-}OCH_3)]_{free}$ (0.66 mM) in methanol at ambient temperature, $^{s}_{s}$pH 9.8 ± 0.1.

Time (h)	Relative Product Peak Area
0	0
23.2	0.12
29.5	0.20
33.6	0.18
51.0	0.34
72.7	0.35

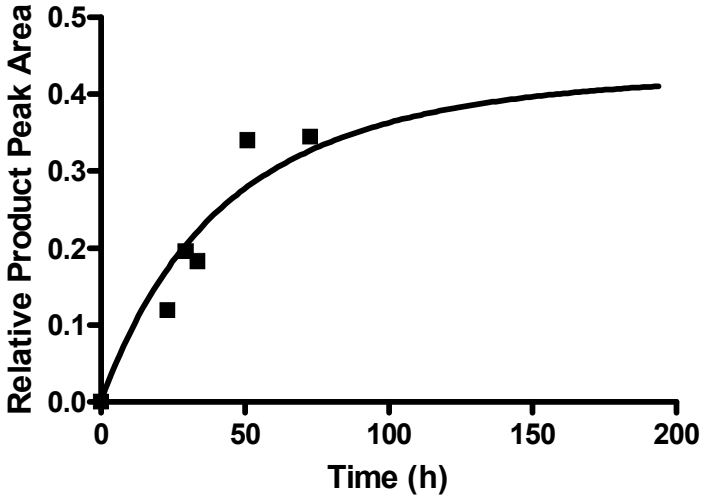

Figure 20S. The decomposition of UpU (0.25 mM) catalyzed by [**36**:$Zn(II)_2$:$(^{-}OCH_3)]_{free}$ (0.66 mM) in methanol at ambient temperature, $^{s}_{s}$pH 9.8 ± 0.1. Fitting the relative product peak area (see text) vs time data in Table 32S to Eq. (6) gives k_{obs}=(5.99 ± 0.61) x 10^{-6} s^{-1}, y_{max} = 0.599, and r^2 = 0.903.

Table 33S. The decomposition of UpU (0.25 mM) catalyzed by [**36**:$Zn(II)_2$:$(^{-}OCH_3)]_{free}$ (0.66 mM) in methanol at ambient temperature, $^{s}_{s}$pH 9.8 ± 0.1.

Time (h)	Relative Product Peak Area
0	0
24.8	0.11
31.5	0.17
48.5	0.20
54.7	*0.31*
72.7	0.28

Values in italics were excluded from the determination of the first order rate constant.

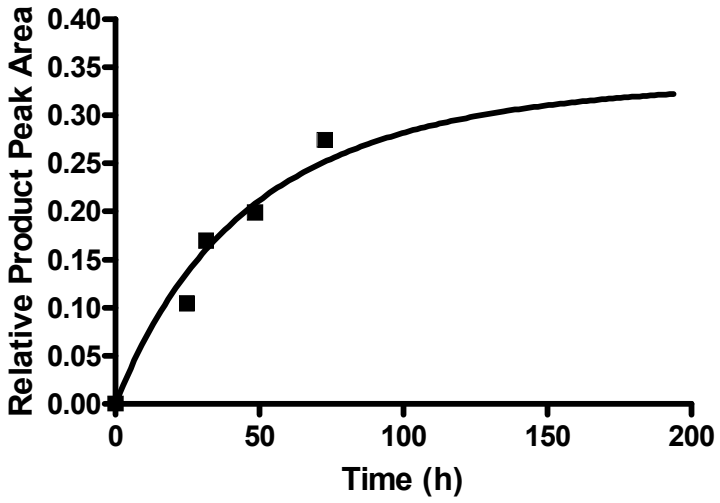

Figure 21S. The decomposition of UpU (0.25 mM) catalyzed by [**36**:$Zn(II)_2$:$(^{-}OCH_3)]_{free}$ (0.66 mM) in methanol at ambient temperature, $^{s}_{s}$pH 9.8 ± 0.1. Fitting the relative product peak area (see text) vs time data in Table 33S to Eq. (6) gives k_{obs}=(5.12 ± 0.36) x 10^{-6} s^{-1}, y_{max} = 0.514, and r^2 = 0.960.

Table 34S. The decomposition of UpU (0.25 mM) catalyzed by [**36**:Zn(II)$_2$:($^-$OCH$_3$)]$_{free}$ (0.79 mM) in methanol at ambient temperature, ^s_spH 9.8 ± 0.1.

Time (h)	Relative Product Peak Area
0	0
3.3	0.09
5.7	0.12
7.9	0.20
10.2	0.31
12.4	*0.38*
14.7	0.32
22.2	*0.32*
27.7	0.38

Values in italics were excluded from the determination of the first order rate constant.

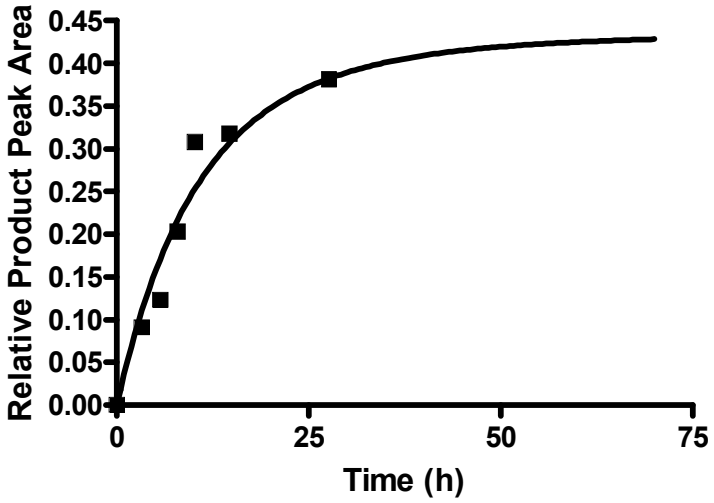

Figure 22S. The decomposition of UpU (0.25 mM) catalyzed by [**36**:Zn(II)$_2$:($^-$OCH$_3$)]$_{free}$ (0.79 mM) in methanol at ambient temperature, ^s_spH 9.8 ± 0.1. Fitting the relative product peak area (see text) vs time data in Table 34S to Eq. (6) gives k_{obs}=(2.54 ± 0.24) x 10^{-5} s^{-1}, y_{max} = 0.436, and r^2 = 0.948.

Table 35. The decomposition of UpU (0.25 mM) catalyzed by [**36**:$Zn(II)_2$:$(^{-}OCH_3)]_{free}$ (0.79 mM) in methanol at ambient temperature, $^{s}_{s}$pH 9.8 ± 0.1.

Time (h)	Relative Product Peak Area
0	0
1.8	0
6.0	0.16
9.2	0.19
11.4	0.24
13.7	*0.30*
16.0	0.26
23.5	0.30
29.1	0.33

Values in italics were excluded from the determination of the first order rate constant.

Table 36S. The decomposition of UpU (0.25 mM) catalyzed by [**36**:$Zn(II)_2$:$(^{-}OCH_3)]_{free}$ (0.91 mM) in methanol at ambient temperature, $^{s}_{s}$pH 9.8 ± 0.1.

Time (h)	Relative Product Peak Area
0	0
1.6	0.09
4.0	0.10
6.9	0.17
8.6	0.21
10.9	0.38
13.1	*0.45*
22.9	0.41
28.4	0.44

Values in italics were excluded from the determination of the first order rate constant.

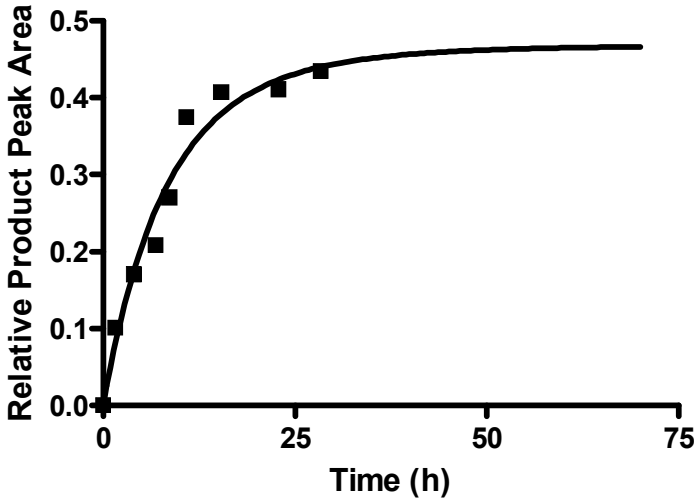

Figure 23S. The decomposition of UpU (0.25 mM) catalyzed by [**36**:$Zn(II)_2$:$(^{-}OCH_3)]_{free}$ (0.91 mM) in methanol at ambient temperature, $^{s}_{s}$pH 9.8 ± 0.1. Fitting the relative product peak area (see text) vs time data in Table 36S to Eq. (6) gives k_{obs}=(2.77 ± 0.20) x 10^{-5} s^{-1}, y_{max} = 0.469, and r^2 = 0.969.

Table 37S. The decomposition of UpU (0.25 mM) catalyzed by [**36**:Zn(II)$_2$:($^-$OCH$_3$)]$_{free}$ (0.91 mM) in methanol at ambient temperature, ^s_spH 9.8 ± 0.1.

Time (h)	Relative Product Peak Area
0	0
2.0	0.07
4.4	0.15
6.7	0.26
8.9	0.29
11.1	0.35
13.2	0.38
20.9	0.50
26.4	*0.41*

Values in italics were excluded from the determination of the first order rate constant.

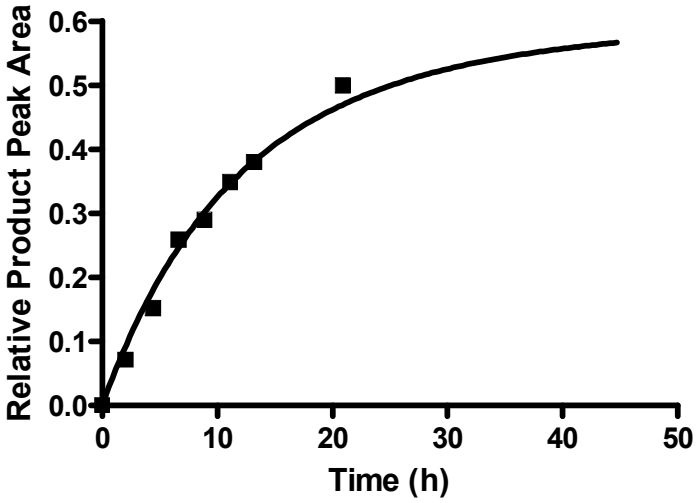

Figure 24S. The decomposition of UpU (0.25 mM) catalyzed by [**36**:Zn(II)$_2$:($^-$OCH$_3$)]$_{free}$ (0.91 mM) in methanol at ambient temperature, ^s_spH 9.8 ± 0.1. Fitting the relative product peak area (see text) vs time data in Table 37S to Eq. (6) gives k_{obs}=(1.91 ± 0.07) x 10^{-5} s^{-1}, y_{max} = 0.605, and r^2 = 0.988.

Table 38S. The decomposition of UpU (0.25 mM) catalyzed by [**36**:Zn(II)$_2$:($^-$OCH$_3$)]$_{free}$ (1.07 mM) in methanol at ambient temperature, ^s_spH 9.8 ± 0.1.

Time (h)	Relative Product Peak Area
0	0
2.0	0.14
4.4	0.26
6.6	0.35
8.9	*0.44*
11.1	*0.53*
13.4	0.47
20.9	0.39
26.4	0.40

Values in italics were excluded from the determination of the first order rate constant.

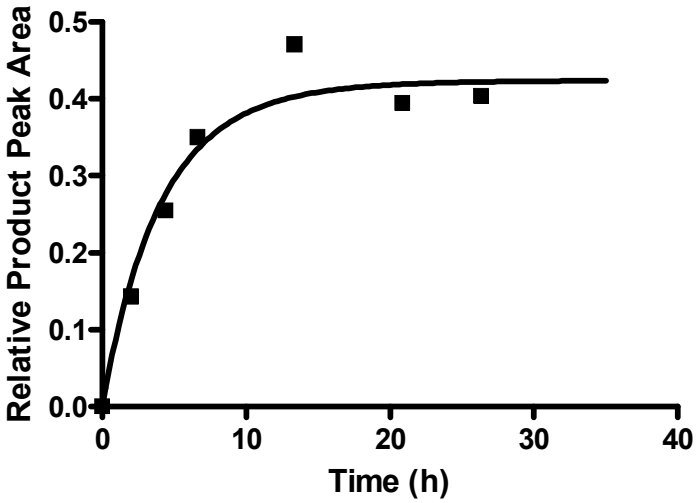

Figure 25S. The decomposition of UpU (0.25 mM) catalyzed by [**36**:Zn(II)$_2$:($^-$OCH$_3$)]$_{free}$ (1.07 mM) in methanol at ambient temperature, ^s_spH 9.8 ± 0.1. Fitting the relative product peak area (see text) vs time data in Table 38S to Eq. (6) gives k_{obs}=(4.55 ± 0.60) x 10^{-5} s^{-1}, y_{max} = 0.424, and r^2 = 0.960.

Table 39S. The decomposition of UpU (0.25 mM) catalyzed by [**36**:$Zn(II)_2$:$(^{-}OCH_3)]_{free}$ (1.07 mM) in methanol at ambient temperature, $^{s}_{s}$pH 9.8 ± 0.1.

Time (h)	Relative Product Peak Area
0	0
2.4	0.17
4.6	0.25
6.9	0.35
9.1	*0.52*
11.4	*0.56*
18.9	0.45
24.4	*0.38*

Values in italics were excluded from the determination of the first order rate constant.

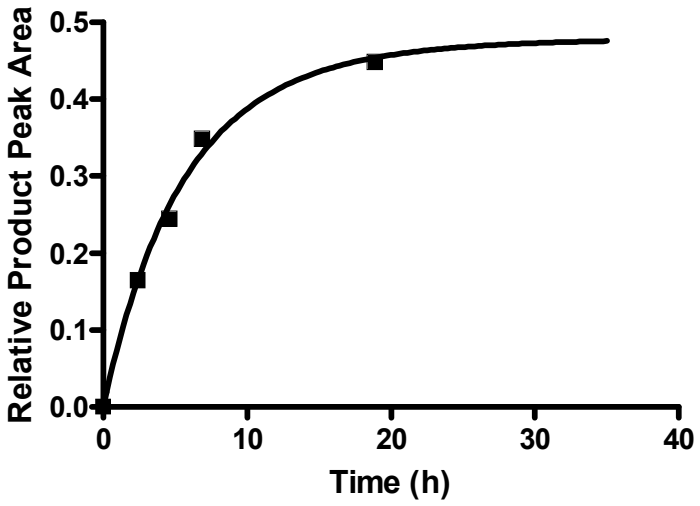

Figure 26S. The decomposition of UpU (0.25 mM) catalyzed by [**36**:$Zn(II)_2$:$(^{-}OCH_3)]_{free}$ (1.07 mM) in methanol at ambient temperature, $^{s}_{s}$pH 9.8 ± 0.1. Fitting the relative product peak area (see text) vs time data in Table 39S to Eq. (6) gives k_{obs}=(3.28 ± 0.15) x 10^{-5} s^{-1}, y_{max} = 0.479, and r^2 = 0.994.

Table 40S. The k_{obs} vs [**53**:$Zn(II)_2$:($^{-}OCH_3$)]$_{free}$ data for the catalyzed methanolysis of UpU (0.25 mM) determined from the rate of appearance of product peaks corresponding to methyl 2'-UMP, methyl 3'-UMP, and uridine at 260nm, $^{s}_{s}$pH 9.47 ± 0.17, and ambient temperature.

[**53**:$Zn(II)_2$: ($^{-}OCH_3$)]$_{free}$ (mM)	k_{obs} (x 10^{-4}, s^{-1})
0.55	0.3
0.55	0.2
0.64	1.0
0.64	0.7
0.72	2.0
0.72	2.0
0.82	3.0
0.82	4.1
0.90	3.4
0.90	5.8
0.95	4.1

Table 41S. The k_{obs} vs [**36**:$Zn(II)_2$:($^{-}OCH_3$)]$_{free}$ data for the catalyzed methanolysis of UpU (0.25 mM) determined from the rate of appearance of product peaks corresponding to methyl 2'-UMP, methyl 3'-UMP, and uridine at 260nm, $^{s}_{s}$pH 9.8 ± 0.1, and ambient temperature.

[**36**:$Zn(II)_2$: ($^{-}OCH_3$)]$_{free}$ (mM)	k_{obs} (x 10^{-5}, s^{-1})
0.52	0.1
0.66	0.6
0.66	0.5
0.79	1.6
0.79	2.5
0.91	2.8
0.91	1.9
1.07	4.4
1.07	3.3

Appendix III. Supplementary material to Chapter 5

NMR data

2-Hydroxylpropyl methyl phosphate (8:92 ratio of **54a/54**). ^{1}H NMR (600MHz, CD_3OD, 25 ^{o}C) δ 1.175 (**54** CHC$\underline{H}_3$, d, J = 6 Hz), δ 1.265 (**54a** CHC$\underline{H}_3$, d, J = 6 Hz), δ 3.595 (**54/54a** OC$\underline{H}_3$, d, J_{P-H} = 18 Hz), δ 3.725 (2H, m, J = 6 Hz), δ 3.930 (1H, m, J = 6 Hz).

Supplementary kinetic data, figures, schemes, and equations

Table 42S. The relative peak area vs time data for the methanolysis of **56** promoted by 500 mM $NaOCD_3$ in CD_3OD at 25.0 ± 0.1 ^{o}C.

Time (h)	Accumulative ½ Relative Peak Area of **54** and **54**a	Relative Peak Area of **56**
0.2	0.37	1.69
1.7	0.72	1.44
3.3	1.04	1.09
5.0	1.26	0.88
6.7	1.35	0.76
8.3	1.52	0.61
10.0	1.75	0.53
11.7	1.68	0.48
13.3	1.69	0.44
15.0	1.76	0.40
26.5	1.85	0.38
28.0	1.79	0.36
50.0	1.64	0.40
66.0	1.76	0.38

Table 43S. The relative peak areas (peak area of interest/reference peak area) for the methanolysis of HPNPP (2.82 mM) and **56** catalyzed by 3.13 mM of [**36**:$Zn(II)_2$:($^{-}OCH_3$)]$_{total}$ determined from: the disappearance of the signals at δ 7.345 (d, $^3J_{H-H}$ = 6 Hz) corresponding to the *ortho* protons of HPNPP (■); the disappearance of the signal at δ 1.355 (3H, d, $^3J_{H-H}$ = 6 Hz) belonging to the methyl group of HPNPP (□□), the appearance of the signal at δ 6.915 (d, $^3J_{H-H}$ = 6 Hz) belonging to the *ortho* protons of released *p*-nitrophenol (▲); the disappearance of the signal at δ 1.355 (d, $^3J_{H-H}$ = 6 Hz) belonging to **56** (▼); and the accumulative appearance of peaks at δ 1.185 (d, $^3J_{H-H}$ = 6 Hz) and δ 1.285 (d, $^3J_{H-H}$ = 6 Hz) belonging to **54** (♦) and **54a** (●), respectively, at $^{s}_{s}$pH 9.8 ± 0.1 and ambient temperature.

Reaction Time/s	**HPNPP *ortho* protons (■)**	**HPNPP methyl group protons (□)**	***p*-NO_2 phenol *ortho* protons (▲)**	**2-hydroxypropyl moiety methyl protons of 56 (▼)**	**2-hydroxypropyl moiety methyl protons of 54 (♦)**	**2-hydroxypropyl moiety methyl protons of 54a (●)**
0	2.00	3.00	---	---	---	---
0.1	1.30*	2.23*	0.70*	1.01*	0.00	0.00
1	0.41	0.63	1.59	1.72	0.73	0.41
2	0.12	0.21	1.88	0.94	1.50	0.69
3	0.00	0.00	2.00*	1.05*	1.58*	0.71*
4	0.00	0.00	2.00*	0.07	2.45	1.02
5	0.00	0.00	2.00*	0.00	2.45	1.01

Values with an asterix (*) were excluded from the determination of rate constants.

Table 44S. The relative peak area vs. time data for the interconversion of **54** and **54a** catalyzed by [**36**:$Zn(II)_2$:($^{-}OCH_3$)]$_{total}$ (3.13 mM) in CH_3OH at ambient temperature, $^{s}_{s}$pH 9.8 ± 0.1.

Time (min.)	Relative Peak Area of **54**	Relative Peak Area of **54a**
0	0.30	0.70
1.0	0.41	0.59
4.0	0.54	0.46
8.0	0.60	0.40
12.0	0.64	0.36
16.0	0.65	0.35

Table 45S. The isomerization of **54/54a** (2.025 mM) catalyzed by 2.25 mM [**36**:Zn(II)$_2$:($^-$OCD$_3$)]$_{total}$ in CD$_3$OD at 25.0 ± 0.1 ^{o}C as a function of time. Relative ratios of **54/54a** were determined.

Time (min.)	Relative Ratio of **54**	Relative Ratio of **54a**
0	88	12
10	82	18
20	75	25
30	71	29
40	69	31
50	68	32
60	68	32
140	68	32

Table 46S. The decomposition of **54** and **54a** (2.025 mM) catalyzed by 2.25 mM [**36**:Zn(II)$_2$:($^-$OCD$_3$)]$_{total}$ in CD$_3$OD at 25.0 ± 0.1 ^{o}C. The relative peak area of **54** and **54a** was determined over the course of time.

Time (min.)	Relative Peak Area of **54**
10	0.57
20	0.38
30	0.32
40	0.28
50	0.21

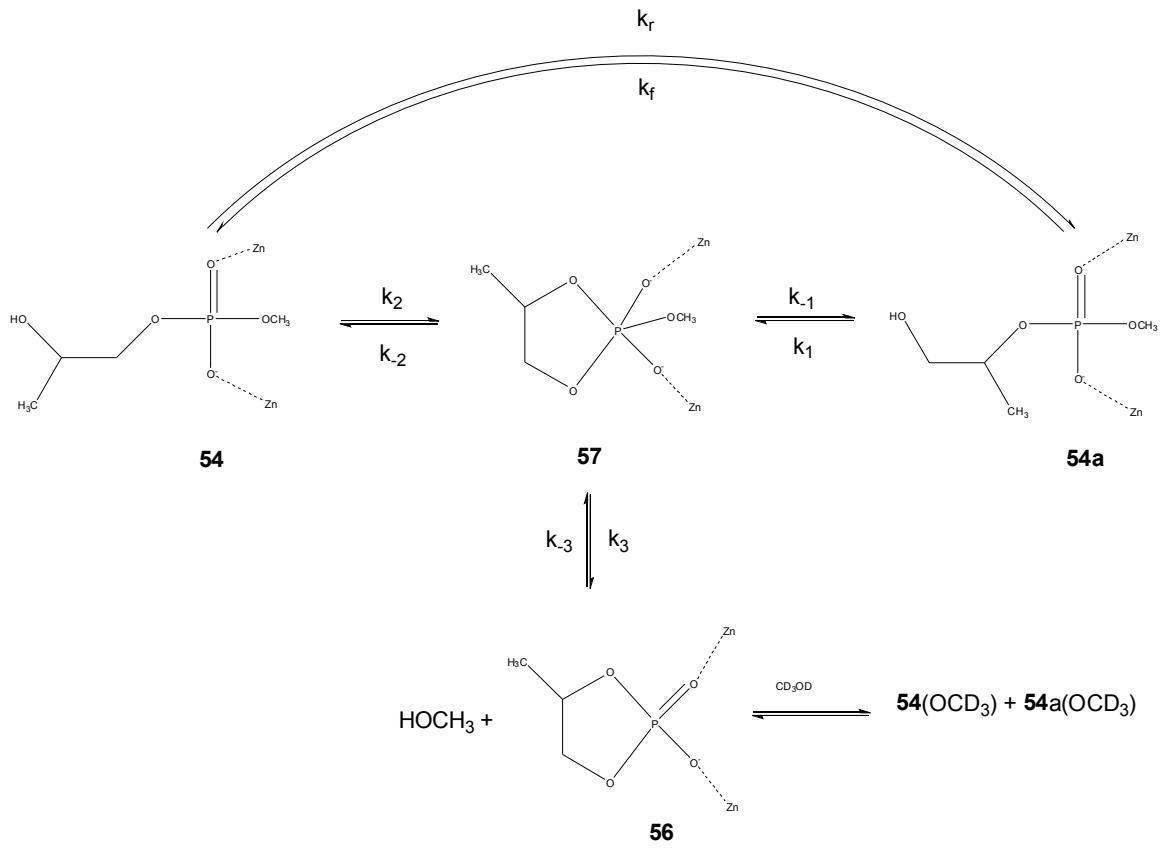

Scheme 1S. Interconversion of the various species of interest catalyzed by **36**:Zn(II)$_2$:($^-$OCD$_3$) in methanol-D4 and the relevant rate constants.

The 36:Zn(II)$_2$:($^-$OCH$_3$)-catalyzed equilibration of 54 and 54a in CH$_3$OH.

The rate constant for the equilibration of **54a/54** to a final thermodynamic ratio of 35/65 catalyzed by **36**:Zn(II)$_2$:($^-$OCH$_3$) (3.13 mM) in CH$_3$OH is obtained from Eq. (1S).

(1S) $k_{obs} = k_f + k_r = 4.7 \times 10^{-3}\ s^{-1}$

where, at equilibrium $k_f/k_r = 65/35$ and so, $k_f = 0.65*(4.7 \times 10^{-3}s^{-1}) = 3.07 \times 10^{-3}s^{-1}$ and $k_r = 0.35*(4.7 \times 10^{-3}s^{-1}) = 1.65 \times 10^{-3}s^{-1}$.

Assuming steady-state conditions for the formation and breakdown of phosphorane intermediate **57**, Eq. (2S) can be derived.

(2S) $d[\mathbf{57}]/dt = [\mathbf{54a}]k_1 + [\mathbf{54}]k_2 + [\mathbf{56}]k_{-3} - [\mathbf{57}](k_{-1} + k_{-2}) - [\mathbf{57}]k_3 = 0$

Steady-state conditions can also be applied to **56** and its transesterification to

yield **54** and **54a** has been experimentally proven to be fast and Eq. (3S) follows.

(3S) $d[\mathbf{56}]/dt = [\mathbf{56}]k_{-3} - [\mathbf{57}]k_3 = 0$

Substitution of (3S) into (2S) yields Eq. (4S).

(4S) $d[\mathbf{57}]/dt = [\mathbf{54a}]k_1 + [\mathbf{54}]k_2 - [\mathbf{57}](k_{-1} + k_{-2}) = 0$

The suite of phosphorane intermediates (**57**) depicted in Scheme 1S partition into **54**, **54a**, and **56**. The 3.13 mM of **36**:$Zn(II)_2$:($^-OCH_3$)-catalyzed partitioning of **57** into **54** and **54a** gives $k_{-1}/k_{-2} = 79/21 = 2.45$ in CH_3OH. Rate constants for the forward and reverse isomerization reactions are indicated in Eq. (5S) and (6S), respectively, from which rate constants for the formation of **57** from **54** and **54a** (k_1 and k_2, correspondingly) can be determined.

(5S) $k_f = k_1k_{-2}/(k_{-1} + k_{-2}) = k_1(29/100)$

where, $k_1 = 3.07 \times 10^{-3} /0.29 = 1.06 \times 10^{-2}\ s^{-1}$.

(6S) $k_r = k_2k_{-1}/(k_{-1} + k_{-2}) = k_2(71/100)$

where, $k_2 = k_r/0.71 = 2.32 \times 10^{-3} s^{-1}$.

The 36:$Zn(II)_2$:($^-OCH_3$)-catalyzed formation of 56 from 54 and 54a in CD_3OD.

It can be assumed that formation of **56** proceeds through the cleavage of P-OCH_3 and the loss of methoxide. The kinetic isotope effect of 3.9 observed for the isomerization of **54a/54** to the final thermodynamic 35/65 ratio in CD_3OD was assumed to hold for the exchange of OCH_3/OCD_3 in CD_3OD. The rate constant for CH_3O exchange is $3.9 \times (4.2 \times 10^{-4}\ s^{-1}) = 1.62 \times 10^{-3}\ s^{-1}$ in CH_3OH.

The partitioning of **57** into **54**, **54a**, and **56** can be determined with the rate \ constants reported above and from the knowledge that the intial kinetic ratio of **54a/54** is 71/29. Eq. (7S) can be derived to determine the relative partitioning of **57**.

(7S) $d[\mathbf{56}]/dt = k_{obs}[\mathbf{54}]_{tot} = \{k_1(\text{fraction } \mathbf{54a})k_3/(k_{-1}+ k_{-2} + k_{-3}) + k_2(\text{fraction } \mathbf{54})k_3/(k_{-1}+ k_{-2} + k_{-3})\}[\mathbf{54}]_{tot}$

$= 1.62 \times 10^{-3}\ s^{-1}[\mathbf{54}]_{tot}$

$= \{(0.71k_1 + 0.29k_2)\ k_3/(k_{-1}+ k_{-2} + k_{-3})\}[\mathbf{54}]_{tot}$

where, $1.62 \times 10^{-3}/(8.2 \times 10^{-3}) = k_3/(k_{-1} + k_{-2} + k_3) = 0.20$. Thus, intermediate **57** partitions to form **56** about 20% of the time, forms **54** about 23% of the time, and forms **54a** about 57% of the time.

Appendix IV. Supplementary material to Chapter 6

Supplementary kinetic data

Table 47S. The percent reaction progress vs time data for the methanolysis of **2** (0.9 mM) catalyzed by [**36**:$Zn(II)_2$:($^{-}OCD_3$)]$_{total}$ (1.0 mM) in CD_3OD at ambient temperature.

Time (h)	Percent Progress (%)
0	0
7.3	2.09
7.3	3.84
18.3	7.41
24.0	9.10
24.0	8.56